NATIONAL TECHNICAL UNIVERSITY OF ATHENS

SCHOOL OF CIVIL ENGINEERING

MASTER OF SCIENCE

ANALYSIS AND DESIGN OF EARTHQUAKE RESISTANT STRUCTURES

MASTER THESIS

A plasticity model for the one dimensional soil response analysis

Anthi Maria

Diploma in Civil Engineering, N.T.U.A.

Supervised by: Associate Professor Nikos Gerolymos

June 2017

ΕΘΝΙΚΟ ΜΕΤΣΟΒΙΟ ΠΟΛΥΤΕΧΝΕΙΟ

ΣΧΟΛΗ ΠΟΛΙΤΙΚΩΝ ΜΗΧΑΝΙΚΩΝ

ΔΙΑΤΜΗΜΑΤΙΚΟ ΠΡΟΓΡΑΜΜΑ ΜΕΤΑΠΤΥΧΙΑΚΩΝ ΣΠΟΥΔΩΝ

ΔΟΜΟΣΤΑΤΙΚΟΣ ΣΧΕΔΙΑΣΜΟΣ ΚΑΙ ΑΝΑΛΥΣΗ ΤΩΝ ΚΑΤΑΣΚΕΥΩΝ

ΜΕΤΑΠΤΥΧΙΑΚΗ ΕΡΓΑΣΙΑ

Προσομοίωμα πλαστικής συμπεριφοράς για την μονοδιάστατη ανάλυση εδαφικής απόκρισης

Άνθη Μαρία

Διπλωματούχος Πολιτικός Μηχανικός, Ε.Μ.Π.

Επιβλέπων: Αναπλ. Καθηγητής Νίκος Γερόλυμος

Ιούνιος 2017

Προλεγόμενα

Θα ήθελα να εκφράσω τις ειλικρινείς μου ευχαριστίες, σε όλους όσους συνέβαλλαν, άμεσα ή έμμεσα, στην προσπάθεια μου αυτή.

Ξεκινώντας, θα ήθελα να ευχαριστήσω τον αναπληρωτή καθηγητή κ. Νίκο Γερόλυμο, για την πολύτιμη βοήθεια και τις συμβουλές του. Η καθοδήγηση και η υποστήριξη του ήταν ανεκτίμητες, από την αρχή των σπουδών μου μέχρι και σήμερα. Το πάθος και ο ενθουσιασμός του για την δουλειά και την επιστήμη με ενέπνεαν πάντα και μετέτρεπαν την εκπαιδευτική διαδικασία σε ένα ευχάριστο ταξίδι. Θα ήθελα να του εκφράσω την ευγνωμοσύνη μου για τον απεριόριστο χρόνο και ενέργεια που μου διέθεσε για την μετάδοση των αστείρευτων γνώσεων του αλλά και της αγάπης του για την επιστήμη. Η συνεργασία μαζί του με έκανε πλουσιότερη όχι μόνο σε γνώσεις, αλλά και σε ηθικές αρχές και αξίες.

Ιδιαίτερες ευχαριστίες, οφείλω στην Παναγιώτα Τασιοπούλου που ήταν πρόθυμη να μου μεταδώσει τις γνώσεις της και να με συμβουλέψει. Η δουλειά της υπήρξε πηγή έμπνευσης και κίνητρο για μένα.

Θα ήθελα επίσης να ευχαριστήσω τους καλούς φίλους και συναδέλφους Κέλλυ Κουνιάκη, Κωνσταντίνο Καπασακάλη και Παναγιώτη Τσαρπαλή που υπήρξαν συνοδοιπόροι σε αυτήν την πορεία των δύο ετών του μεταπτυχιακού αλλά και τις Βάλια Ζωντανού, Χαρά Καλογεράκη, Λήδα Κρημπένη και Νάσια Κουδουνά που συνέβαλλαν στην πραγματοποίηση του σκοπού αυτού είτε μέσω της ηθικής υποστήριξης, είτε μέσω της ανταλλαγής απόψεων επί του επιστημονικού.

Τέλος, θα ήθελα να ευχαριστήσω την οικογένεια μου για την αμέριστη υποστήριξη και ενθάρρυνση τους σε κάθε μου βήμα και ιδιαίτερα τους γονείς μου, Σπύρο και Ζωζώ, τους πιο σημαντικούς ανθρώπους στη ζωή μου. Χωρίς αυτούς τίποτα δεν θα ήταν δυνατό.

NATIONAL TECHNICAL UNIVERSITY OF ATHENS
SCHOOL OF CIVIL ENGINEERING
MASTER OF SCIENCE
ANALYSIS AND DESIGN OF EARTHQUAKE RESISTANT STRUCTURES

A plasticity model for the one dimensional soil response analysis

Master Thesis

Anthi Maria

A B S T R A C T

A plasticity model is presented for the non-linear ground response analysis of layered sites. The model is the one-dimensional version of that recently proposed by Tasiopoulou and Gerolymos (2016) for sand behavior, designated as TA-GER sand model. Critical state compatibility for monotonic and cyclic loading, anisotropic plastic flow rule and Bouc-Wen motivated hardening law are among the key-features of the developed 1D model, offering considerable flexibility in representing complex patterns of cyclic behavior such as stiffness decay and increase in strength due to build-up of pore-water pressure. Implemented through an explicit finite–difference algorithm into an in-house computer code which performs integration of the wave equations to obtain the nonlinear response of layered soil deposits, the model is first calibrated to match published experimental shear modulus and damping curves and is then validated against results from two wave-propagation codes available in literature

.

ΕΘΝΙΚΟ ΜΕΤΣΟΒΙΟ ΠΟΛΥΤΕΧΝΕΙΟ
ΣΧΟΛΗ ΠΟΛΙΤΙΚΩΝ ΜΗΧΑΝΙΚΩΝ
ΔΙΑΤΜΗΜΑΤΙΚΟ ΠΡΟΓΡΑΜΜΑ ΜΕΤΑΠΤΥΧΙΑΚΩΝ ΣΠΟΥΔΩΝ
ΔΟΜΟΣΤΑΤΙΚΟΣ ΣΧΕΔΙΑΣΜΟΣ ΚΑΙ ΑΝΑΛΥΣΗ ΤΩΝ ΚΑΤΑΣΚΕΥΩΝ

Προσομοίωμα πλαστικής συμπεριφοράς για την μονοδιάστατη ανάλυση εδαφικής απόκρισης

Μεταπτυχιακή εργασία

Άνθη Μαρία

Π Ε Ρ Ι Λ Η Ψ Η

Αναπτύσσεται ένα προσομοίωμα πλαστικής συμπεριφοράς για τη μη γραμμική ανάλυση εδαφικής απόκρισης πολύστρωτων σχηματισμών. Το μοντέλο αποτελεί τη μονοδιάστατη έκδοση του μοντέλου Ta-Ger για αμμώδη εδάφη, που προτάθηκε πρόσφατα από τους Τασιοπούλου και Γερόλυμο (2016). Εξέχοντα χαρακτηριστικά του μοντέλου αποτελούν η συμβατότητα με την θεωρία κρίσιμης κατάστασης για μονοτονική και ανακυκλική φόρτιση, ο ανισοτροπικός πλαστικός νόμος ροής και ο εμπνευσμένος από τους Bouc – Wen νόμος κράτυνσης, προσφέροντας αξιοσημείωτη ευελιξία στην αναπαράσταση σύνθετων μηχανισμών ανακυκλικής συμπεριφοράς όπως η μείωση της δυσκαμψίας και η απώλεια της αντοχής λόγω ανάπτυξης υπερπιέσεων πόρων. Το μοντέλο εισάγεται σε έναν αλγόριθμο επίλυσης άμεσης μεθόδου πεπερασμένων διαφορών, που πραγματοποιεί ολοκλήρωση της διαφορικής εξίσωσης διάδοσης κύματος, για τη μη γραμμική απόκριση πολύστρωτων εδαφικών σχηματισμών και στην συνέχεια βαθμονομείται βάσει των δημοσιευμένων πειραματικών καμπυλών μείωσης του μέτρου διάτμησης και αύξησης της απόσβεσης. Τέλος, το μοντέλο επικυρώνεται σύμφωνα με αποτελέσματα δύο εναλλακτικών μεθόδων πρόβλεψης της απόκρισης σε διάδοση διατμητικού κύματος, διαθέσιμων στη βιβλιογραφία.

EXTENDED ABSTRACT

INTRODUCTION

Several constitutive models and numerical codes have been proposed over the last decades for 1D seismic response analysis of horizontally layered soils subjected to vertically-polarized S waves. In general, they can be categorized into three major groups: (a) The equivalent linear viscoelastic models (e.g. [1], [2]), (b) the nonlinear hysteretic (or phenomenological) models (e.g. [3], [4], [5]), and (c) the plasticity-based models (e.g. [6], [7])

Equivalent linear models are the most popular owing to their computational convenience and simplicity. Their main limitations include their inability to efficiently predict the behavior of a nonlinear system under strong ground motions where large cyclic shear strains dominate the response and the violation of the principle of physical causality [8]. Well identified features of cyclic soil behavior, such as: densification, cyclic mobility, stiffness decay and loss of strength due to pore pressure generation, asymmetric response with loading direction are inherently impossible to be reproduced.

Hysteretic models are plausible alternatives to plasticity-based models, but, while capable of overcoming most of the aforementioned limitations, the calibration process is often an arduous task in which the physical meaning of the model parameters is often jeopardized in favour of case-specific accuracy. The absence of a physical law for relating volumetric with shear strains is the main source of this drawback.

Present work presents a downscale version of the recently developed plasticity-based model by Tasiopoulou and Gerolymos for sand behavior [9], [10]. A methodology for the calibration of the model parameters is developed, so that the constitutive stress–strain loops are consistent with experimental shear modulus and damping curves available in the literature. The finite difference wave-propagation code, into which the aforementioned model was implemented, is validated through comparison with results from the equivalent-linear code STRATA [2] and the nonlinear hysteretic code NL-DYAS [4], [5].

BRIEF MODEL DESCRIPTION

Tasiopoulou and Gerolymos [9], [10] developed a new plasticity-based model for sand behavior formulated in the 6-dimenional stress-strain space. In the present work, a 2-dimensional (in p-q space) version of the model is presented for the 1D seismic response analysis of layered soils.

According to this version, the incremental stress-strain relationship is given in the following matrix form:

$$\begin{bmatrix} dp \\ dq \end{bmatrix} = \eta \begin{bmatrix} K - \dfrac{-K^2 M_s d}{-KM_s d + 3G}\zeta_a{}^n & \dfrac{3KGd}{-KM_s d + 3G}\zeta_a{}^n \\ \dfrac{-3KGM_s}{-KM_s d + 3G}\zeta_a{}^n & 3G - \dfrac{9G^2}{-KM_s d + 3G}\zeta_a{}^n \end{bmatrix} \begin{bmatrix} d\varepsilon_p \\ d\varepsilon_q \end{bmatrix}$$

in which K and G are the elastic (small strain) bulk modulus and shear modulus respectively, d is the ratio of the plastic volumetric strain increment $d\varepsilon_p{}^{\mathrm{p}}$, over the plastic deviatoric strain increment $d\varepsilon_q{}^{\mathrm{p}}$ and is based on Rowe's dilatancy theory as it depends on the distance of the current stress ratio q/p from the phase transformation line M_{pt} and M_s is the failure stress ratio representing the ultimate strength. Parameter ζ_a is a hysteretic dimensionless quantity that provides the loading and unloading rule and is a function of the Bouc–Wen parameter ζ, while the exponent n controls the rate of transition from the elastic state to the perfectly plastic one. Finally, η is inserted as a multiplier of the hardening elastoplastic matrix expressing the dissipated hysteretic energy. It is expressed in a ductility based form, as it is a function of μ which is a reference ductility defined in terms of shear strain, as follows:

$$\eta = \frac{s_1}{s_1 + \mu^{s_2}}$$

where s_1 and s_2 are model parameters. Indicative model predictions for characteristic values of the aforementioned parameters, for monotonic and cyclic drained shear tests will emphasize progressing stiffening and evolution to the critical state as loading cycles accumulate and densification builds up. Monotonic and cyclic element tests also depict the evolution of the phase transformation and the ultimate strength parameters M_{pt} and M_s, from their initial values to their critical state value M_{sc}, in a large strain.

PARAMETERS CALIBRATION

To determine the parameters of the model G_{max} is first obtained (e.g., from resonant column tests, crosshole / downhole tests, etc.); then, the parameters n, s_1, and s_2 must be assessed. The calibration is based on matching some established experimental G : γ and ξ : γ curves from the literature. To this end, the Lavenberg–Marquardt optimization procedure is used, available in mathematical code MATLAB. Two published families of G : γ , ξ : γ curves have been utilized: (a) the Vucetic & Dobry curves for sand [11] and (b) the pressure (σ'_0)-dependent curves of Darendeli et al. [12].

Starting from the Vucetic & Dobry (1991) curves, the agreement between computed and experimental curves is quite satisfactory. Small discrepancies are observed for small strain levels.

Darendeli et al. [12] recommended a new family of normalized shear modulus and material damping curves, as functions of plasticity index and mean effective stress. Four confining pressures *(σ'_0 = 25, 100, 400, 1600 kPa)* are examined herein. The set of calibrated parameters is unique for each family of curves and there is no need for recalibration to account for different values of mean confining pressure.

COMPARISON WITH OTHER METHODS

The 2-dimensional version of the TA-GER sand model [9], [10] is implemented into a computer code which uses the explicit finite-difference technique to integrate the equations of motion for the nonlinear one-dimensional ground response analysis of layered sites.

The effectiveness of the proposed model is checked against the hysteretic model by Gerolymos and Gazetas [4] implemented in the finite difference code NL-DYAS ([4], [5]).

To compare NL-DYAS with TA-GER, a 30-m deep *dense sand* profile with density ρ = 2.1 Mg/m^3, constant with depth, and a certain shear wave velocity distribution is excited at its base and its response is calculated.

A strong motion, the JMA 090 record from the Kobe (1995) earthquake and a moderate one from Kalamata 1986 earthquake are used as excitations at the base of the soil column. We consider the sand to behave according to the Derendeli curves.

To serve as a yardstick, an equivalent linear soil response analysis was also carried out with the use of code STRATA [2] — one of the current state-of-practice soil amplification codes.

The results of the three analyses (TA–GER, NL-DYAS, STRATA) in terms of the acceleration time histories at the ground surface, the distributions with depth of the peak values of acceleration, displacement, shear strain, and shear stress, the stress–strain hysteresis loops of the two nonlinear models at the depth of 5m and 15m and the corresponding acceleration response spectra will raise the following conclusions:

- For the moderate excitation, all three codes (and corresponding soil models) predict similar response in terms of distributions with depth and quite similar acceleration time histories, with STRATA exhibiting slightly higher amplitudes.
- Regarding the strong seismic excitation, a fairly similar response is predicted by the two non-linear models. On the other hand, STRATA significantly exaggerates the long-period pulses, while it depresses the high-frequency components — a performance within expectations, as such "depression" of high frequencies has been already noted in the literature (e.g. [13], [14], [15], [16]). The response acceleration spectra from the three codes reinforce this conclusion: whereas the two inelastic soil models produce almost identical spectra, the equivalent-linear analysis, having filtered-out the short-period components, underpredicts the spectral values for periods less than 0.45 sec. It is worth mentioning that an improved equivalent-linear method that avoids the overdamping of high frequencies has been developed by Assimaki and Kausel [14]. Such overdamping stems from the facts that damping is a function of strain amplitude and that high frequencies are usually associated with small amplitudes of motion; thus, these components experience substantially less damping than the dominant frequencies and are artificially suppressed when hysteretic damping is taken as constant. The overestimation of the long period spectral accelerations by the equivalent linear method is due to resonance phenomena that take place in a linear analysis. Such phenomena phenomena cannot be developed when nonlinearity is accounted for, as the shear modulus, therefore the natural periods of soil, are not fixed but change over time.
- The distributions with depth of the peak values of acceleration, shear stress, and horizontal displacement computed with the two nonlinear models for the JMA 090 record are in well agreement, considerably deviating from those of the equivalent linear method. The similarity between the $\tau - \gamma$ diagrams of TA-GER and NL-DYAS analyses is evident for the moderate motion. There are sharp differences for the strong seismic excitation, however, with the TA-GER model predicting broader hysteresis loops that are more regular in shape.

CONCLUSIONS

A plasticity-based model implemented into a finite differences computer code was presented and found capable of predicting efficiently the 1D nonlinear site response. The model is a simplified version of that originally proposed by Tasiopoulou and Gerolymos [9], [10]. The few model parameters were calibrated against experimental results in terms of the shear modulus reduction and damping ratio increase curves available in the literature. The capability of the model in simulating the nonlinear response of horizontally layered deposits was checked through comparison with two codes available in the literature: NL-DYAS and STRATA. While the three codes exhibited similar results for the moderate seismic excitation case, validating the proposed plasticity-based model, the equivalent linear method fails to yield satisfactory results for the strong motion case, significantly underestimating the high-frequency components of the ground response and overestimating the low-frequency ones.

Table of Contents

Chapter 1
Subject of study and literature review

1.1 Scope

The scope of the Thesis is to develop a two – dimensional model, deriving from a plasticity based three – dimensional constitutive model, that can conduct one – dimensional ground response analyses of horizontally layered soils subjected to vertically-polarized S waves. It is aimed that the proposed model can be used in practice for relevant geotechnical problems. In this line of thought, calibration of the constitutive relationship parameters according to experimental data and validation against relevant methods for predicting ground response in seismic shaking is intended in order to enhance the reliability and applicability of the model.

1.2 Layout

Dynamic soil response

The dynamic response of a soil element under cyclic loading is characterized by the hysteretic loop that connects the stress with the strain.

Numerous constitutive models have been developed lately for the representation of the soil cyclic response. The complexity of these models is usually strongly associated to the range of their applicability. A broad categorization of the soil models could be the following:

- viscoelastic models
- hysteretic or non – linear cyclic models
- plasticity theory based models

When the shear strain amplitude that seismic loading imposes is around 10^{-4} to 10^{-5} cyclic soil response is adequately described by the classical theory of linear viscoelasticity. For these small strains soil response is almost elastic and is characterized by small hysteretic damping, which influences, however, the response. The main defect of these models is the correlation between the damping (and the shear modulus in a Maxwell type model) and the frequency. This has not been ascertained by laboratory tests, which converge that soil damping and stiffness are practically independent of the imposed rate of deformation.

The range of application of the viscoelastic models is extended in the study of the cyclic soil response in medium strains around 10^{-4} to 10^{-3}, through the usage of the equivalent – liner analysis methods. In these strain amplitudes the influence of loading cycles in mechanical soil properties is adequately described by only two parameters: the secant shear modulus and the damping.

For strain amplitudes greater than 10^{-3} soil properties are conspicuously affected by the strain amplitude as well as by the number of loading cycles and more general by the exact relationship between the stress and the strain. Viscoelasticity theory is incapable of describing complex non – linear characteristics of cyclic soil response, such as stiffness degradation and loose of strength with the loading cycles, irregular response depending on loading direction, residual strain etc.

Aiming at the realistic soil response analysis in large strains, a bunch of in – elastic (hysteretic) models has been developed. In almost every proposed hysteretic model for describing the stress – strain relationship Masing 's unloading – reloading rule is being utilized. This criterion was proposed in 1926 for the representation of metals cyclic response. Despite of being incapable of realistically representing the diverse soil response in loading – unloading, it is being widely used in geotechnical earthquake engineering thanks to its simplicity.

A considerable drawback of the non – linear cyclic (hysteretic) models nis their difficulty in representing the response under a big number of stress paths. The overcome this problem a number of constitutive models based in plasticity theory has been developed

Advanced constitutive modeling

The most accurate and general methods for representation of soil behavior are based on advanced constitutive models that use basic principles of mechanics to describe observed soil behavior for (a) general initial stress conditions, (b) a wide variety of stress paths, (c) rotating principal axes, (d) cyclic or monotonic loading, (e) high or low strain rates and (f) drained or undrained conditions.

Such models generally require a *yield surface* that describes the limiting stress conditions for which elastic behavior is observed, a *hardening law* that describes changes in the size and shape of the yield surface as plastic deformation occurs, and a *flow rule* that relates increments of plastic strain to increments of stress. The Cam – Clay (Roscoe and Schofield, 1963) and modified Cam – Clay (Roscoe and Burland, 1968) models were among the first of this type. Improvements in the prediction of shear strains have resulted from the use of multiple nested yield loci within the yield surface (Mroz, 1967; Prevost, 1977) and the development of bounding surface models (Dafalias and Popov, 1979) which incorporate a smooth transition from elastic to plastic behavior.

Although advanced constitutive models allow considerable flexibility and generality in modeling the response of soils to cyclic loading, their description usually requires many more parameters than equivalent linear models or cyclic non linear models. Evaluation of these parameters can be difficult, and the parameters obtained from one type of test can be different from those obtained from another. Additionally, the development of plasticity based models is mainly based on the depiction of the soil response under static loading. Their competency in dynamic conditions is not yet equally satisfactory. Although the use of advanced constitutive models will undoubtedly increase, these practical problems have, to date, limited their use in geotechnical earthquake engineering practice.

A hierarchy of models are available for characterization of the stress – strain behavior of cyclically loaded soils. The models range considerably in complexity and accuracy; a model that is appropriate for one type of problem may not be appropriate for another. No single stress – strain model is appropriate for all problems. Selection of a stress – strain model requires careful consideration of the problem to which it is to be applied, recognition of the assumptions and limitations of the available models, and a good understanding of how the model is used in all required analyses.

1.3 Monotonic and cyclic behavior of sand

The behavior of sand has been extensively studied in literature both experimentally and theoretically. Experimental observations provided an insight on the behavioral trends and mechanisms developed under various loading conditions. These observations constituted the basis upon which Critical State Theory by Roscoe et al. (1958) and Schofield and Wroth (1968) was formulated, aiming to accommodate and interpret the basic behavioral characteristics of sand. In the following, a review of the most characteristic aspects of sand response is held within the framework of Critical State Theory.

Monotonic behavior of sand

After numerous experimental observations, it has become common knowledge that sand tends to undergo shear-induced volume change until a critical state is reached, upon which shearing occurs with no volumetric change. Whether shearing tends to develop positive (contraction) or negative (dilation) volume change depends on the initial state of the material relative to the critical state which is a function of the relative density and the confining pressure. The critical state is defined by a surface formed in e-p-q space, which is projected as a line (CSL) in the e-p and q-p planes; e being the void ratio, q the deviatoric stress and p being the mean effective stress. Critical state is considered to be unique for each type of sand. Figure 1.1 illustrates the critical state line (CSL) in e-p plane. Initial loose states, located at the right-hand side of CSL, exhibit contractive behavior which is reflected through reduction of: (i) void ratio, e, in case of drained p-constant loading and (ii) mean effective stress, p, in case of undrained loading, until CSL is reached. Dense states, located at the left-hand side, initially exhibit contractive response until phase transformation line (PTL) is reached. Thereafter, dilative response dominates which is interpreted as increase of: (i) void ratio, e, in case of drained p-constant loading and (ii) mean effective stress, p, in case of undrained loading, until CSL is reached.

This kind of behavior is confirmed experimentally, as shown in Figure 1.2(a). As the initial void ratio increases for a given initial confining pressure, the response tends to be more contractive. In terms of stress-strain curves, a hardening type of response is observed which becomes more intense as the initial void ratio increases. It should be noticed that the void ratio reaches practically the same residual value, known as critical void ratio, irrespectively of the initial value, as it is predicted by the Critical State Theory. It is also worth mentioning that critical state is also reached in p-q space at large strains, as shown by Figure 1.2(b). The stress ratio q/p reaches a unique residual critical stress ratio, irrespectively of the initial conditions.

Apart from the dependency of sand response on the initial void ratio (or initial relative density, Dr), Figure 1.3 demonstrates the impact of initial confining pressure, p. For a given initial relative density, the response becomes more dilative as initial confining pressure decreases. In stress-strain terms, the effect of dilatancy is exhibited by an increase in maximum obtained strength followed by strain softening.

The tendency of positive (dilatancy) or negative (contraction) volumetric change in case of drained loading conditions is expressed through increase or reduction of mean effective stress, respectively, in case of undrained loading, as characteristically shown in Figure 1.4. Experimental results of Figure 1.5 illustrate the behavioral trend under undrained conditions for various initial relative densities and confining pressures. All the evolving stress paths in p-q space converge to the critical state line, which works as a failure envelope, until the ultimate critical stress state is reached.

So far, it has been shown that the behavior of sand is dependent on the relative position of its initial state, in terms of initial density and means effective stress, to the critical state line in e-p plane. However, experimental results depicted in Figure 1.6 indicate dependency on the loading direction, for a given initial state. Despite the given constant distance between initial state and CSL in e-p space, sand exhibits contractive behavior in case of triaxial extension loading, while its response is dilative under triaxial compression loading. This behavioral diversity is attributed to stress-induced anisotropy

Cyclic Behavior of Sand

Cyclic behavior of sand presents certain differentiations when compared to the monotonic response, which cannot be fully accommodated by the strictly defined Critical State framework. For example, experiments confirm that irrespectively of the initial state relative to the CSL in e-p space, sand exhibits only contractive behavior, in accumulative terms, tending to reach the densest possible configuration, defined by minimum void ratio, e_{min}, under drained conditions, or reach zero values of mean effective stress under undrained conditions, as shown in Figure 1.7. The first tendency leads to densification and increase in strength/stiffness, known as cyclic hardening, (Figures 1.8-1.10), while the latter one is associated with cyclic mobility and liquefaction effects (Figure 1.11(a)). It should be mentioned, though, that the critical state concept applies in p-q space, where the critical stress ratio is reached at large strains, after a sufficient number of cycles, irrespectively of the drainage conditions.

In other words, the dependency of sand behavior on the initial state relative to CSL in e-p space is not reflected in the same way as in case of monotonic loading, where it determines whether the response will be dilative or contractive. In case of cyclic loading, the above mentioned dependency determines the number of loading cycles needed to achieve either: (i) $e = e_{min}$ (drained conditions) or (ii) $p = 0$ (undrained conditions). The correlation between number of cycles and initial relative density is shown in Figures 1.10 and 1.11(b).

Figures

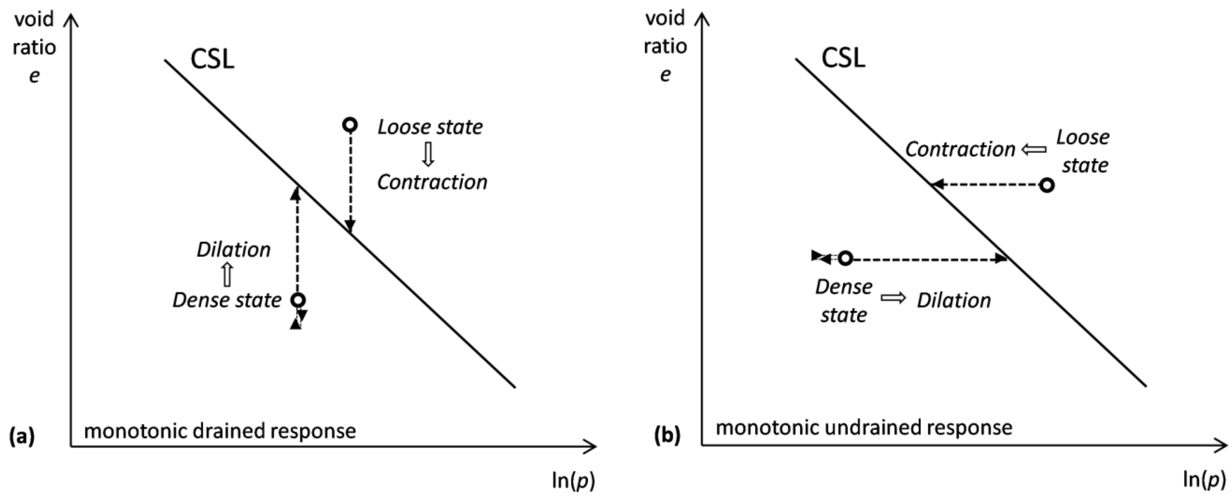

Figure 1.1. Illustration of monotonic behavior of sand in e-p space, where e is the void ratio and p is the mean effective stress: (a) drained and (b) undrained conditions.

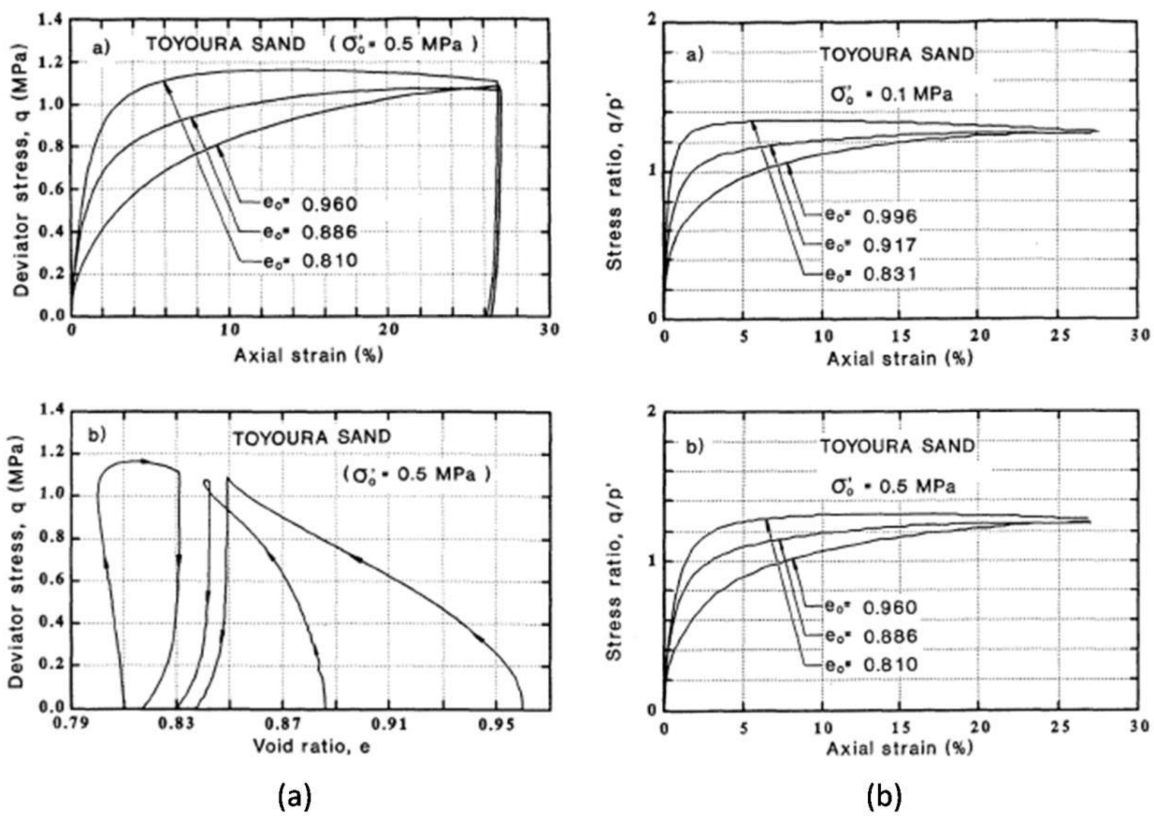

Figure 1.2. Drained triaxial tests: (a) stress-strain curves and void ratio versus deviatoric stress, (b) stress ratio versus axial strain (Verdugo and Ishihara, 1996).

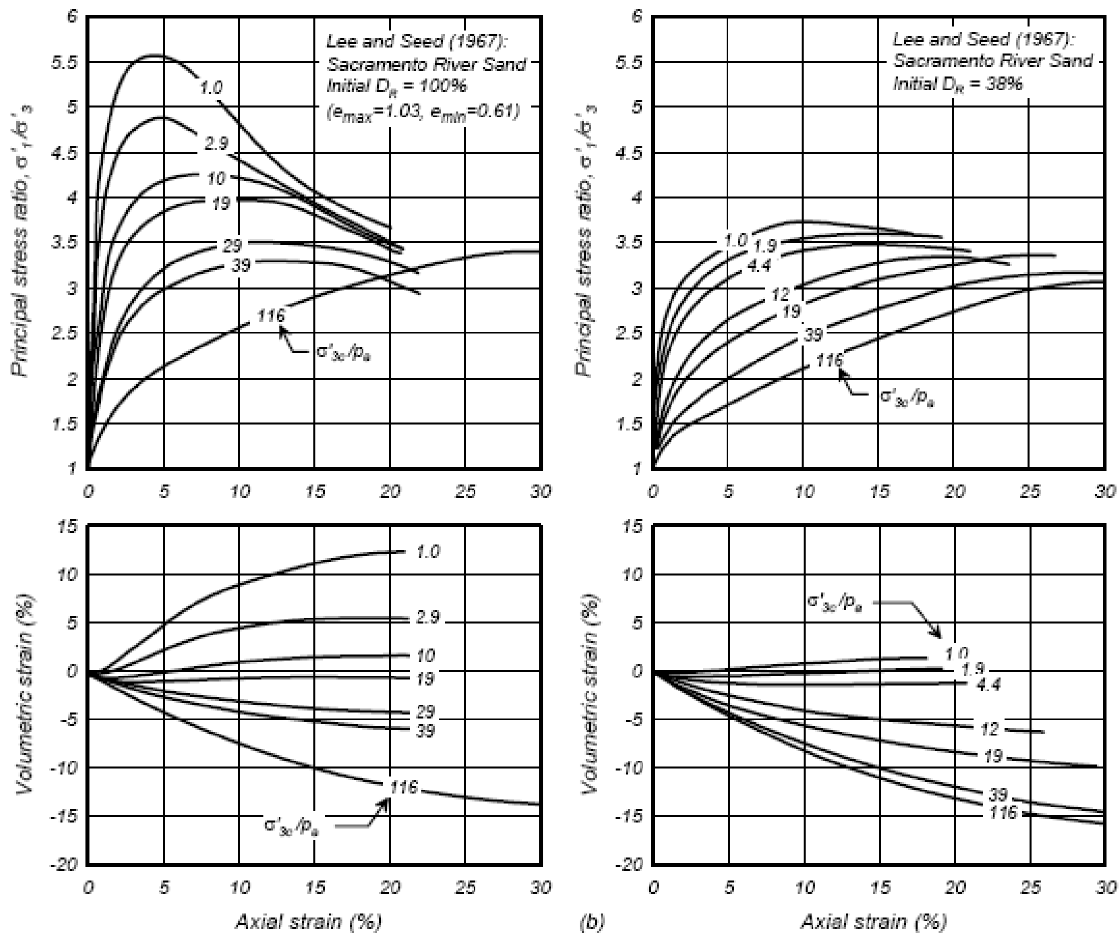

Figure 1.3. Drained triaxial compression tests on loose and dense sand specimens under a range of effective confining stresses (Lee and Seed, 1967).

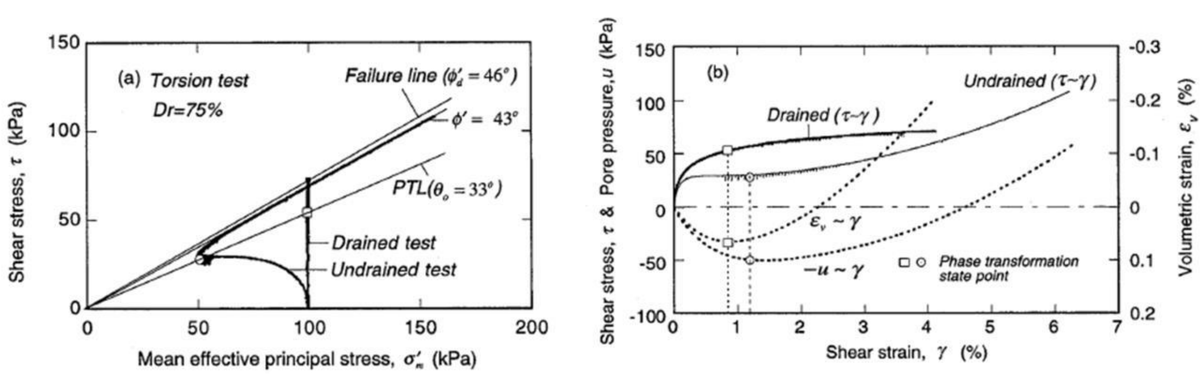

Figure 1.4. Influence of drainage conditions on sand response (Zhang et al., 1997).

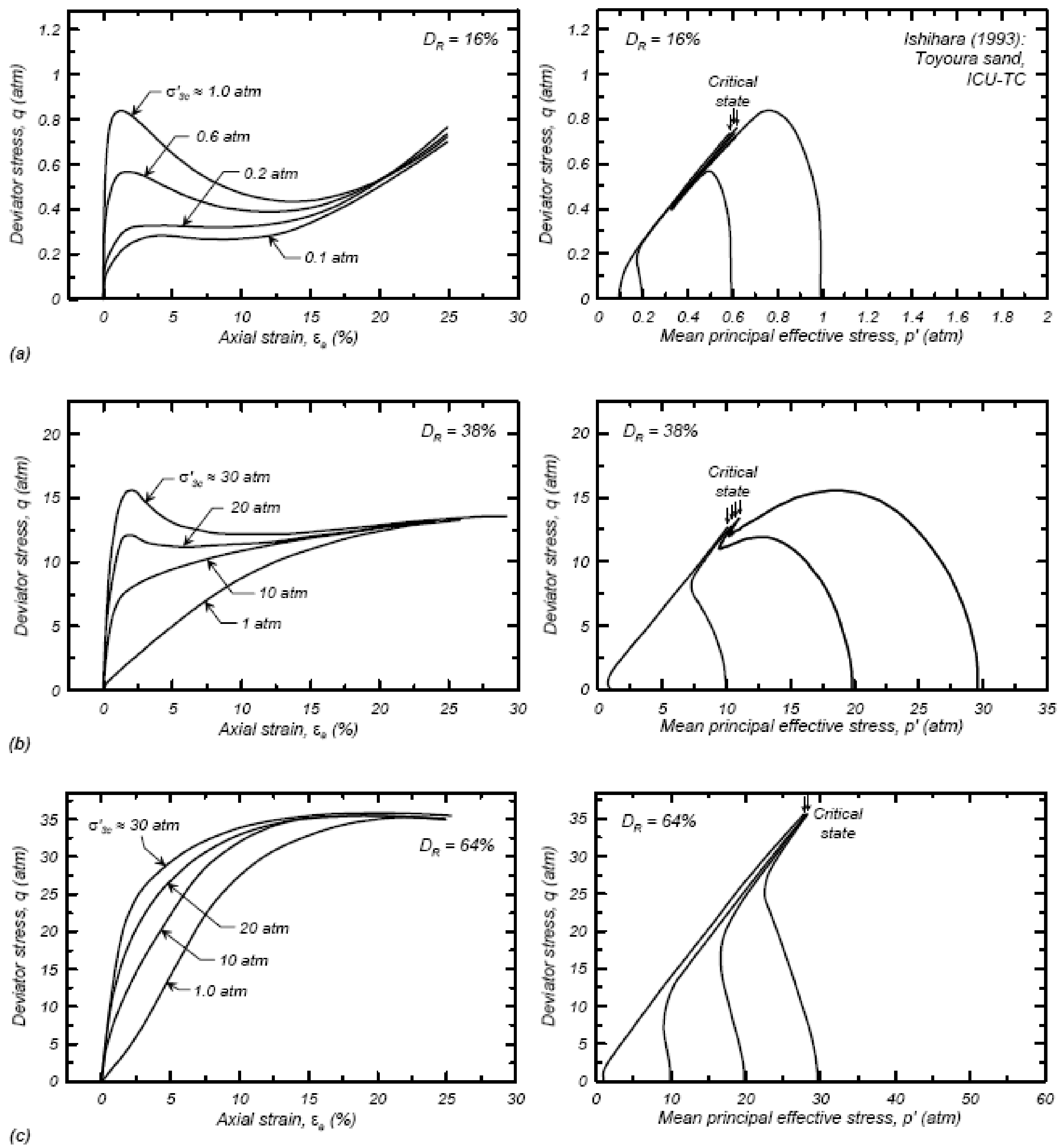

Figure 1.5. Undrained triaxial compression tests on sand specimens of various initial relative densities under a range of effective consolidation stresses (Verdugo and Ishihara, 1996).

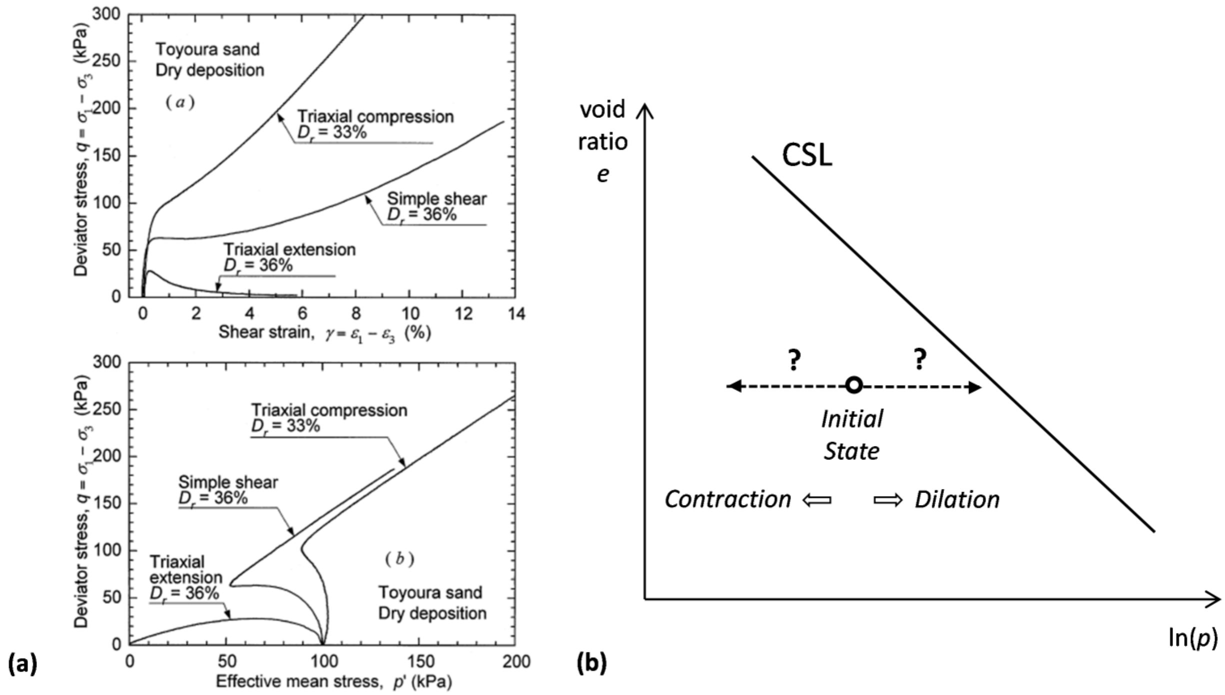

Figure 1.6. (a) Influence of loading direction on sand response (Yoshimine et al., 1998) and (b) how it can be predicted within the critical state framework.

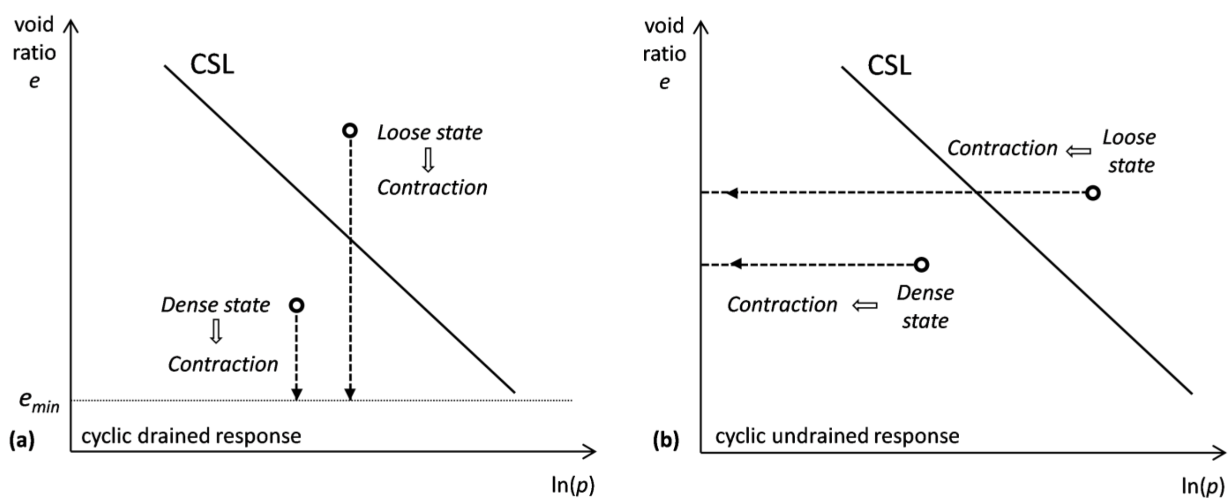

Figure 1.7. Illustration of cyclic behavior of sand in e-p space, where e is the void ratio and p is the mean effective stress: (a) drained and (b) undrained conditions.

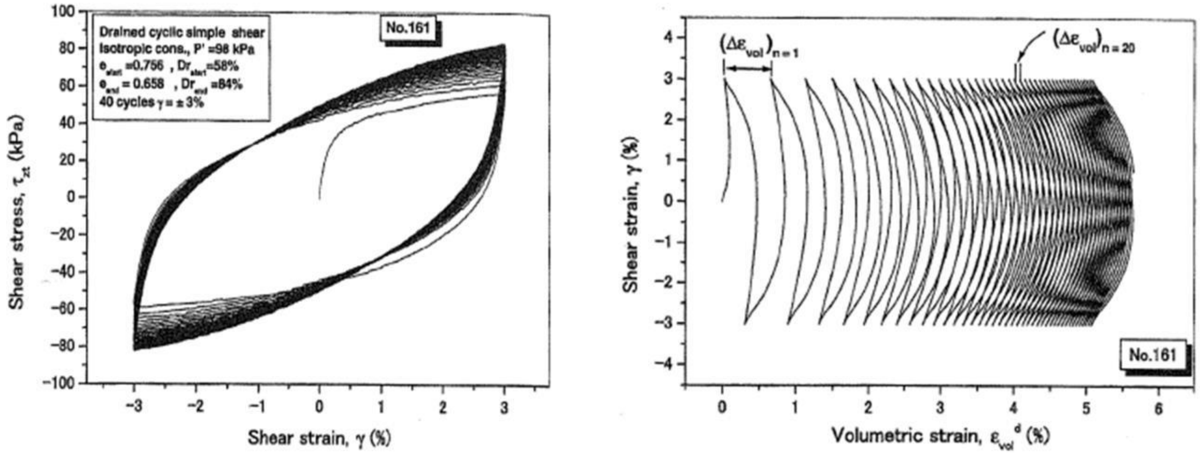

Figure 1.8. Stress-strain curves (left) and volumetric strain versus shear strain for a medium dense sand specimen subjected to drained cyclic simple shear under constant strain amplitude (Shahnazari and Towhata, 2002).

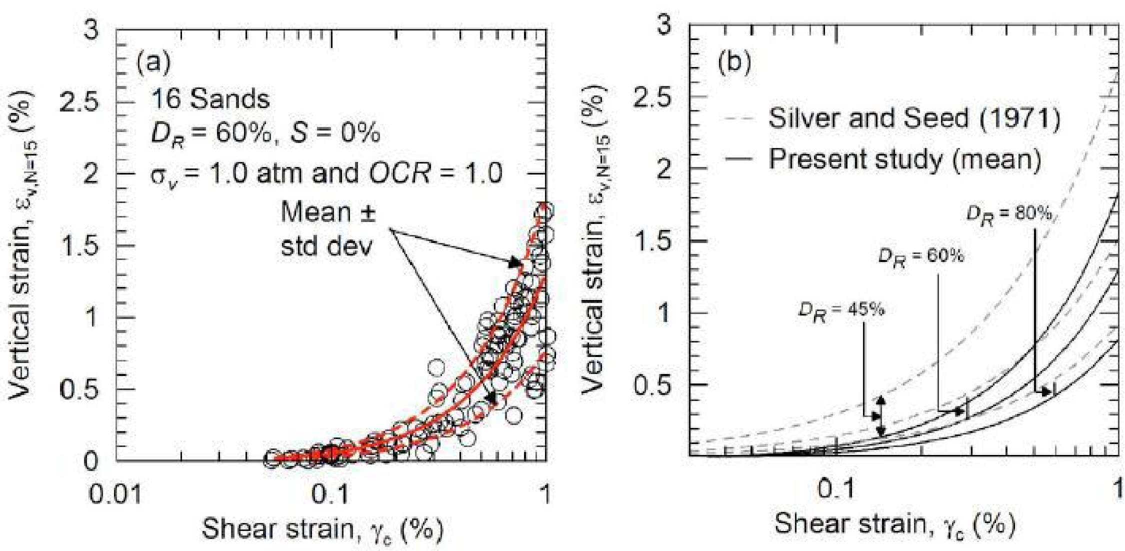

Figure 1.9. Volumetric strains in drained cyclic direct simple shear tests on clean sands (Duku et al. 2008): (a) Results from 16 sands at a relative density of about 60% with an overburden stress of 1.0 atm, and (b) Comparison of trends with earlier relationships by Silver and Seed (1971) for sands at relative densities of 45, 60, and 80%.

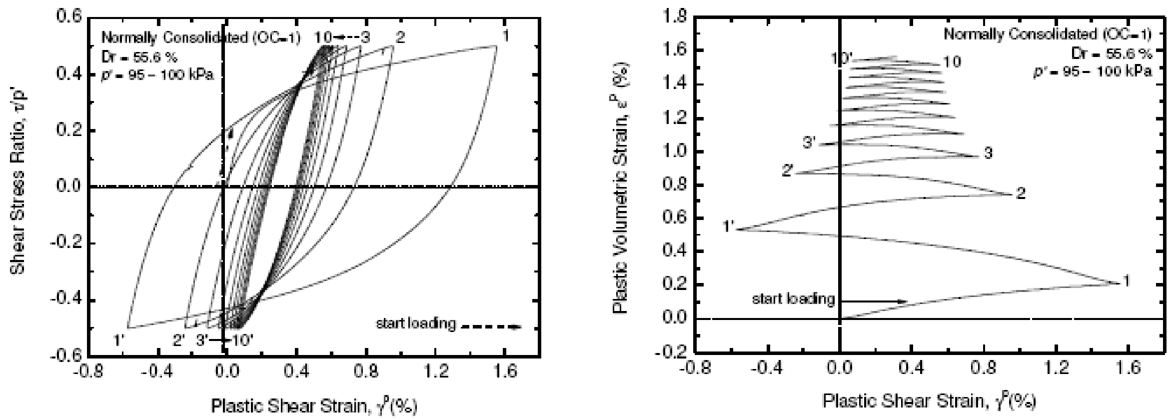

Figure 1.10. Stress-strain curves (left) and volumetric strain versus shear strain for a medium dense sand specimen subjected to drained cyclic simple shear under constant shear stress amplitude (Wahyudi et al., 2010).

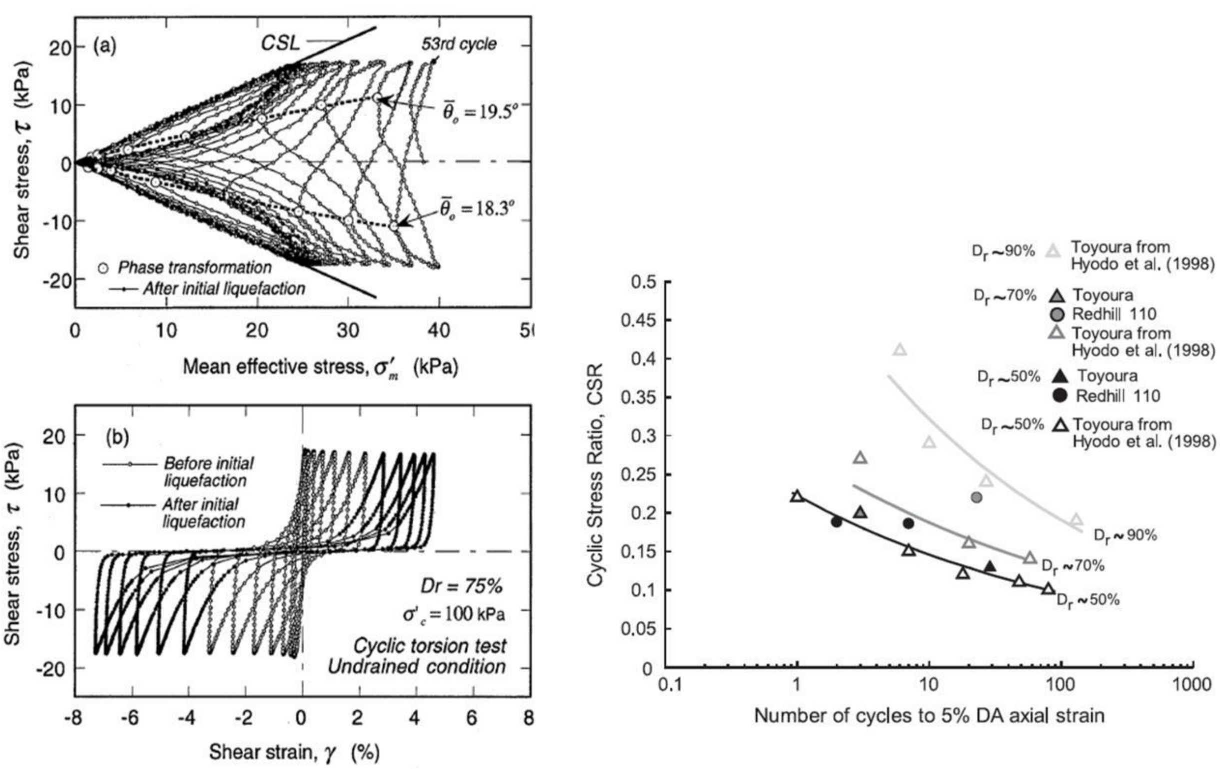

(a) (b)

Figure 1.11. (a) Effective stress path and stress-strain hysteresis observed in a cyclic undrained torsional test (Zhang et al., 1997), (b) Cyclic stress ratio versus number of cycles required to cause 5% of DA axial strain for samples with relative density, Dr of 50%, 70% and 90% (Lombardi et al., 2014).

Chapter 2
Downgrade of the 3D constitutive model Tager for sand in triaxial space

2.1 Introduction

Performance based analysis is increasingly gaining ground in daily practice against conventional pseudostatic analysis. The necessity of developing economically efficient solutions without jeopardizing safety, is the main reason for this drastic change in the way we you used to design our structures.

However, the effectiveness of a performance based design approach strongly hinges on the ability of the utilized numerical tool to realistically calculate the soil and structural displacements for a wide range of loading paths and initial conditions. Apparently, the constitutive modeling of soil behavior plays a decisive role on this. The behavioral diversity of sand for different loading (drained /undrained, monotonic/cyclic), initial stress and fabric conditions, renders its modeling a difficult and challenging task. The suitability of the used constitutive model is evaluated by its capability to capture the trends across all these conditions without recalibration of its parameters for each specific case, but also by its simplicity. Too many parameters might increase the versatility of the model at the risk, however, of losing its physical meaning.

In the last three decades, many constitutive models for sand have been proposed, each with varying degree of accuracy and applicability (a brief discussion about this was made in Ch. 1). The most promising ones are plasticity-based and incorporate the effective stress and critical state concepts (e.g. Ishihara and Towhata, 1980; Cubrinovski and Ishihara, 2000; Dafalias and Manzari, 2004; Park and Byrne, 2004; Boulanger et al., 2011).

In this paragraph, a brief reference to the constitutive model for sand Ta-Ger will be made, as it was published by Panagiota Tasiopoulou and Nikos Gerolymos in 2016. This constitutive model, formed in multiaxial space was based on a new theoretical framework that combines features of perfect elastoplasticity and Bouc-Wen type hardening plasticity. It adopts an open-end, cone-type bounding surface with the elastic region being trivialized to a single point, coupling perfect elastoplasticity with pre-failure smooth hysteresis. This alternative plasticity formulation exhibits critical state compatibility for monotonic and cyclic loading and uniqueness of its parameters for a given type of sand, irrespective of loading conditions. It aims to provide a continuous function between an input (displacement, strain etc.), and an output (force, stress etc.), for nonlinear, hysteresis systems, by defining a continuous expression of an elastoplastic matrix, connecting the strain with the stress. Using a new plastic flow rule based on a revision of Rowe's dilatancy theory (1962), it is versatile enough to account for anisotropic distribution of the dilatancy to the plastic strain increments as well as densification due to cyclic loading. The Drucker-Prager failure envelope is used as bounding surface, but modifications can be easily implemented to account for Lode angle dependency. The combined influence of density and confining stress on the response is efficiently taken into account through the critical state approach. Among the other benefits is the ability of the model to realistically reproduce complex patterns of monotonic and cyclic behavior such as hysteretic response, dilation, contraction, loss of strength and cyclic mobility in undrained monotonic and cyclic loading, respectively.

The aforementioned constitutive model for sand was downscaled to p-q space and reformulated in a way that hysteretic loops and densification can be predicted for an input strain time history. In what follows, the formulation and some of the key parameters of the model, accounting for drained conditions, are presented.

2.2 Model Concept and Parameters

An alternative plasticity concept

Classic elastoplasticity framework imposes that the elasto-plastic matrix is given by:

$$\boldsymbol{E^{ep}} = \boldsymbol{E^e}\left[\boldsymbol{I} - \boldsymbol{\Phi_g}\left(\boldsymbol{\Phi_f}^{\boldsymbol{T}}\boldsymbol{E^e}\boldsymbol{\Phi_g}\right)^{-1}\boldsymbol{\Phi_f}^{\boldsymbol{T}}\boldsymbol{E^e}\right]$$

in which $\boldsymbol{\Phi} f$ and $\boldsymbol{\Phi} g$ account for the gradient to the failure surface and plastic flow rule, respectively:

$$\boldsymbol{\Phi_f} = \frac{\partial f}{\partial \boldsymbol{\sigma}}$$

$$\boldsymbol{\Phi_g} = \frac{\partial g}{\partial \boldsymbol{\sigma}}$$

For a perfectly plastic material, the yield surface is fixed in stress space, and therefore plastic deformation occurs only when the stress path moves on the yield surface. The plastic strain increment is obtained from the flow rule that is assumed to imply normality to the plastic potential function g, according to the above formulation.

In the present modified elasto – plasticity framework hardening and hysteretic behavior is introduced by inserting the matrices H and η:

$$\boldsymbol{E_h}^{\boldsymbol{ep}} = \boldsymbol{E}^{\boldsymbol{e}}(\boldsymbol{I} - \boldsymbol{BH})\boldsymbol{\eta}$$

The terms in matrix **H** are functions of the dimensionless hardening parameter ζ, which is inspired by the Bouc-Wen smooth hysteresis model Bouc (1971) and its extended versions (Wen, 1976 ; Gerolymos and Gazetas, 2005), and η (Gerolymos and Gazetas, 2005; Drosos et al., 2012) accounts for stiffness degradation by modifying the shape and size of the hysteretic loops according to the amplitude of the deviatoric strain εq . Finally, **B** is the abbreviation of the right-hand side term inside the parentheses of the formulation of the classic elasto – plastic matrix:

$$\boldsymbol{B} = \boldsymbol{\Phi_g}\left(\boldsymbol{\Phi_f}^{\boldsymbol{T}}\boldsymbol{E}^{\boldsymbol{e}}\boldsymbol{\Phi_g}\right)^{-1}\boldsymbol{\Phi_f}^{\boldsymbol{T}}\boldsymbol{E}^{\boldsymbol{e}}$$

<u>Elastic Parameters</u>

In order to form the elastic matrix $\boldsymbol{E}^{\boldsymbol{e}}$, it is necessary to define the elastic shear modulus G and the elastic bulk modulus K which are expressed as functions of the mean effective stress and the relative soil density using Seed and Idriss published experimental data and Souliotis and Gerolymos curve fitting, as follows:

$$G_{max} = 1592{,}6 * p_a * D_{ro}^{0.6464} * \left(\frac{p}{p_a}\right)^m \quad \text{and} \quad K = G$$

in which:

pa is the atmospheric pressure
Dro is the initial soil relative density
m is a dimensionless parameter determining the rate of variation of G and K with p.

The elastic bulk modulus K, is considered to be equal to G_{max}, assuming a Poisson ratio of v=0.15 which is typical for relatively uniform sands at confining pressures greater than 50 KPa (e.g. Gu and Yang, 2013).

The elastic matrix in triaxial space is given by:

$$\boldsymbol{E^e} = \begin{bmatrix} K & 0 \\ 0 & 3G \end{bmatrix}$$

since the deviatoric, dq , and mean effective, dp , stress increments are calculated using the elastic deviatoric and volumetric strain increments, in respect:

$$dp = K d{\varepsilon_p}^e$$

$$dq = 3G d{\varepsilon_q}^e$$

<u>Yield surface</u>

The model incorporates the Drucker-Prager failure envelope as the bounding surface:

$$f = q - M_s p = 0$$

in which, Ms is the ultimate strength line in q-p space. This equation implies the following consistency condition at failure:

$$f = 0 \leftrightarrow \frac{q}{M_s p} = 1$$

Thus the hardening parameter ζ, is defined as:

$$\zeta = \left|\frac{q}{M_s p}\right|$$

The hardening parameter, ζ, is bounded, strictly obtaining values within the range [0, 1]. At reversal points, ζ is transformed to ζα , according to:

$$\zeta_\alpha = \left|\frac{\zeta - \zeta_p}{1 + |\zeta_p|}\right|$$

which ζp is the maximum value of ζ at the previous reversal (pivot) point. Hence, hardening parameter ζα becomes equal to 0 at the occurrence of loading reversal, indicating elastic response at the beginning of unloading/reloading.

The hardening matrix H, for monotonic loading, is defined as:

$$H = \begin{bmatrix} \zeta^n & 0 \\ 0 & \zeta^n \end{bmatrix}$$

where n is an exponential parameter which “controls” the rate of transition from the elastic state to the perfectly plastic one (Gerolymos and Gazetas, 2005). For cycling loading parameter ζα is used for the formation of the plastic matrix

$$H = \begin{bmatrix} {\zeta_\alpha}^n & 0 \\ 0 & {\zeta_\alpha}^n \end{bmatrix}$$

Flow rule

The stress-dilatancy relationship, adopted by the model, is based on Rowe's dilatancy theory (Rowe 1962). Dilatancy, defined as the ratio of the plastic volumetric strain increment, $d\varepsilon_p{}^p$ over the plastic deviatoric strain increment, $d\varepsilon_p{}^q$depends on the distance of the current stress ratio, *q / p = ζ Ms* from the phase transformation line, *Mpt*, as follows:

$$d = R_d \frac{d\varepsilon_p{}^p}{d\varepsilon_q{}^p} = R_d \left(M_{pt} - \left| \frac{q}{p} \right| \right) = R_d \left(M_{pt} - \zeta M_s \right)$$

Parameter R_d is given by:

$$R_d = e^{-a(D_r - D_{ro})}$$

Where Dr is the current relative density, Dro is the initial relative density and a is a constant. Evidently, increase of Dr causes decrease of parameter Rd and subsequent decrease of quantity d, resulting in densification for the case of a drained cyclic simple shear element test. Influence of parameter a in densification line for various relative densities is depicted in Fig. 3.1.

Modified hardening elasto – plastic matrix

The modified elastoplastic matrix is calculated according to the above mentioned:

$$E_h{}^{ep} = \begin{bmatrix} K - \dfrac{-K^2 M_s d}{-K M_s d + 3G} \zeta^n & \dfrac{-3KGd}{-K M_s d + 3G} \zeta^n \\ \dfrac{-3KGM_s}{-K M_s d + 3G} \zeta^n & 3G - \dfrac{9G^2}{-K M_s d + 3G} \zeta^n \end{bmatrix}$$

The only difference between the modified elastoplastic matrix, $E_h{}^{ep}$, and the elastoplastic matrix, $E_h{}^{ep}$, resulting from elastic-perfectly plastic formulation is attributed to the introduction of hardening parameter ζn, which provides a smooth hysteretic interpolation, Bouc-Wen motivated, between elastic and perfect plastic stress states.

If matrix η, which consists of only diagonal terms:

$$\boldsymbol{\eta} = \begin{bmatrix} \eta & 0 \\ 0 & \eta \end{bmatrix}$$

is incorporated into the ${E_h}^{ep}$ formulation, then the elastoplastic matrix is modified as:

$${E_h}^{ep} = \eta \begin{bmatrix} K - \dfrac{-K^2 M_s d}{-K M_s d + 3G} \zeta^n & \dfrac{3KGd}{-K M_s d + 3G} \zeta^n \\ \dfrac{-3KGM_s}{-K M_s d + 3G} \zeta^n & 3G - \dfrac{9G^2}{-K M_s d + 3G} \zeta^n \end{bmatrix}$$

<u>Parameter η</u>

Parameter η is inserted as a multiplier of the hardening elastoplastic matrix.η expresses the dissipated hysteretic energy and it affects the expansion of the stress – strain loop. It is expressed in a ductility based form as it is a function of μ which is a reference ductility defined in terms of shear strain at the most current stress reversal, at the maximum attained shear strain before the start of the current unloading or reloading cycle:

$$\eta = \frac{s_1}{s_1 + \mu^{s_2}}$$

Figs. 3.2 and 3.3 illustrate the influence of parameters s_1 and s_2 in the shear modulus reduction and damping curves.

<u>Critical state concept</u>

The essence of the critical state concept is that no change in volume occurs when the current stress state reaches the critical state, while the shear deformation continuously increases. In order to achieve this kind of performance upon critical state, both the phase transformation line, M_{pt} and the ultimate strength line, M_s, should evolve in p-q space converging to the critical state line, M_{cs} and producing zero plastic volumetric change when $M_{pt} = M_s = M_{cs}$. The evolution of the ultimate strength line is expressed as a function of the cumulative total deviatoric strain, $\sum|d_{\varepsilon q}|$:

$$M_s = M_{cs} + \left[M_{sp} + \left(M_{s0} - M_{sp}\right)e^{-c_1 \sum|d_{\varepsilon q}|} - M_{cs}\right]e^{-c_1 \sum|d_{\varepsilon q}|}$$

where M_{s0} is an initial value of the ultimate strength, and M_{sp} is a maximum value that can be potentially reached depending on the model parameter c_1. The phase transformation line evolves according to following expression:

$$M_{pt} = M_{cs} + (M_{pt0} - M_{cs})e^{-c_2 \sum|d_{\varepsilon q}|}$$

in which M_{pt0} is the initial value of M_{pt} , c_2 is a model parameter and $\sum|d_{\varepsilon q}|$ expresses the accumulation of total deviatoric strain increments. The influence of parameters c_1 and c_2 is illustrated in Figs. 3.4 and 3.5. in terms of shear stress, volumetric strain and evolution of M_{pt} and M_s for a monotonic shear test. In case of cyclic drained loading, slower evolution of phase transformation line towards critical state leads to less accumulation of volumetric strain for a certain number of cycles, due to generation of greater “uplift” of the *ep*-*eq* curve, close to the reversal points.

2.3 Model Performance

Simulation of drained behavior of sand under monotonic and cyclic loading have been performed in p-q space. Simulation is strain controlled; thus, the applied deviatoric strain increment dεq is considered known and the mean effective stress, p, is assumed constant, so that dp = 0 . The 2x2 matrix connecting the strain with the stress increments is formed as follows:

$$\begin{bmatrix} dp \\ dq \end{bmatrix} = \begin{bmatrix} A & B \\ C & D \end{bmatrix} \begin{bmatrix} d\varepsilon_p \\ d\varepsilon_q \end{bmatrix}$$

where :

$$A = K - \frac{-K^2 M_s d}{-K M_s d + 3G} \zeta^n$$

$$B = \frac{3KGd}{-K M_s d + 3G} \zeta^n$$

$$C = \frac{-3KGM_s}{-K M_s d + 3G} \zeta^n$$

$$D = 3G - \frac{9G^2}{-K M_s d + 3G} \zeta^n$$

The deviatoric stress increment, *dq*, is calculated as

$$dq = \left(-\frac{BC}{A} + D \right) d\varepsilon_q$$

and the volumetric strain increment, *dεp*, is obtained by:

$$dep = -\frac{B}{A} \left| d\varepsilon_q \right|$$

The results are afterwards transformed in terms of shear stress and shear strain.

Regarding the monotonic loading, three different relative densities were examined under the same mean effective stress and also three different mean effective stresses were examined for the same initial relative density. Results are depicted in Fig. 3.6-3.9 in terms of shear stress, volumetric strain, void ratio, boundary line M_s, phase transformation line M_{pt} and the evolution of the last two parameters *vs* the stress state line *q/p*. The evolution of the friction angle with shear strain along with its maximum value ϕ_{peak}, its initial value ϕ_{s0} and its critical state value ϕ_{cs} are also presented in Fig. 3.10.

The evolution of phase transformation and ultimate strength lines with strain, demonstrate that both lines reach the critical state line at large strains. Moreover, it is worth noting that for loose sands the phase transformation line is initially located above the ultimate strength line in p-q space and vice versa for denser sands. This is attributed to the more contractive behavior which leads them directly to the critical state with no phase transformation (Yoshimine and Ishihara, 1998). The opposite behavior is observed for denser sand crossing the phase transformation line (contractive response) before "moving" towards the critical state (dilative response). The same remarks can be made for the sands under a small mean effective stress and sands under a heavy mean effective stress, which correspond to denser and looser sands respectively. As expected, ultimate strength line is never exceeded from the stress state line q/p either for dense or loose sands.

Cyclic drained shear tests were also carried out (Fig. 3.11 – 3.16.) and three different relative densities were examined under the same mean effective stress for three different levels of mean effective stress. Cyclic drained shear tests will emphasize progressive stiffening as loading cycles accumulate and densification builds up. Maximum attained shear stress is, as expected, greater for denser sands and those under a big mean effective stress. It is worth noting, that in the volumetric strain figure the distance between two consecutive loading cycles becomes smaller as loading cycles accumulate, proceeding to the critical state, as is also pointed by the coincidence of M_{pt} and M_s with their critical state value M_{cs}. The shape of the densification line is indicative to a more dilative behavior for denser sands and sands under small mean effective stresses.

Figures

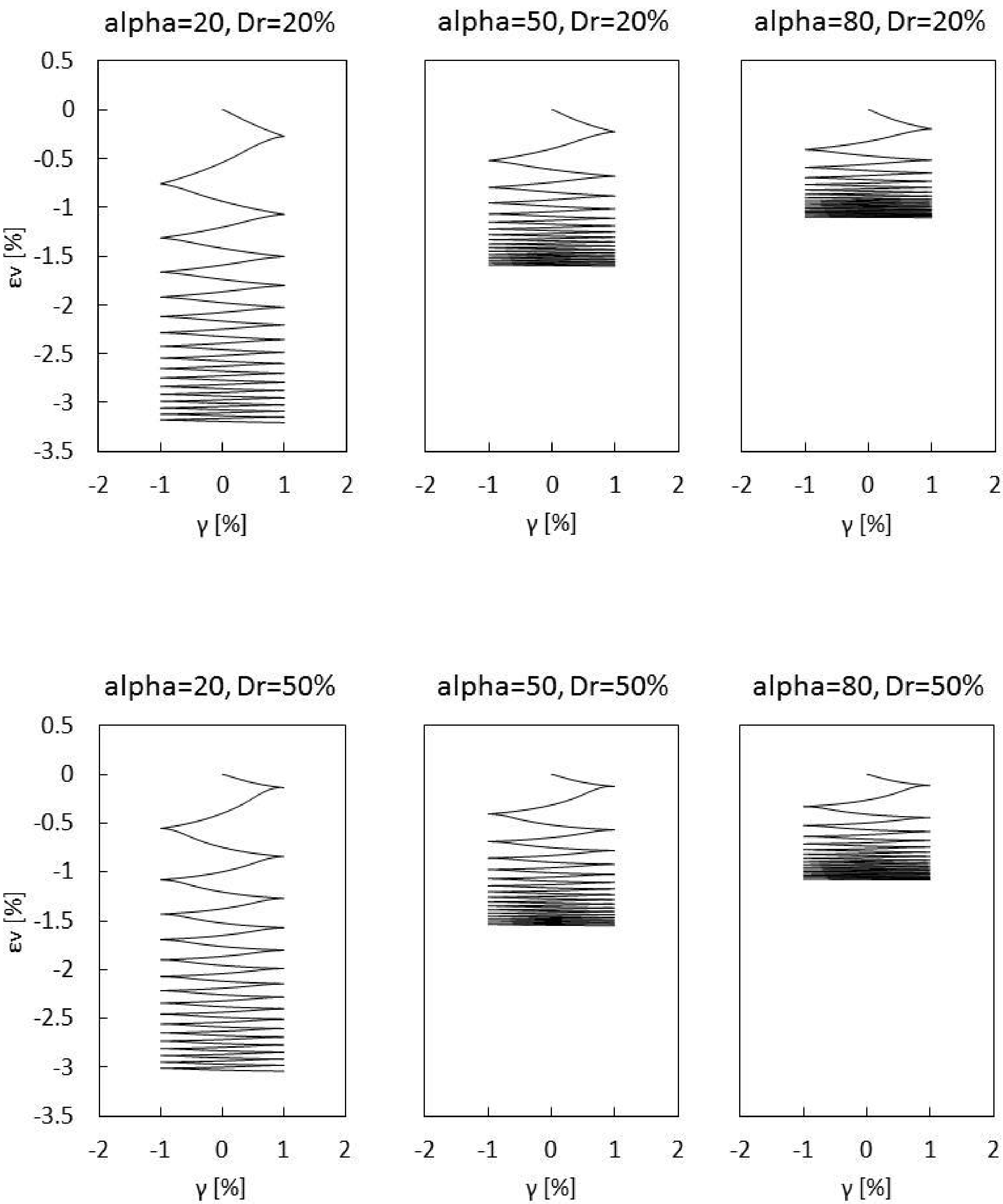

alpha=20, Dr=20%
alpha=50, Dr=20%
alpha=80, Dr=20%
alpha=20, Dr=50%
alpha=50, Dr=50%
alpha=80, Dr=50%
εv [%]
γ [%]
0.5
0
-0.5
-1
-1.5
-2
-2.5
-3
-3.5
-2
-1
0
1
2

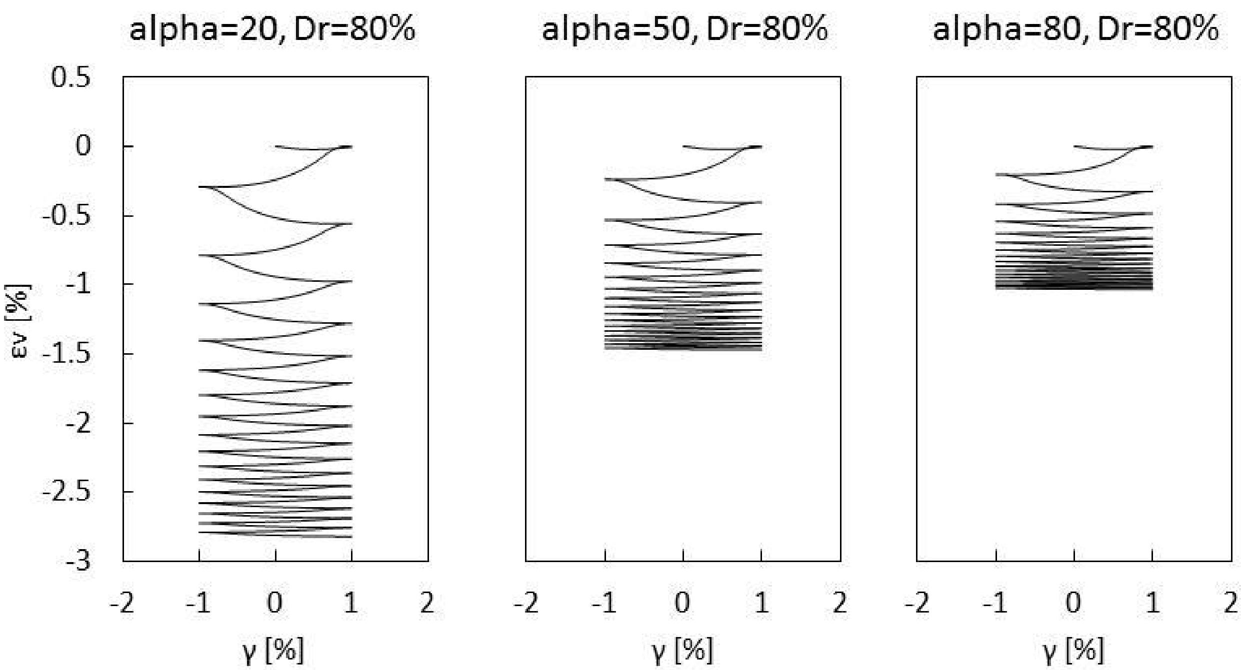

Figure 3.1: (a) Volumetric strain for cyclic drained shear test in respect of shear strain for different values of the exponent a for three relative densities Dr=20%, Dr=50% and Dr=80%

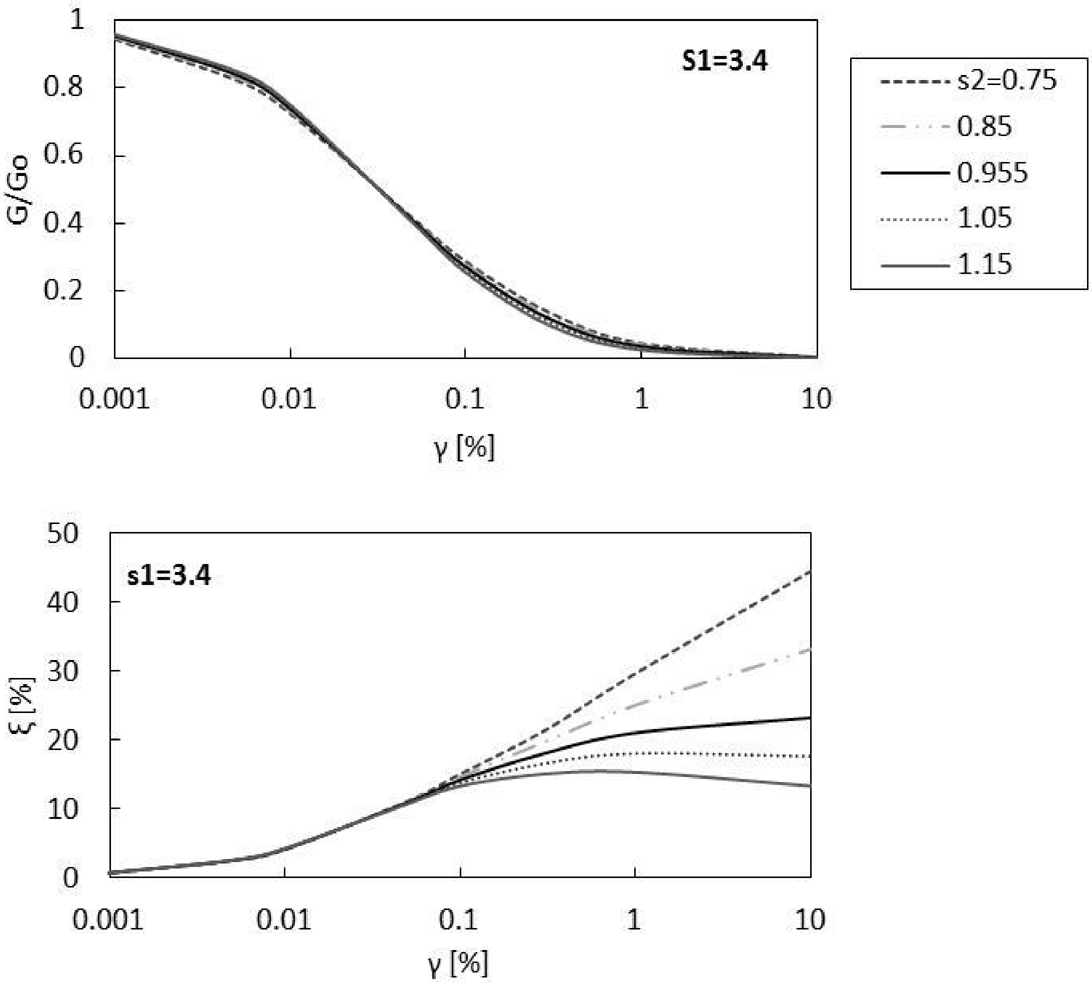

Figure 3.2: Shear modulus reduction and damping curves for various values of the s_2 parameter for s_1=3.4

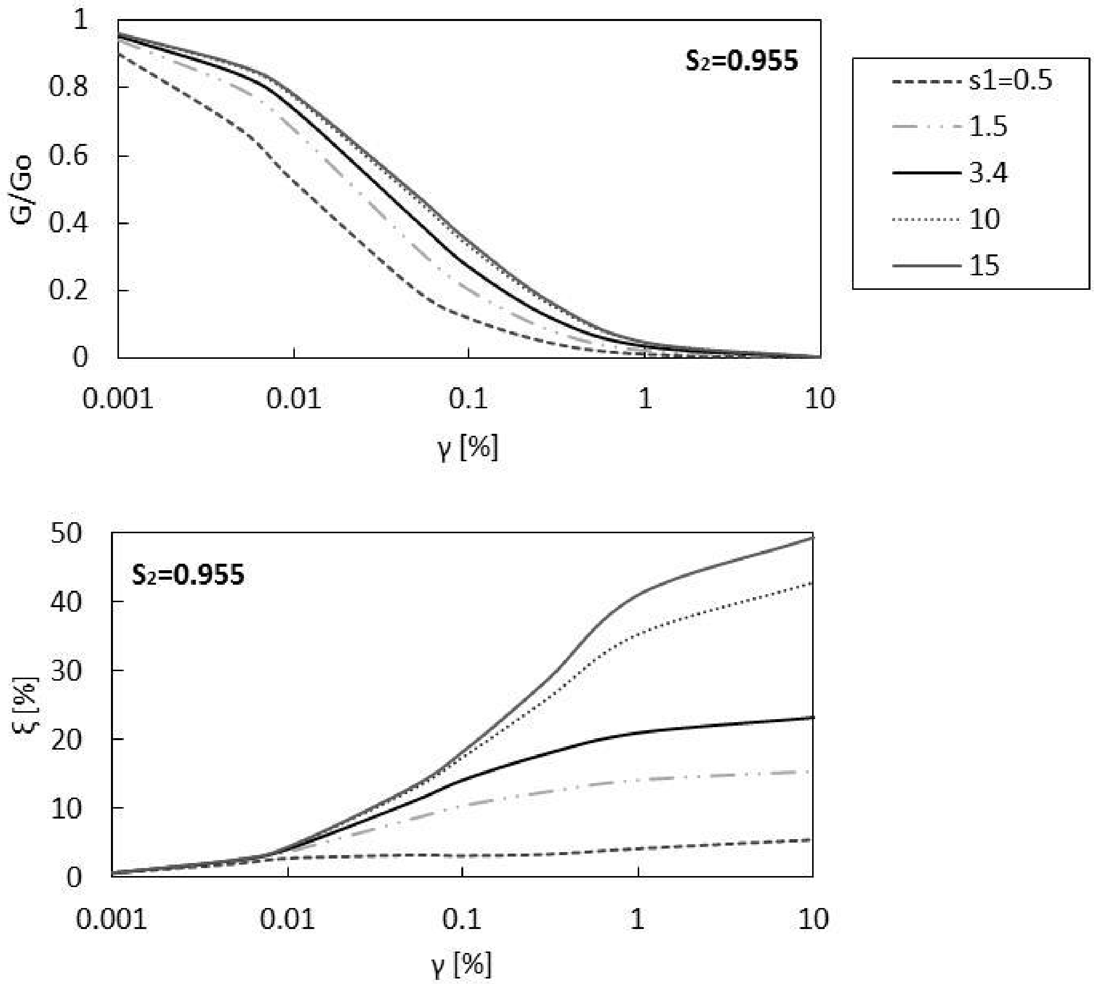

Figure 3.3: Shear modulus reduction and damping curves for various values of the s_1 parameter for s_2=0.955.

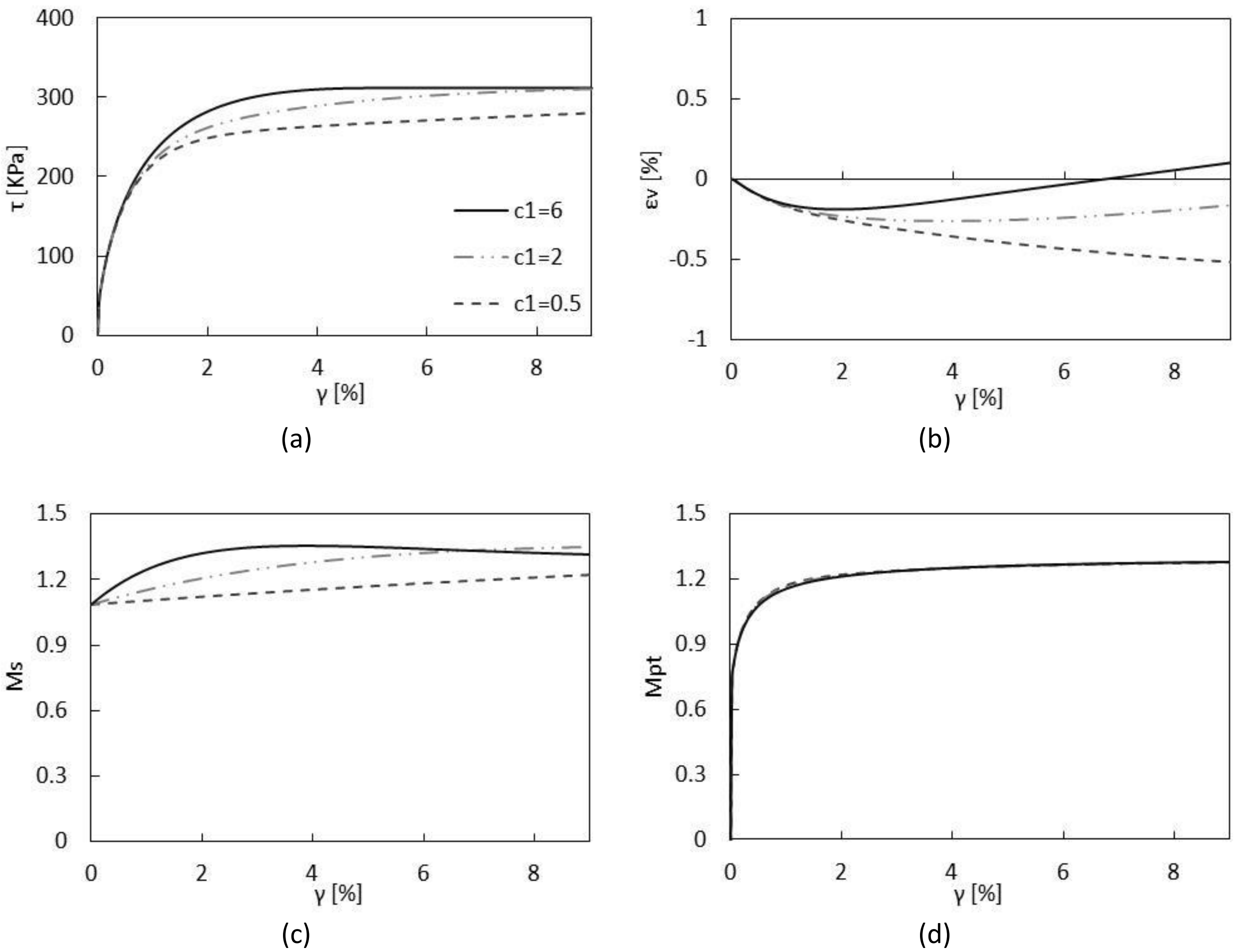

(a) (b)

(c) (d)

Figure 3.4: (a) Influence of the exponent c_1 in a drained monotonic shear test in terms of (a) shear stress, (b) volumetric strain, (c) boundary line Ms and (d) phase transformation line with shear strain for c_1 constant.

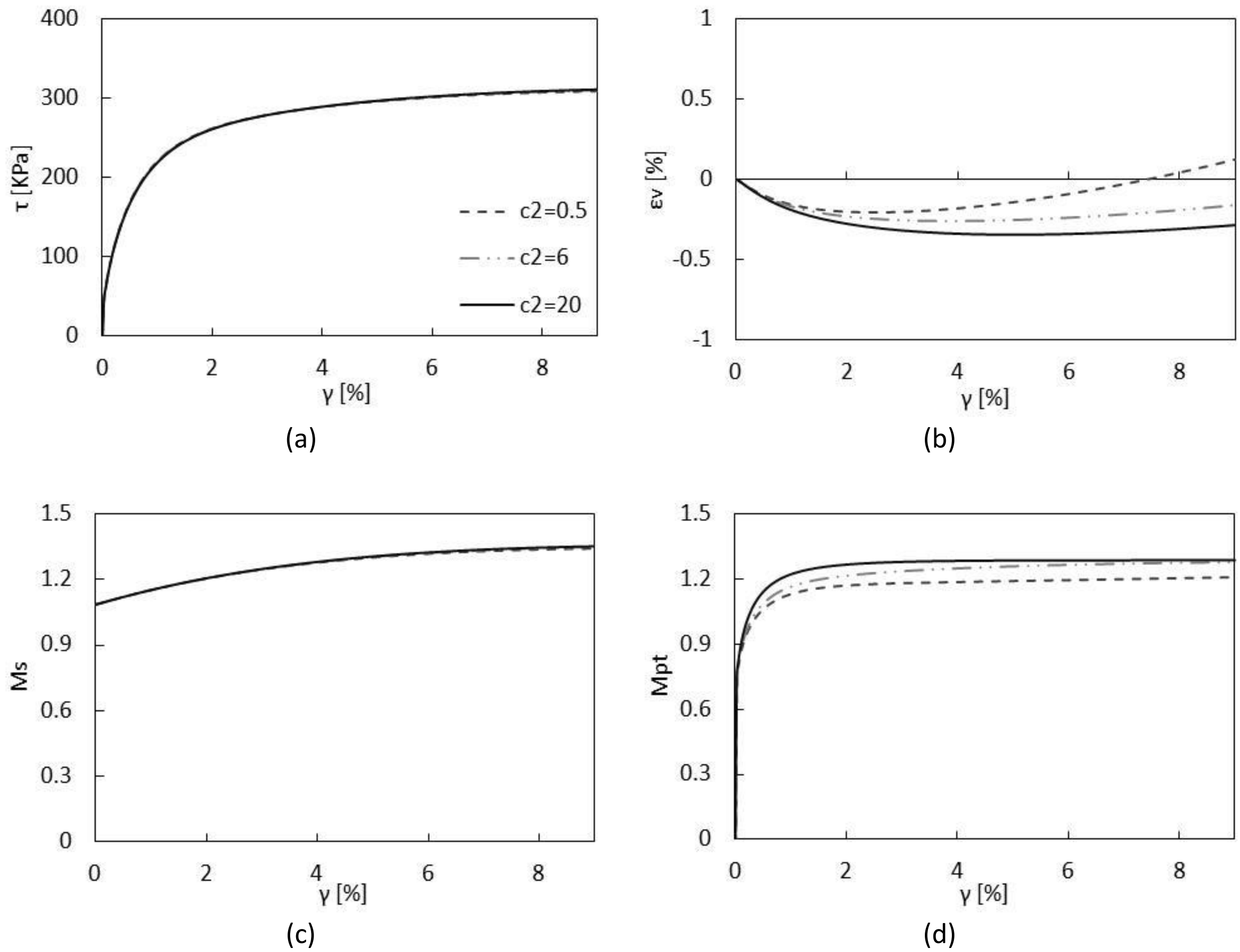

Figure 3.5: (a) Influence of the exponent c_2 in a drained monotonic shear test in terms of (a) shear stress, (b) volumetric strain, (c) boundary line Ms and (d) phase transformation line with shear strain for c_1 constant.

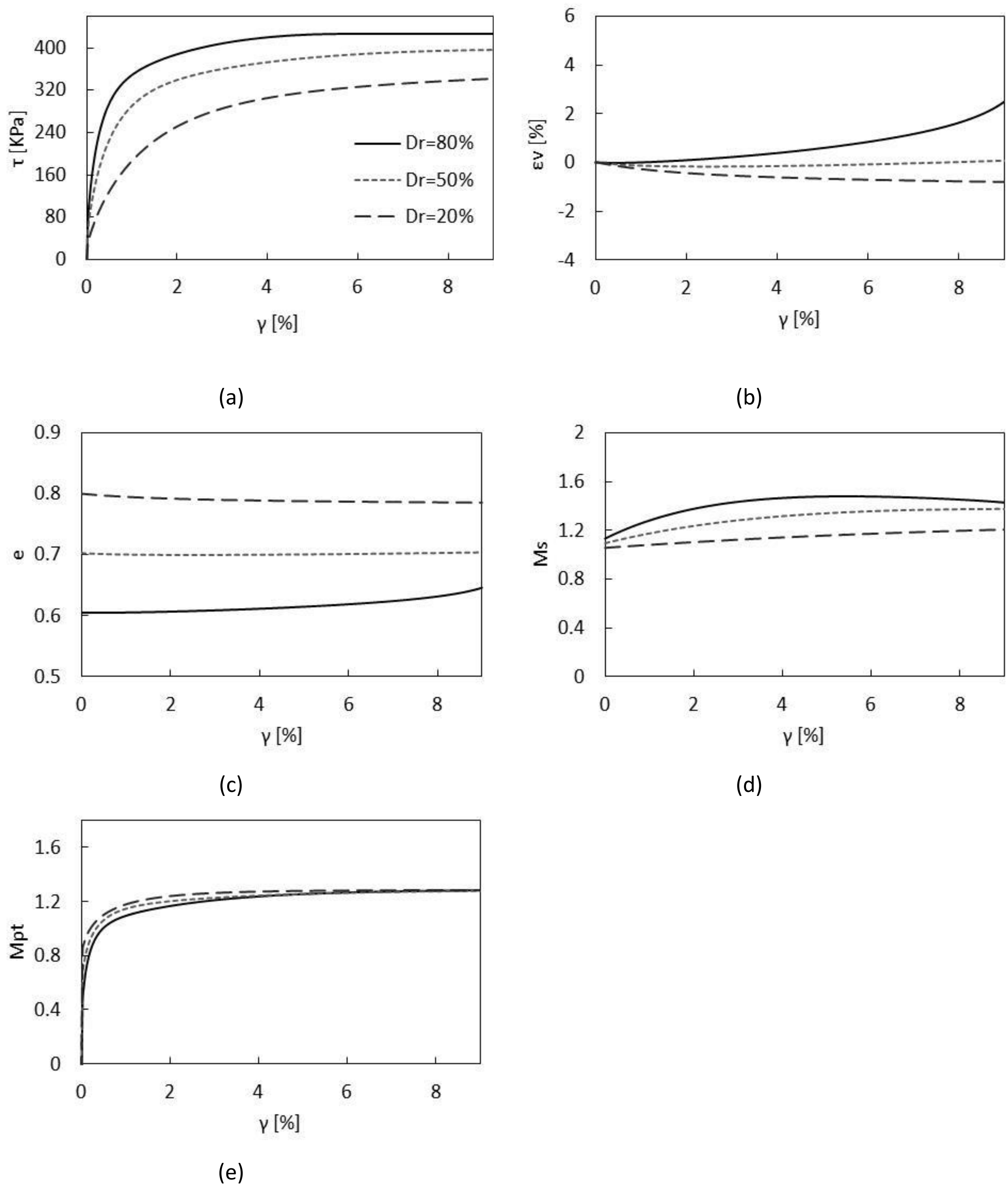

Figure 3.6: (a) Shear stress, (b) volumetric strain, (c) void ratio, (d) boundary line Ms and (e) phase transformation line Mpt for a monotonic shear test for three relative densities Dr=20%, Dr-50% and Dr=80% for mean effective stress p=500KPa.

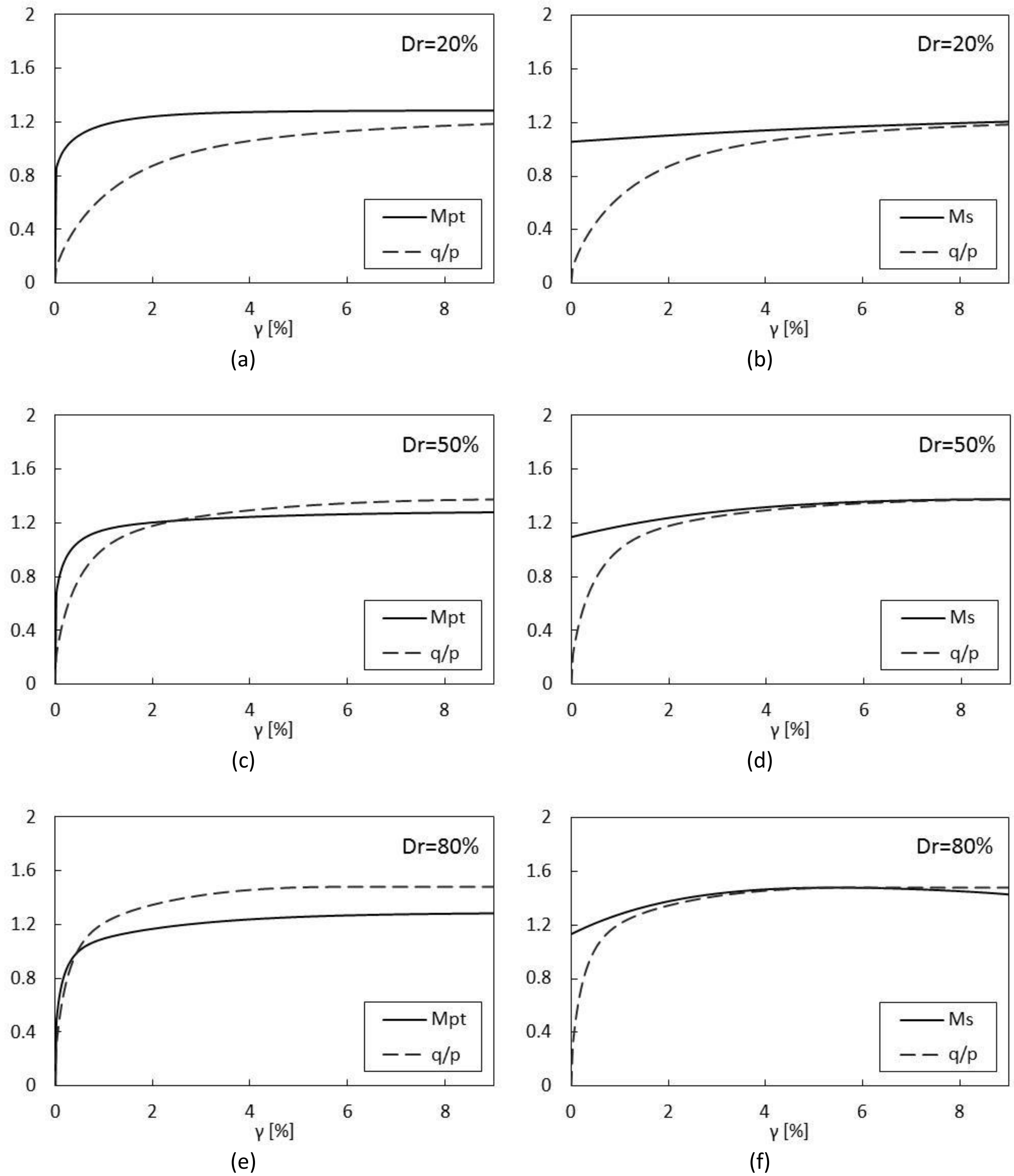

Figure 3.7: (a) , (c), (e) Evolution of phase transformation line Mpt vs the evolution of the stress state line q/p with shear strain for three relative densities Dr=20%, Dr-50% and Dr=80% for mean effective stress p=500KPa and (b), (d) and (f) Evolution of boundary line Ms vs the evolution of the stress state line q/p with shear strain for three relative densities Dr=20%, Dr-50% and Dr=80% for mean effective stress p=500KPa for a drained monotonic shear test

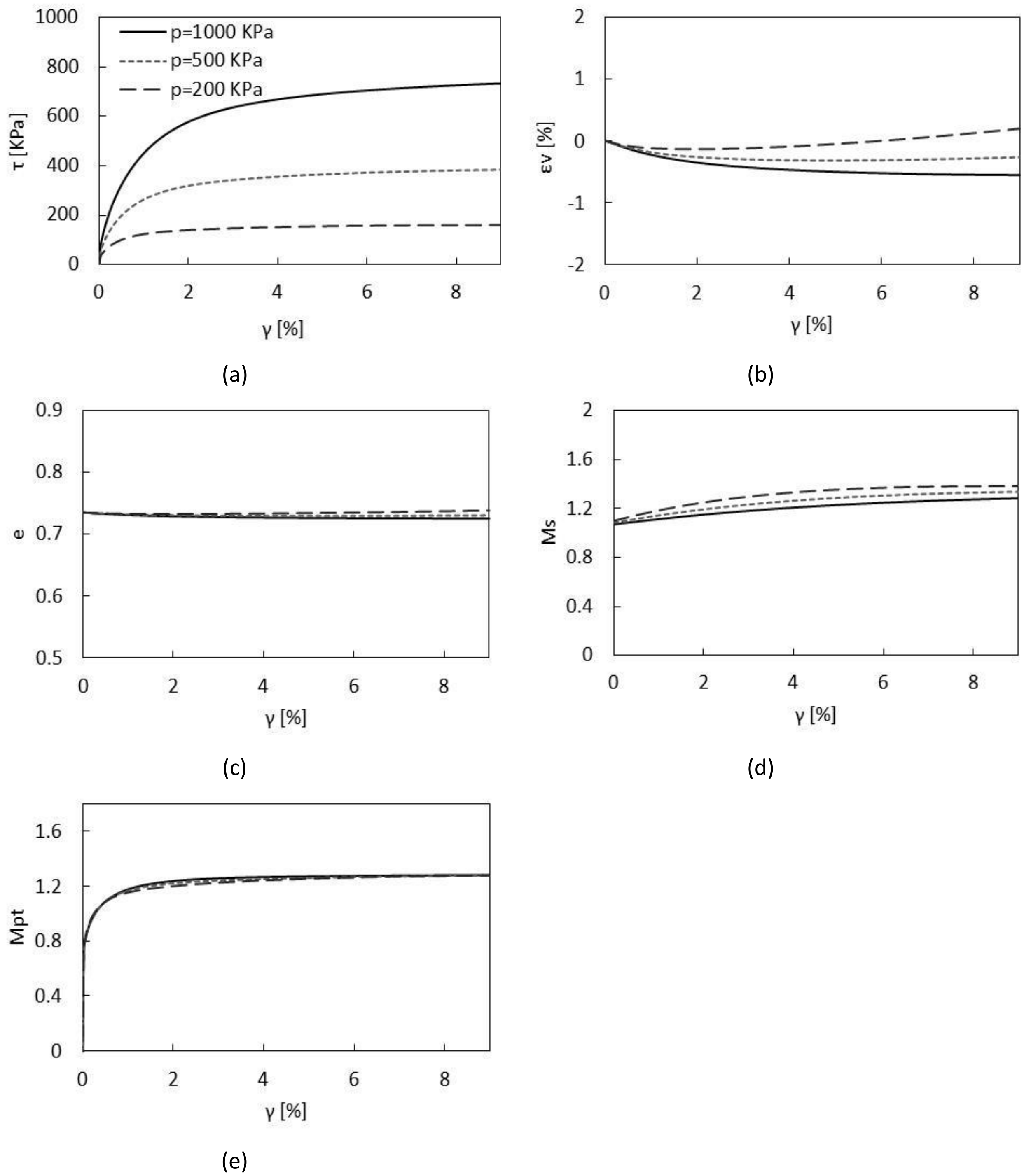

Figure 3.8: (a) Shear stress, (b) volumetric strain, (c) void ratio, (d) boundary line Ms and (e) phase transformation line Mpt for a drained monotonic shear test for three mean effective stresses p=1000KPa, p=500KPa and p=200KPa for a relative density Dr=40%.

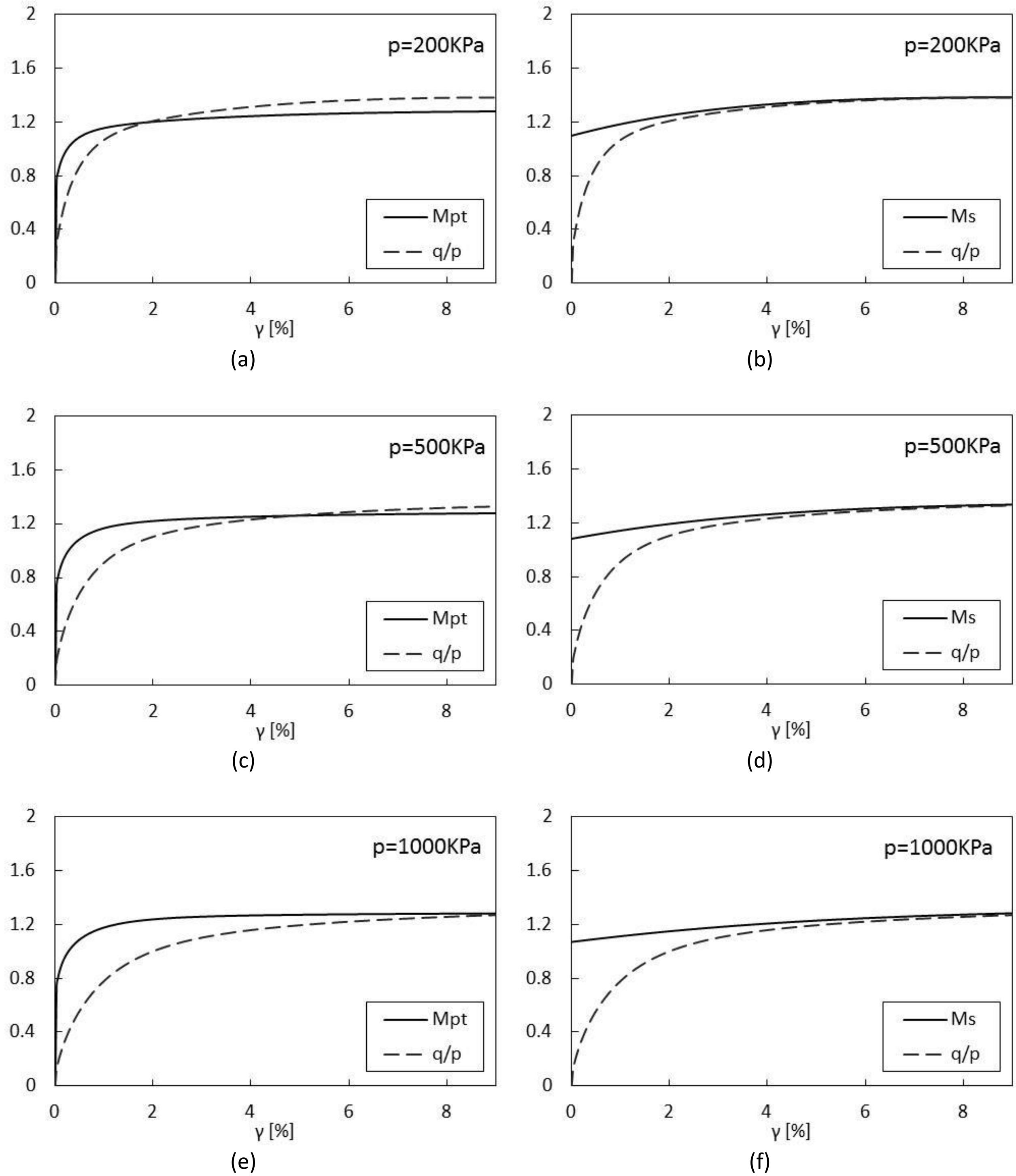

Figure 3.9: (a) , (c), (e) Evolution of phase transformation line Mpt vs the evolution of the stress state line q/p with shear strain for three mean effective stresses p=1000KPa, p=500KPa and p=200KPa for a relative density Dr-40% and (b), (d) and (f) Evolution of boundary line Ms vs the evolution of the stress state line q/p with shear strain three mean effective stresses p=1000KPa, p=500KPa and p=200KPa for a relative density Dr-40% for a drained monotonic shear test

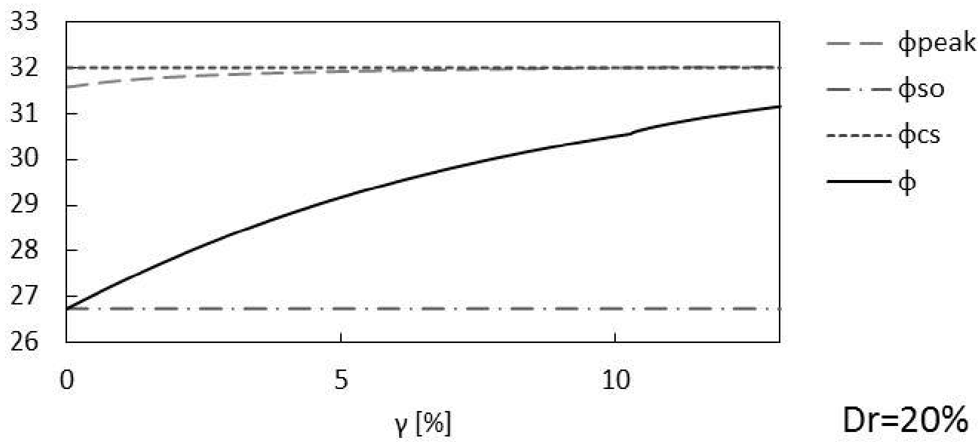

(a)

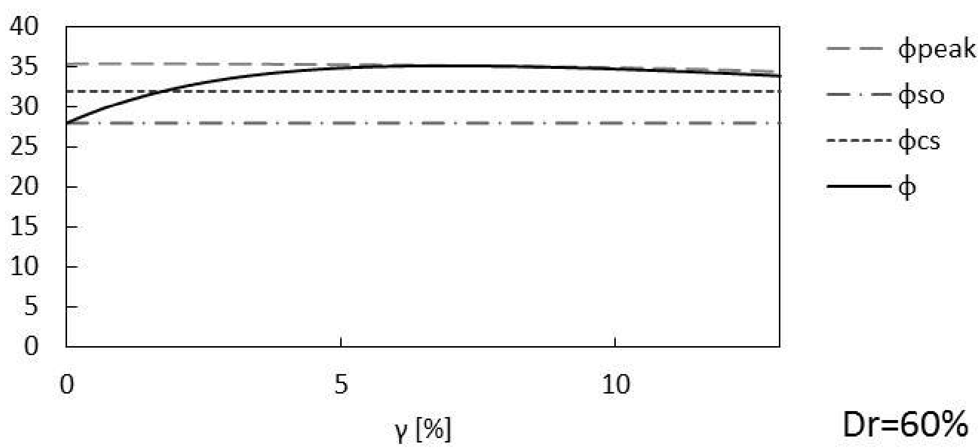

(b)

Figure 3.10: Evolution of friction angle with shear strain for a monotonic drained shear test along with its maximum value φ_{peak}, its initial value φ_{s0} and its critical state value φ_{cs} for (a) initial Dr=20% and mean effective stress p=400KPa and (b) initial Dr=60% and mean effective stress p=400KPa

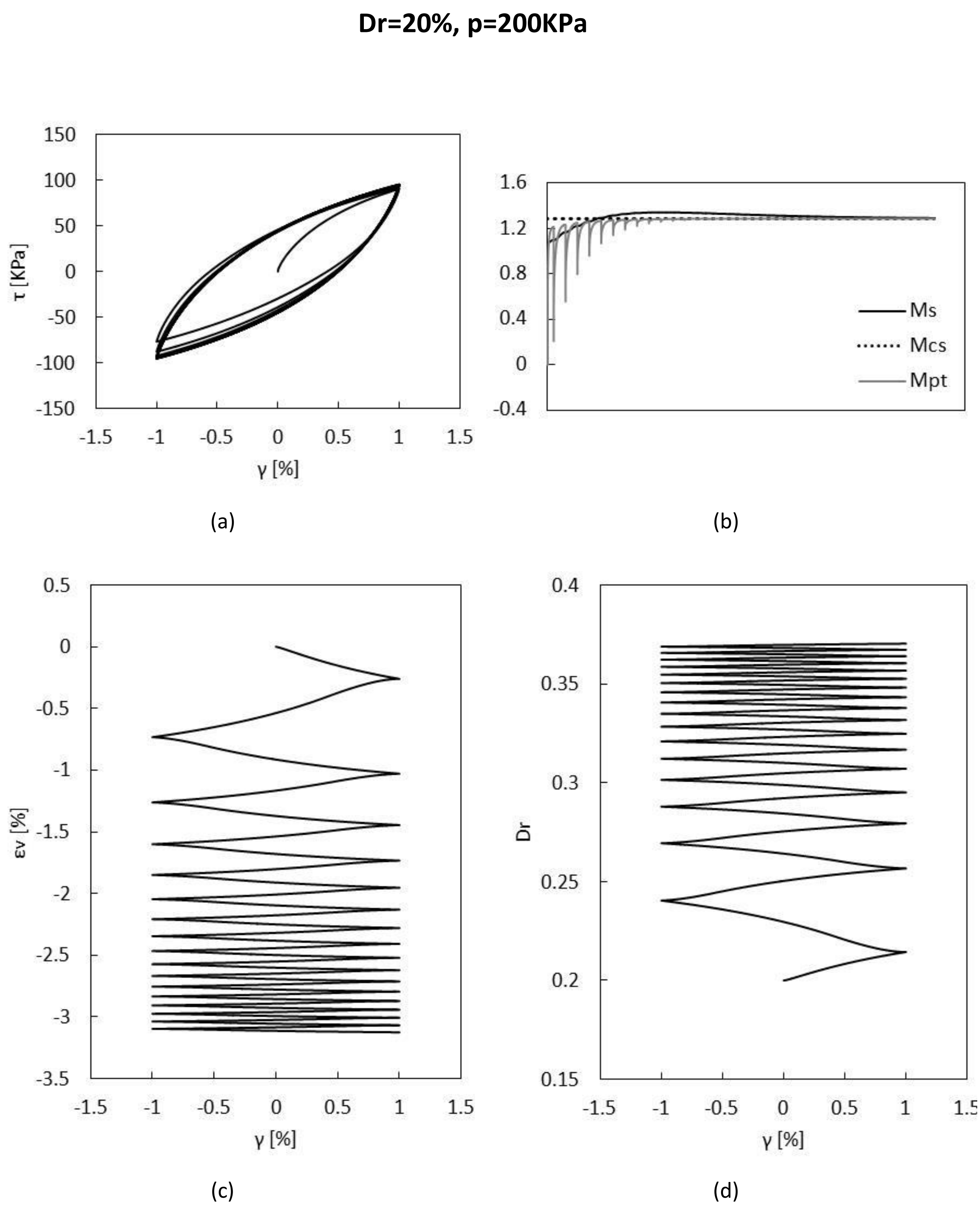

Figure 3.11: (a) Stress-strain hysteretic loops (b) Evolution of M_{pt} and M_s parameters along with their critical state value M_{cs} (c) Volumetric strain and (d) Relative density Dr for initial relative density D_{r0}=20% and mean effective stress p=200KPa for a cyclic drained shear test

Dr=50%, p=200KPa

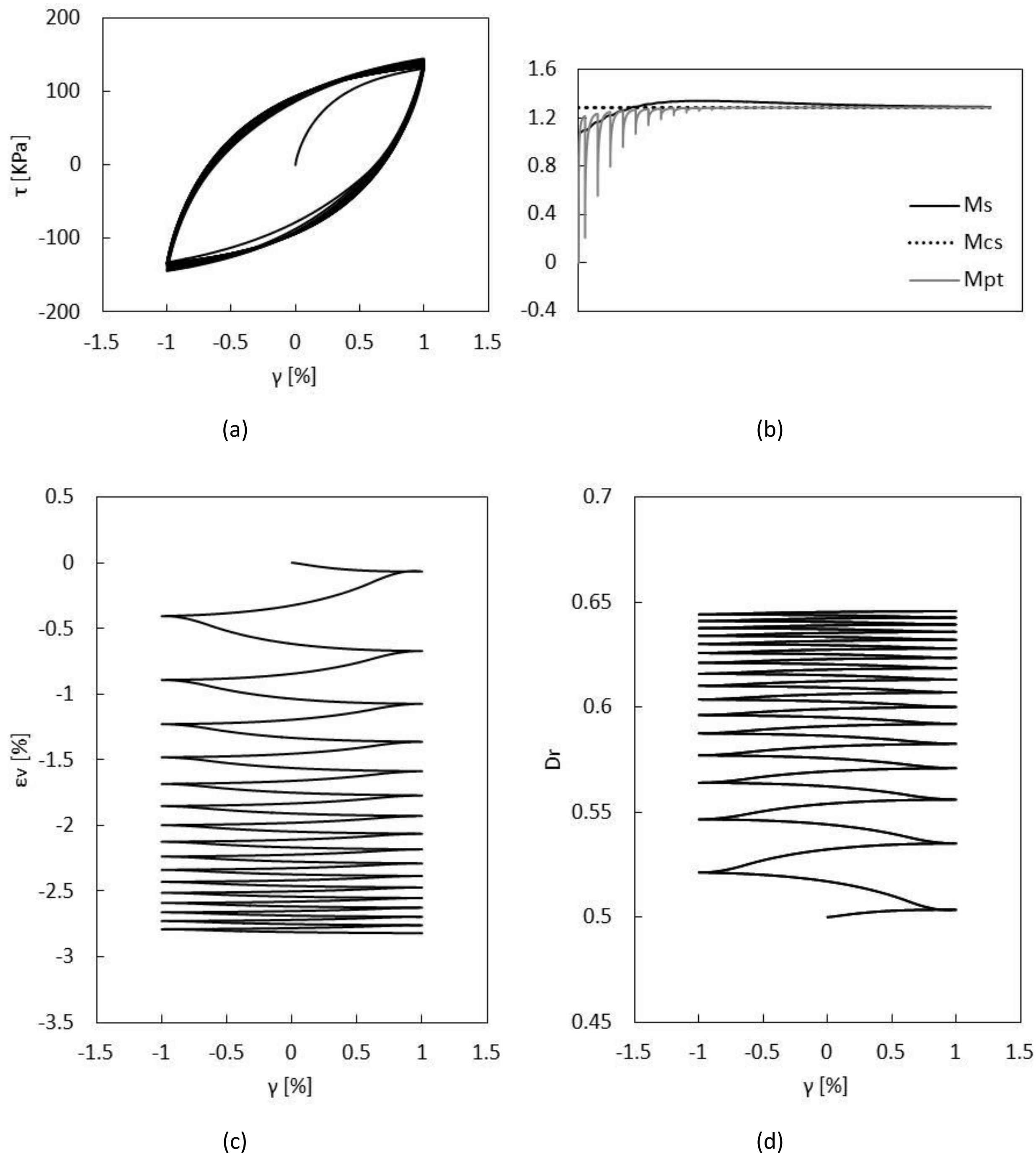

Figure 3.12: (a) Stress-strain hysteretic loops (b) Evolution of M_{pt} and M_s parameters along with their critical state value M_{cs} (c) Volumetric strain and (d) Relative density Dr for initial relative density D_{r0}=50% and mean effective stress p=200KPa for a cyclic drained shear test

Dr=80%, p=200KPa

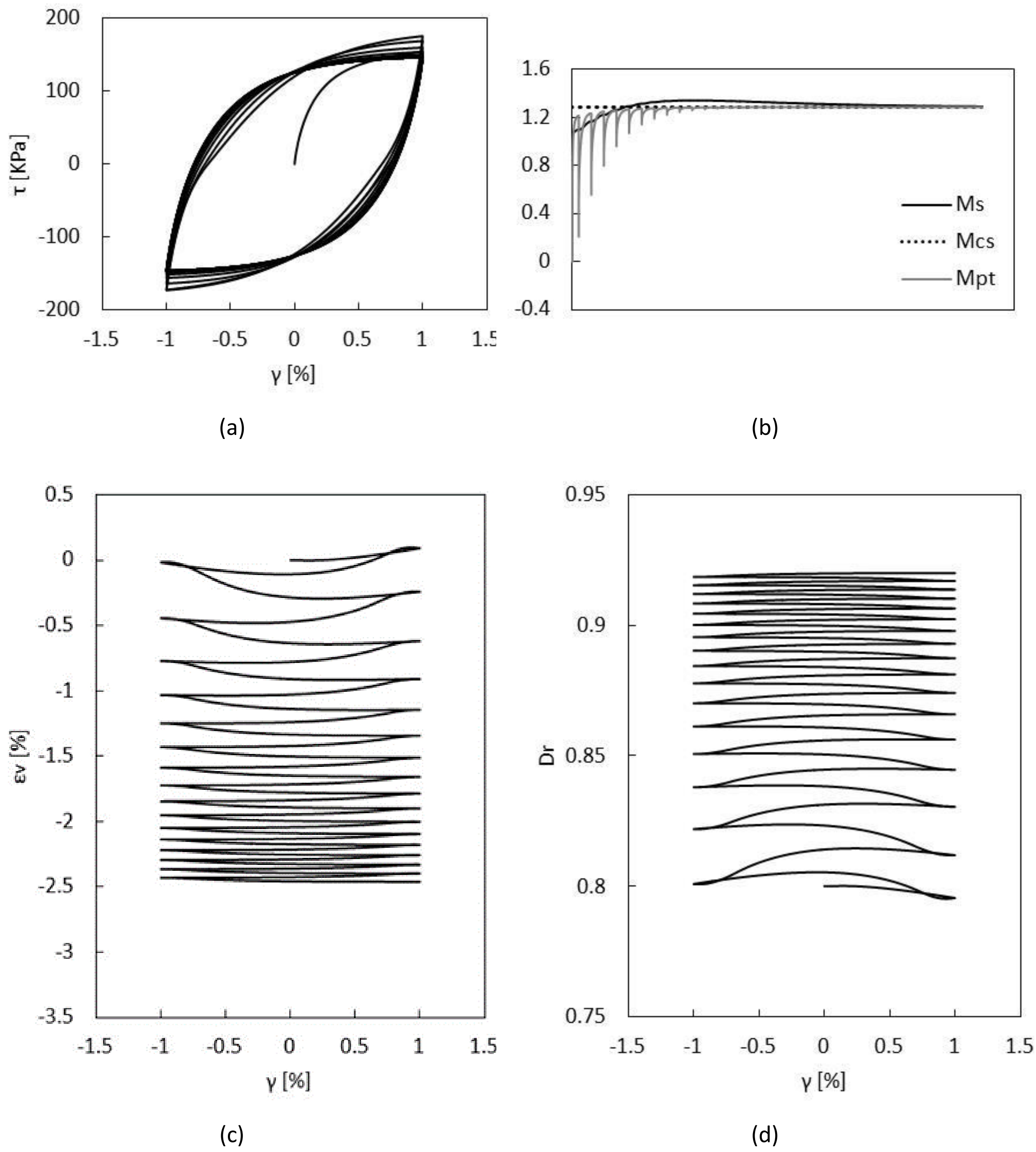

Figure 3.13: (a) Stress-strain hysteretic loops (b) Evolution of M_{pt} and M_s parameters along with their critical state value M_{cs} (c) Volumetric strain and (d) Relative density Dr for initial relative density D_{r0}=80% and mean effective stress p=200KPa for a cyclic drained shear test

Dr=20%, p=500KPa

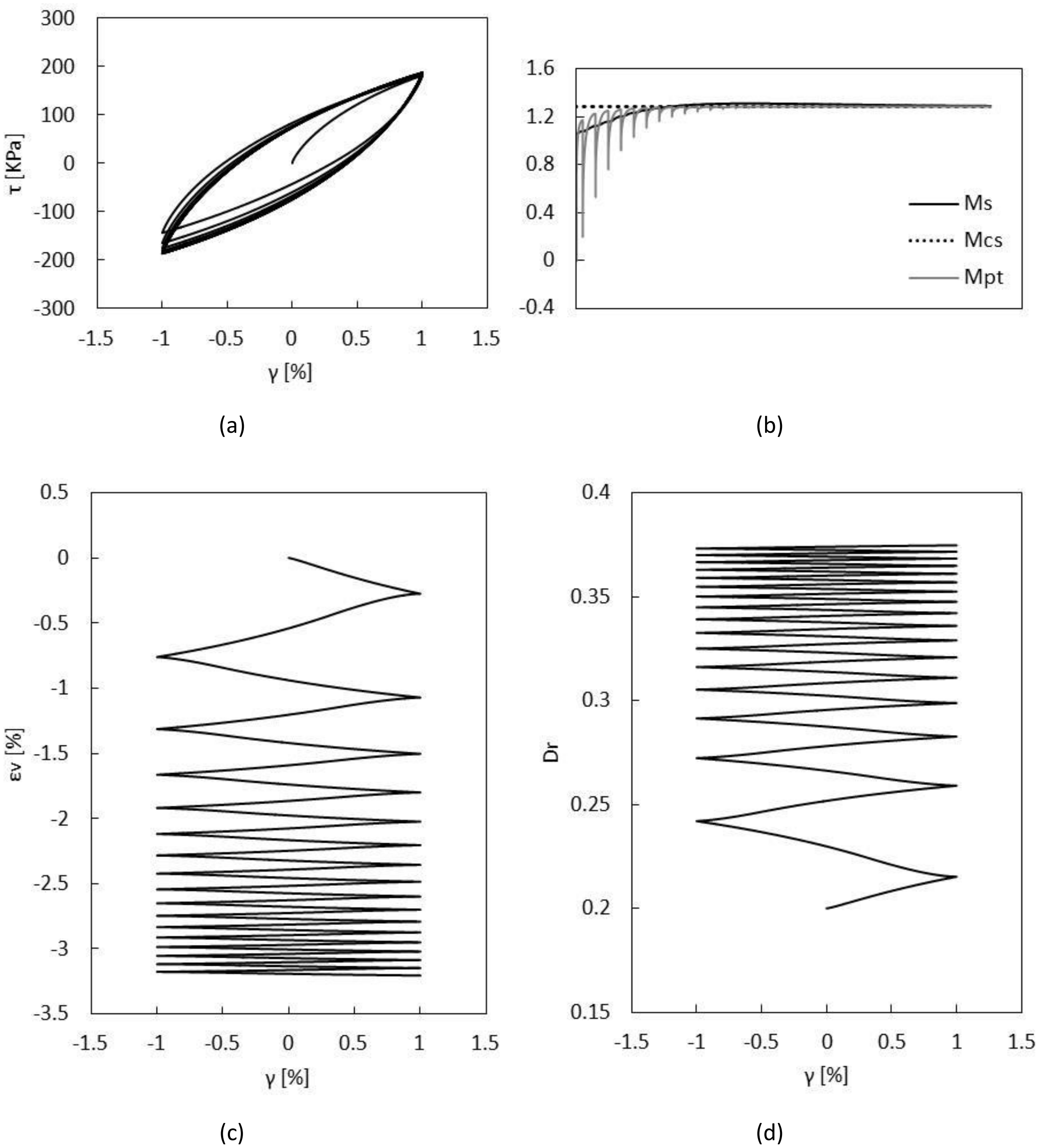

Figure 3.14: (a) Stress-strain hysteretic loops (b) Evolution of M_{pt} and M_s parameters along with their critical state value M_{cs} (c) Volumetric strain and (d) Relative density Dr for initial relative density D_{r0}=20% and mean effective stress p=500KPa for a cyclic drained shear test

Dr=50%, p=500KPa

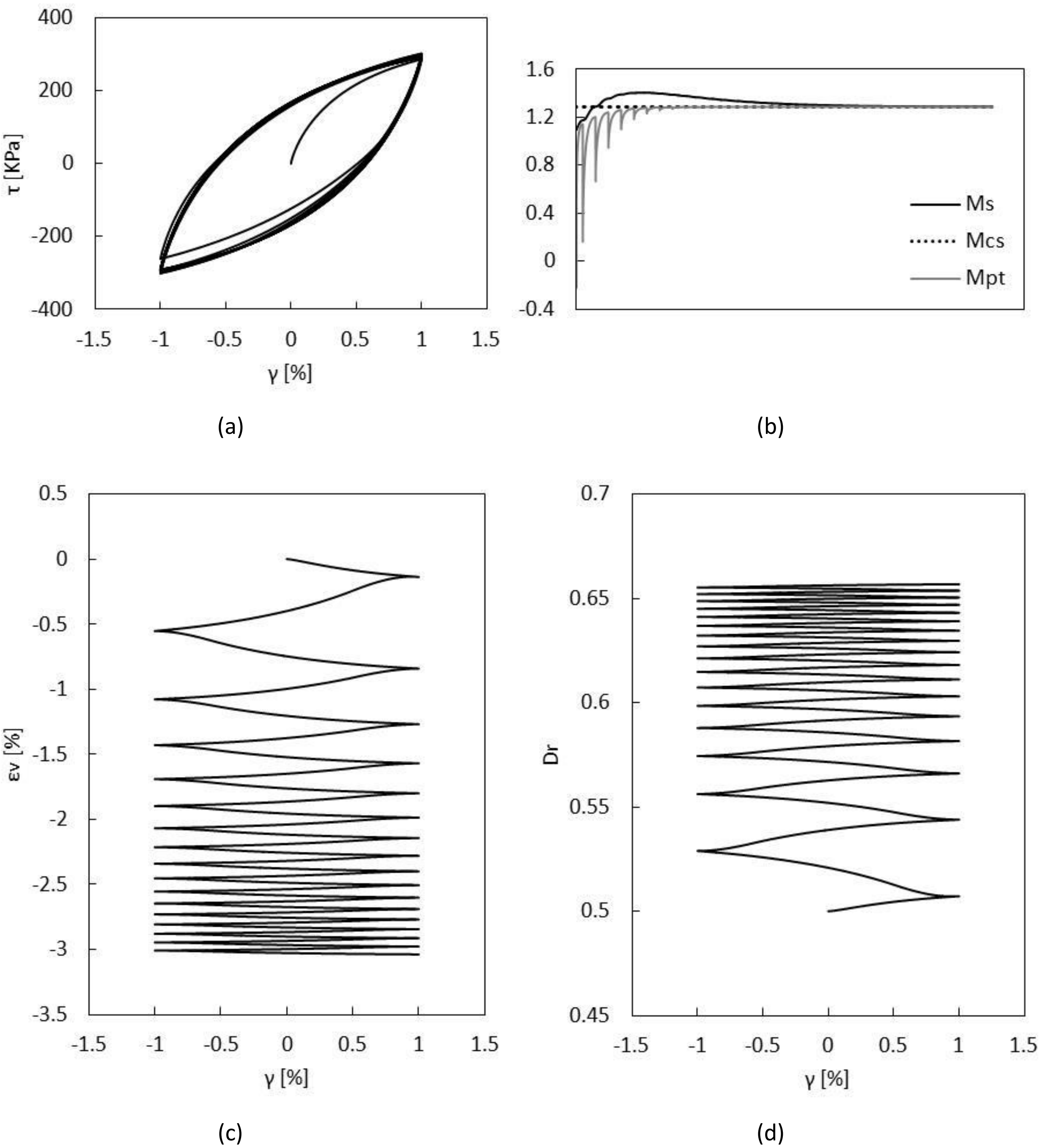

Figure 3.15: (a) Stress-strain hysteretic loops (b) Evolution of M_{pt} and M_s parameters along with their critical state value M_{cs} (c) Volumetric strain and (d) Relative density Dr for initial relative density D_{r0}=50% and mean effective stress p=500KPa for a cyclic drained shear test

Dr=80%, p=500KPa

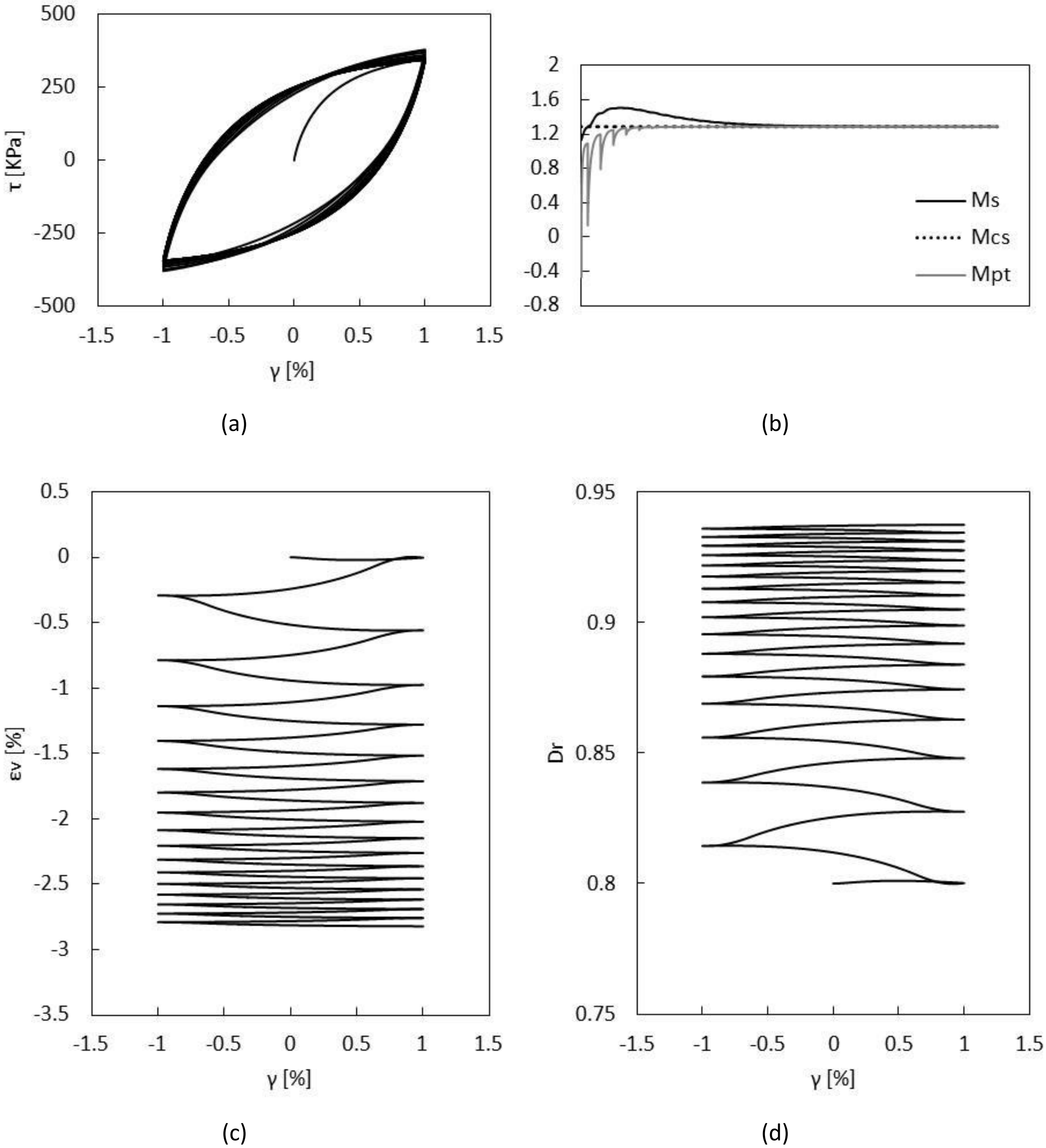

Figure 3.16: (a) Stress-strain hysteretic loops (b) Evolution of M_{pt} and M_s parameters along with their critical state value M_{cs} (c) Volumetric strain and (d) Relative density Dr for initial relative density D_{r0}=80% and mean effective stress p=500KPa for a cyclic drained shear test

Dr=20%, p=1000KPa

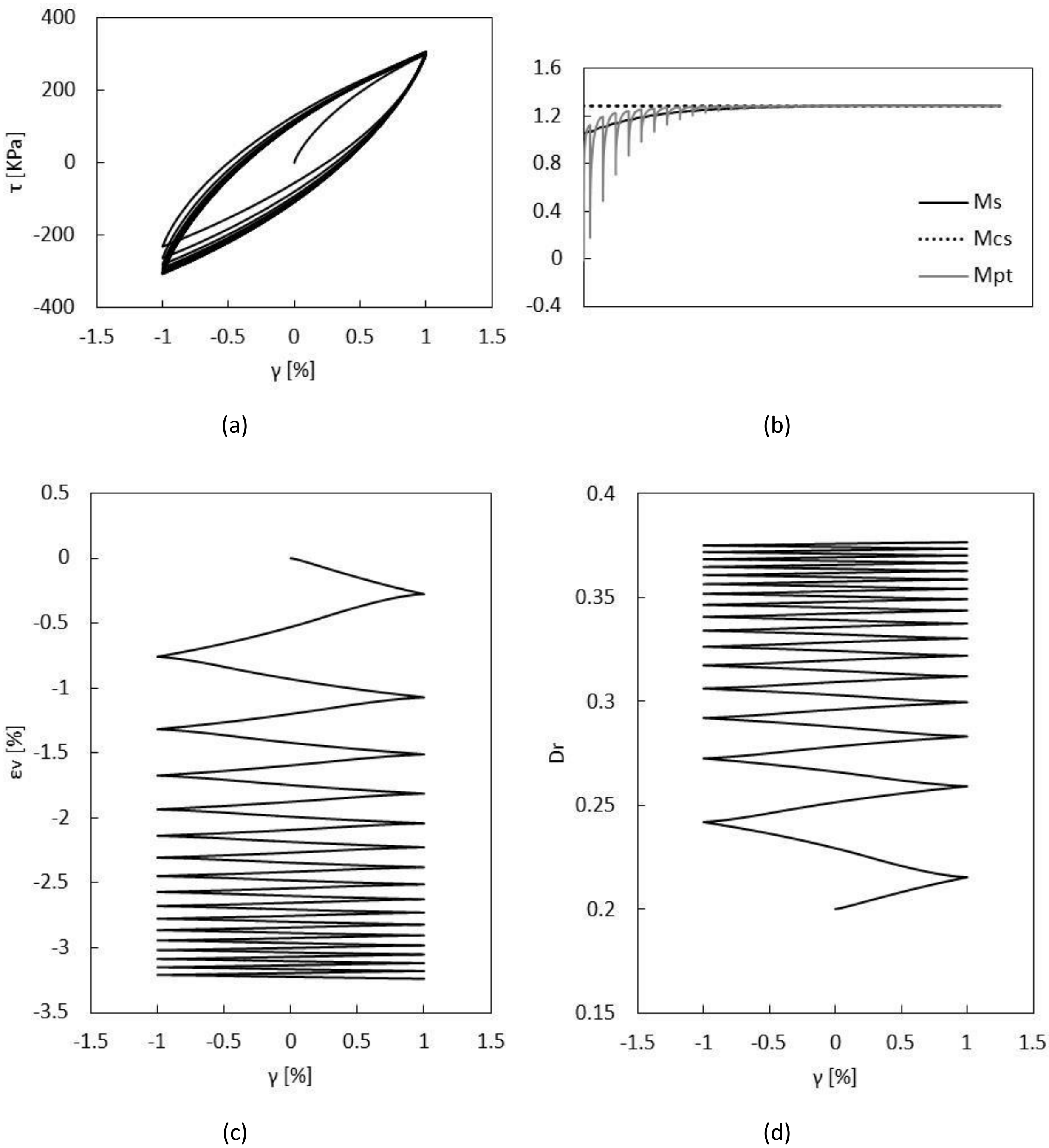

Figure 3.17: (a) Stress-strain hysteretic loops (b) Evolution of M_{pt} and M_s parameters along with their critical state value M_{cs} (c) Volumetric strain and (d) Relative density Dr for initial relative density D_{r0}=20% and mean effective stress p=1000KPa for a cyclic drained shear test

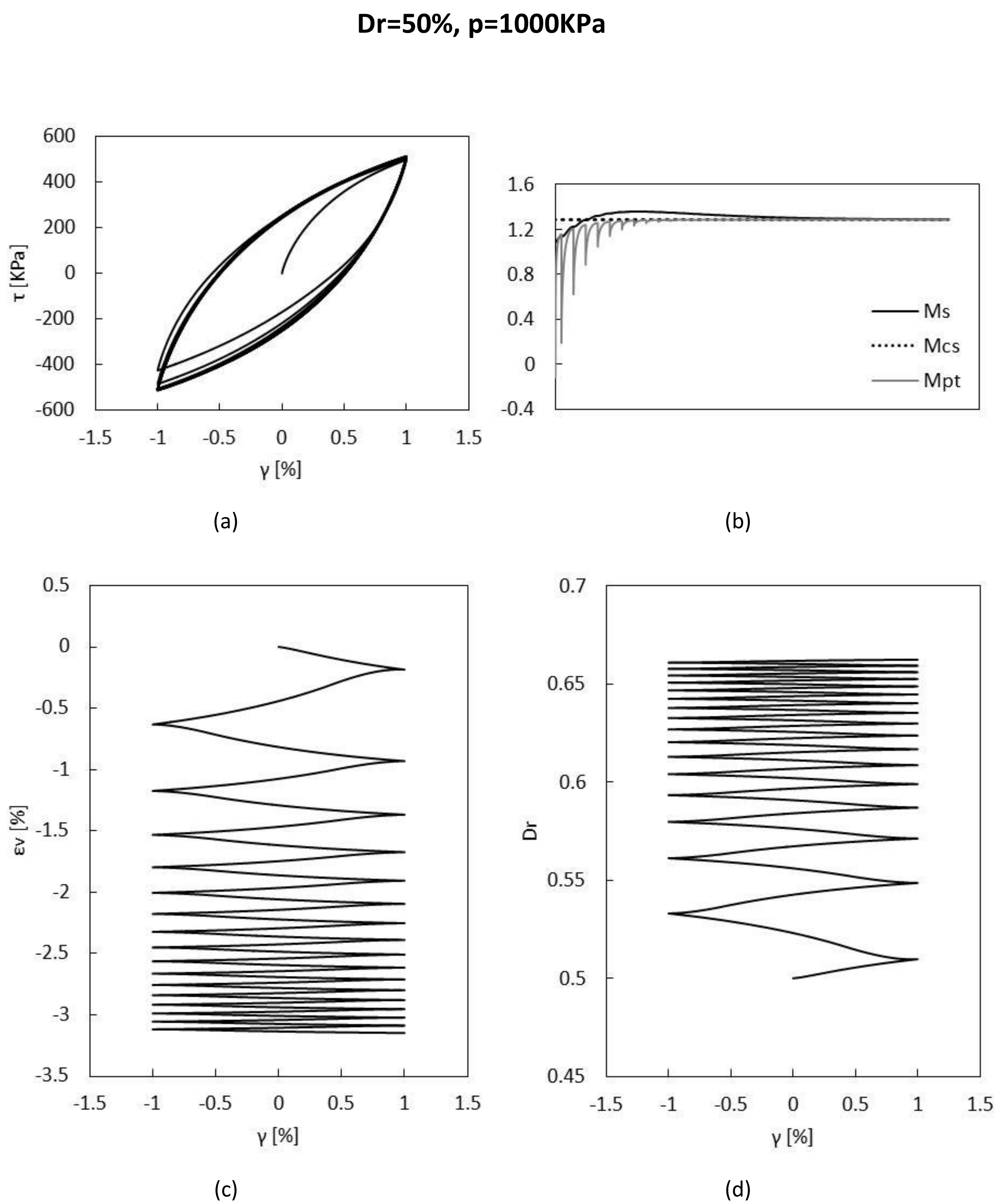

Figure 3.18: (a) Stress-strain hysteretic loops (b) Evolution of M_{pt} and M_s parameters along with their critical state value M_{cs} (c) Volumetric strain and (d) Relative density Dr for initial relative density D_{r0}=50% and mean effective stress p=1000KPa for a cyclic drained shear test

Dr=80%, p=1000KPa

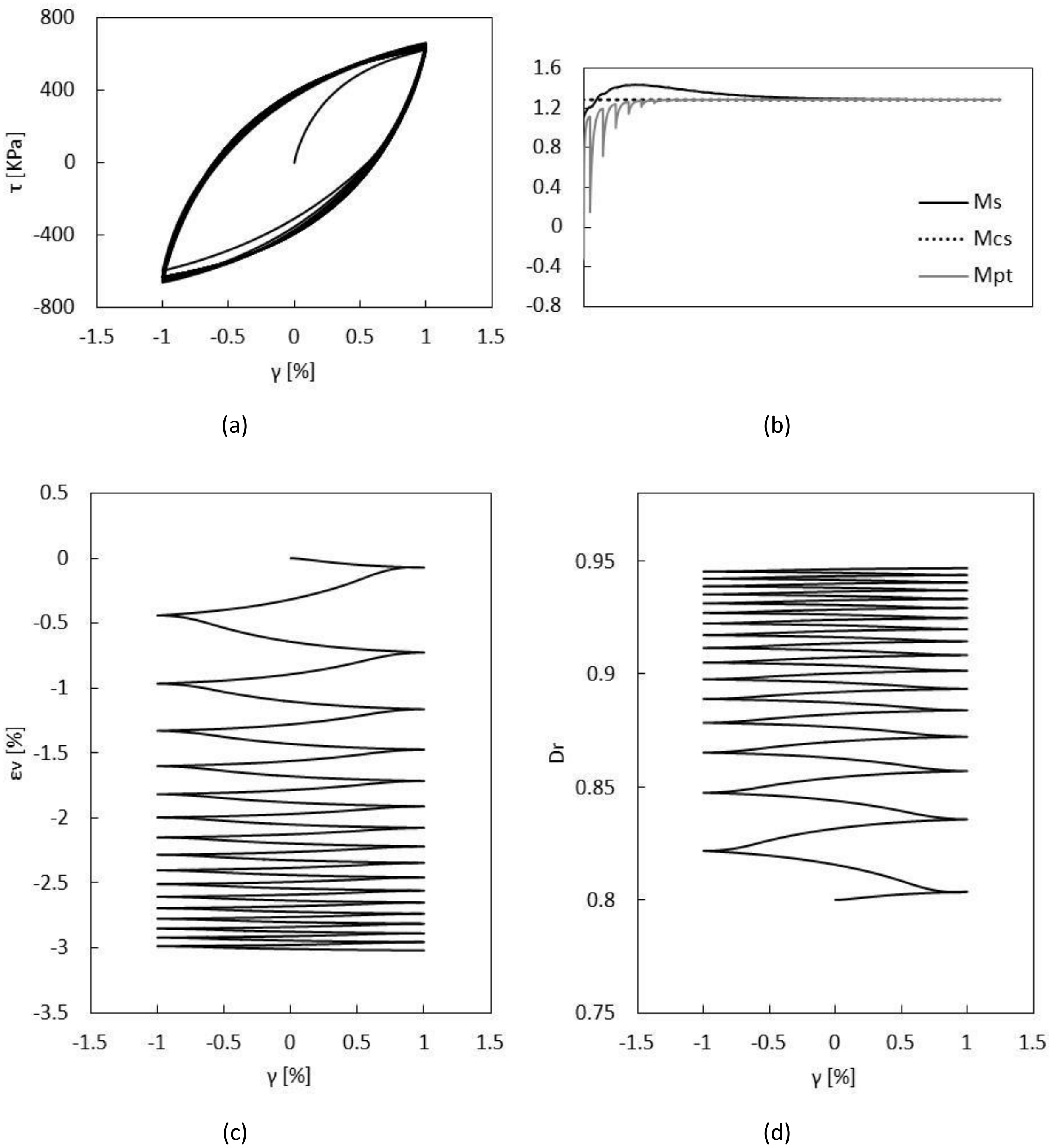

Figure 3.19: (a) Stress-strain hysteretic loops (b) Evolution of M_{pt} and M_s parameters along with their critical state value M_{cs} (c) Volumetric strain and (d) Relative density Dr for initial relative density D_{r0}=80% and mean effective stress p=1000KPa for a cyclic drained shear test

Chapter 3
Model parameters calibration against literature curves

3.1 Laboratory and in situ tests

In order to calibrate Viscoelastic and hysteretic models it is necessary to define the initial shear modulus. This is accomplished through:

- laboratory tests
- in situ tests
- empirical relationships available in literature

Resonance tests are representative of the first category. Through resonance tests the initial shear modulus (which is defined as the initial shear modulus in small strains, $\gamma \leq 10^{-5}$) can be calculated, as well as the hysteretic damping ratios and the secant shear modulus as a function of the strain amplitude. The reliability of each one of the types of resonance tests in defining the initial shear modulus is associated with the soil specimen quality. An alternative laboratory test (which is interesting but not widespread) is the one that uses piezoelectric sensors (transmitter and receiver) in appropriate positions around the specimen. The estimation of *Gmax* is accomplished through the measurement of the arrival time of the shear wave in the receiver. The main drawback of this test is that it does not provide any information about the developed shear strains.

Crosshole and downhole tests are the best in situ geotechnical tests in order to calculate the shear wave propagation velocity. (through soil) in small strains and therefore the initial shear modulus.

It is well known that in large strains cyclic soil response can not be accurately described with the use of only two parameters (*Gsec* and ξ). The knowledge of the hysteretic shear stress – strain relationship is a prerequisite. Its approach is achieved in the laboratory through the conduction of cyclic loading tests. Through these tests one can define the monotonic loading curve and the loading – unloading – reloading rule that define the calibration of a hysteretic model. The most remarkable cyclic tests are:

- the triaxial test
- the simple shear test
- the torsional test

The applicability if the aforementioned tests is related to the initial loading conditions of the soil that we aim to analyze its dynamic response, as well as to the deformation due to the imposed loading. Thus, the cyclic simple shear test for example, is one of the most representative for modeling of the behavior of soil subjected to seismic loading, but only when soil – structure interaction is absent. The cyclic response of a soil element close to a pile subjected to an axial oscillation, is correctly approached through a simple shear test. On the contrary, the response of the same soil element is better described through a triaxial test when the pile oscillates horizontally.

3.2 Shear modulus and damping curves

Model calibration through the hysteretic loops extracted from laboratory tests is not usually implemented, since laboratory data are either not enough for the description of the soil characteristics, or they are not adequate. Empirical relationships for the shear modulus and the hysteretic damping ratio consist an alternative way for calibration.

Shear Modulus

Laboratory tests have shown that soil stiffness is influenced by cyclic amplitude, void ratio, mean principal effective stress, plasticity index, over – consolidation ratio and number of loading cycles. The secant shear modulus of an element of soil varies with cyclic shear strain amplitude. At low strain amplitudes, the secant shear modulus is high, but it decreases as the strain amplitude increases. The locus of points corresponding to the tips of hysteresis loops of various cyclic strain amplitudes is called a *backbone* (or *skeleton*) curve (Fig. 3.1a); its slope at the origin (zero cyclic strain amplitude) represents the largest value of the shear modulus, G_{max}. At greater cyclic strain amplitudes, the modulus ratio G_{sec} / G_{max} drops to values less than 1. Characterization of the stiffness of an element of soil therefore requires consideration of both G_{max} and the manner in which the modulus ratio G / G_{max} varies with cyclic strain amplitude and other parameters. The variation of the modulus ratio with shear strain is described graphically by a *modulus reduction curve* (Fig. 3.1b). The modulus reduction curve presents the same information as the backbone curve; either one can be determined from the other.

Maximum Shear Modulus, Gmax

Since most seismic geophysical tests induce shear strains lower than about $3x10^{-4}$ %, the measured shear wave velocities can be used to compute G_{max} as :

$$G_{max} = \rho \, v_s{}^2$$

The use of measured shear wave velocities is generally the most reliable means of evaluating the in situ value of G_{max} for a particular soil deposit, and seismic geophysical tests are commonly used for that purpose. Care must be taken in the interpretation of shear wave velocity, particularly at sites with anisotropic stress conditions, which can cause measured shear wave velocities to vary with the direction of wave propagation and particle movement (Roesler 1979; Stokoe et al., 1985; Yan and Byrne, 1991).

When shear wave velocity measurements are not available, G_{max} can be estimated in several different ways. Laboratory test data suggest that the maximum shear modulus can be expressed as

$$G_{max} = 625\, F(e)\, (OCR)^k p_a{}^{1-n} (\sigma'_m)^n$$

where *F(e)* is a function of the void ratio, OCR the over consolidation ratio, *k* an over consolidation ratio exponent (Table 3.1), σ'_m the mean principal effective stress, n a stress exponent, and p_a is atmospheric pressure in the same units as σ'_m and G_{max}. Hardin (1978) proposed that $F(e)=1/(0.3+0.7e^2)$, while Jamiolkowski et al. (1991) suggested that $F(e)= 1/e^{1/3}$. The stress exponent is often taken as n=0.5 but can be computed for individual soils from the results of laboratory tests at different effective confining pressures. It should be apparent that G_{max}, p_a, and σ_m' must be expressed in the same units. The above equation can also be used to adjust measured G_{max} values to represent conditions that are different (e.g., increased effective stresses) from those at which the measurements were made.

Other empirical relationships have been proposed for specific soil types. The maximum shear modulus of sand, for example, is often estimated as:

$$G_{max} = 1000K_{2,max}(\sigma_m')^{0.5}$$

Where $K_{2,max}$ is determined from the void ratio or relative density (Table 3.2) and σ_m' is in lb/ft^2 (Seed and Idris, 1970). Field tests have consistently shown that shear wave velocities of gravels are significantly higher than those of sands, indicating that G_{max} of gravel is higher than that of sand. $K_{2,max}$ values for gravels are typically in the range 80 to 180 (Seed et al., 1984). For fine – grained soils, preliminary estimates of the maximum shear modulus can be obtained from plasticity index, overconsolidation ratio and undrained strength (Table 3.3). Because undrained strengths are highly variable and because shear moduli and undrained strengths vary differently= with effective confining pressure, these results must be used carefully.

The maximum shear modulus can also be estimated from in situ test parameters. A number of empirical relationships between G_{max} and various in situ test parameters have been developed. The inherent difficulty of correlating a small strain parameter such as G_{max} with penetration parameters that relate to much larger strains is evident from the scatter in the data on which they are based and from the variability of the results obtained by different investigators. As such, the usefulness of such correlations is currently limited to preliminary estimates of G_{max}.

However, the application of in situ testing to geotechnical earthquake engineering problems is only in its early stages, and significant advances can be expected as additional data become available.

Evaluation of shear modulus can be complicated by rate and time effects (Anderson and Woods, 1975, 1976; Anderson and Stokoe, 1978; Isenhower and Stokoe, 1981). Rate effects can cause G_{max} to increase with increasing soil plasticity. Rate effects can be significant when comparing G_{max} values obtained from field shear wave velocity measurements (usually made with the use of impulsive disturbances which produce relatively high frequencies) with values obtained from laboratory tests. The shear wave velocity and hence Gmax, increases approximately linearly with the logarithm of time past the end of primary consolidation to an extent that cannot be attributed solely to the effects of secondary compression. The change of stiffness with time can be described by

$$\Delta G_{max} = N_G(G_{max})_{1000}$$

where ΔG_{max} is the increase in G_{max} over one log cycle of time and $(G_{max})_{1000}$ is the value of G_{max} at the time of 1000 min past the end of primary consolidation. N_G increases with increasing plasticity index PI and decreases with increasing OCR (Kokushu et al., 1982). For normally consolidated clays, N_G can be estimated from the relationship

$$N_G \approx 0.027\sqrt{PI}$$

Anderson and Woods (1975) showed that some of the discrepancy between G_{max} values from field and laboratory tests could be explained by time effects, and that N_G could be used to correct the G_{max} values from laboratory tests to better represent6 actual in situ conditions.

Modulus reduction G/Gmax

In the early years of geotechnical earthquake engineering, the modulus reduction behaviors of coarse – and fine – grained soils were treated separately (e.g., Seed and Idriss, 1970). Recent research, however, has revealed a gradual transition between the modulus reduction behavior of nonplastic coarse – grained soil and plastic fine – grained soil.

Zen et al., (1978) and Kokushu et al., (1982) first noted the influence of soil plasticity on the shape of the modulus reduction curve; the shear modulus of highly plastic soils was observed to degrade more slowly with shear strain than did low – plasticity soils. After reviewing experimental results from a broad range of materials, Dobry and Vucetic (1987) and Sun et al. (1988) concluded that the shape of the modulus reduction curve is influenced more by the plasticity index than by the void ratio and presented curves of the type shown in Fig. 3.2.a. These curves show that the linear cyclic threshold shear strain, γ_{tl}, is greater for highly plastic soils than for soils of low plasticity. This characteristic is extremely important; It can strongly influence the manner in which a soil deposit will amplify or attenuate earthquake motions. The PI=0 modulus reduction curve from Fig. 3.2.a. is very similar to the average modulus reduction curve that was commonly used for sands (Seed and Idriss, 1970) when coarse – and fine – grained soils were treated separately. This similarity suggests that the modulus reduction curves of Fig. 3.2.a. may be applicable to both fine – and coarse – grained soils (this conclusion should be confirmed for individual coarse – grained soils, particularly those that could exhibit aging or cementation effects). The difficulty of testing very large specimens has precluded the widespread testing of gravelly soils in the laboratory, but available test data indicate that the average modulus reduction curve for gravel is similar to, though slightly flatter than, that of sand (Seed et al., 1986; Yasuda and Matsumoto, 1993).

Modulus redaction behavior is also influenced by effective confining pressures, particularly for soils of low plasticity (Iwasaki et al., 1978; Kokoshu, 1980). The linear cyclic threshold shear strain γ_{lt} , is greater at high effective confining pressures than at low effective confining pressures. The effect of effective confining pressure and plasticity index on modulus reduction behavior were combined by Ishibashi and Zhang (1993) in the form

$$\frac{G}{G_{max}} = K(\gamma, PI)(\sigma'_m)^{m(\gamma PI)-m_0}$$

where

$$K(\gamma, PI) = 0.5\left\{1 + tanh\left[ln\left(\frac{0.000102 + n(PI)}{\gamma}\right)^{0.492}\right]\right\}$$

$$m(\gamma, PI) - m_0 = 0.272\left\{1 - tanh\left[ln\left(\frac{0.000556}{\gamma}\right)^{0.4}\right]\right\}\exp(-0.0145PI^{1.3})$$

$$n(PI) = \begin{cases} 0.0 & \text{for } PI = 0 \\ 3.37x\ 10^{-6}PI^{1.404} & \text{for } 0 < PI \leq 15 \\ 7.0\ x10^{-7}PI^{1.976} & \text{for } 15 < PI \leq 70 \\ 2.7\ x10^{-5}PI^{1.115} & \text{for } PI > 70 \end{cases}$$

The effect of confining pressure on modulus reduction behavior of low – and high – plasticity soils is illustrated in Fig. 3.3 a.

In 2001, Darendeli et al. developed a new family of normalized modulus reduction and material damping curves. Their study focused on developing the empirical framework that can be used to generate normalized modulus reduction and material damping curves. This framework is composed of simple equations, which incorporate the key parameters that control nonlinear soil behavior. The effects of various parameters (such as confining pressure and soil plasticity) on dynamic soil properties were evaluated and quantified within this framework. The normalized curves for modulus reduction are presented in Figure 3.4.a. for a non plastic soil for various confining pressures.

Damping Ratio

Theoretically, no hysteretic dissipation of energy takes place at strains below the linear cyclic threshold shear strain. Experimental evidence, however, shows that some energy is dissipated even at very low strain levels (the mechanism is not well understood), so the damping ratio is never zero. Above the threshold strain, the breadth of the hysteresis loops exhibited by a cyclically loaded soil increase with increasing cyclic strain amplitude, which indicates that the damping ratio increases with increasing strain amplitude.

Just as modulus reduction behavior is influenced by plasticity characteristics, so is damping behavior (Kokushu et al., 1982);Dobry and Vucetic, 1987; Sun et al., 1988). Damping ratios of highly plastic soils are lower than those of low plasticity soils at the same cyclic strain amplitude (Fig. 3.2.b.). The PI damping curve from Fig. 3.2.b., is nearly identical to the average damping curve that was used for coarse – grained soils when they were treated separately from fine – grained soils. This similarity suggests that the damping curves of Fig. 3.2.b. can be applied for both fine – and coarse – grained soils. The damping behavior of gravel is very similar to that of sand (Seed et al., 1984).

Damping behavior is also influenced by effective confining pressure, particularly for soils of low plasticity. Ishibashi and Zhang (1993) developed an empirical expression for the damping ratio of plastic and non plastic soils (Fig. 3.3.b.). Using the equation for modulus reduction *G/Gmax ,* the damping ratio is given by

$$\xi = 0.333\,\frac{1+\exp(-0.0145PI^{1.3})}{2}\left[0.586\left(\frac{G}{G_{max}}\right)^2 - 1.547\,\frac{G}{G_{max}} + 1\right]$$

Material damping curves published by Darendeli et al., are presented in Figure 3.4.b. for various confining pressures for a non plastic soil (PI=0).

3.3 Calibration procedure

In order to fit the model with the literature shear modulus and damping curves (which were discussed in the previous paragraph) a bunch of parameters are selected for calibration.

As it was mentioned in Cp. 2 , shear modulus is expressed as function of the mean effective stress and the relative soil density using Seed and Idriss Published data and Souliotis and Gerolymos curve fitting, as follows:

$$G_{max} = A * p_a * D_{ro}^{0.6464} * \left(\frac{p}{p_a}\right)^m$$

where A is a constant that controls the initial stiffness. Its influence in the formulation of G_{max} is illustrated in Fig 3.5. and is the first parameter selected for calibration.

Then, the hysteretic parameter η that causes the stiffness degradation, and is a function of s_1 , and s_2 must be assessed. η is activated after the end of the first monotonic (backbone) curve in the unloading – reloading curves and affects the expansion of the hysteretic shear stress – strain loop (Fig. 3.6).

Finally, exponent n which controls the rate of transition from the elastic state to the perfectly plastic one, is the last parameter selected for calibration. High values of n lead to decupling between elasticity and perfect plasticity (Fig. 3.7)

The calibration is then based on matching some established experimental G : γ and ξ : γ curves from the literature. To this end, the Lavenberg–Marquardt optimization procedure is used, available in mathematical code MATLAB. Two published families of G : γ , ξ : γ curves have been utilized: (a) the Vucetic & Dobry curves for sand [11] and (b) the pressure (σ'_0)-dependent curves of Darendeli et al. [12]. The values of the parameters A, s_1, s_2 and n for which curve fitting was obtained, are shown in Table 3.4 for each one of the family curves.

Starting from the Vucetic & Dobry (1991) curves, the results of the calibration are illustrated in Fig. 3.8. The PI=0 curve (which corresponds to sand) is being used herein for a confining pressure of 100 KPa. The agreement between computed and experimental curves is quite satisfactory. Small discrepancies are observed for small strain levels. The corresponding hysteretic shear stress – strain loops are also depicted in Fig. 3.10.

Darendeli et al. [12] recommended a new family of normalized shear modulus and material damping curves, as functions of plasticity index and mean effective stress. Four confining pressures *(σ'_0= 25, 100, 400, 1600 kPa)* are examined herein, for PI=0. Comparison of the predicted with the experimental curves is depicted in Fig 3.9.

Figures

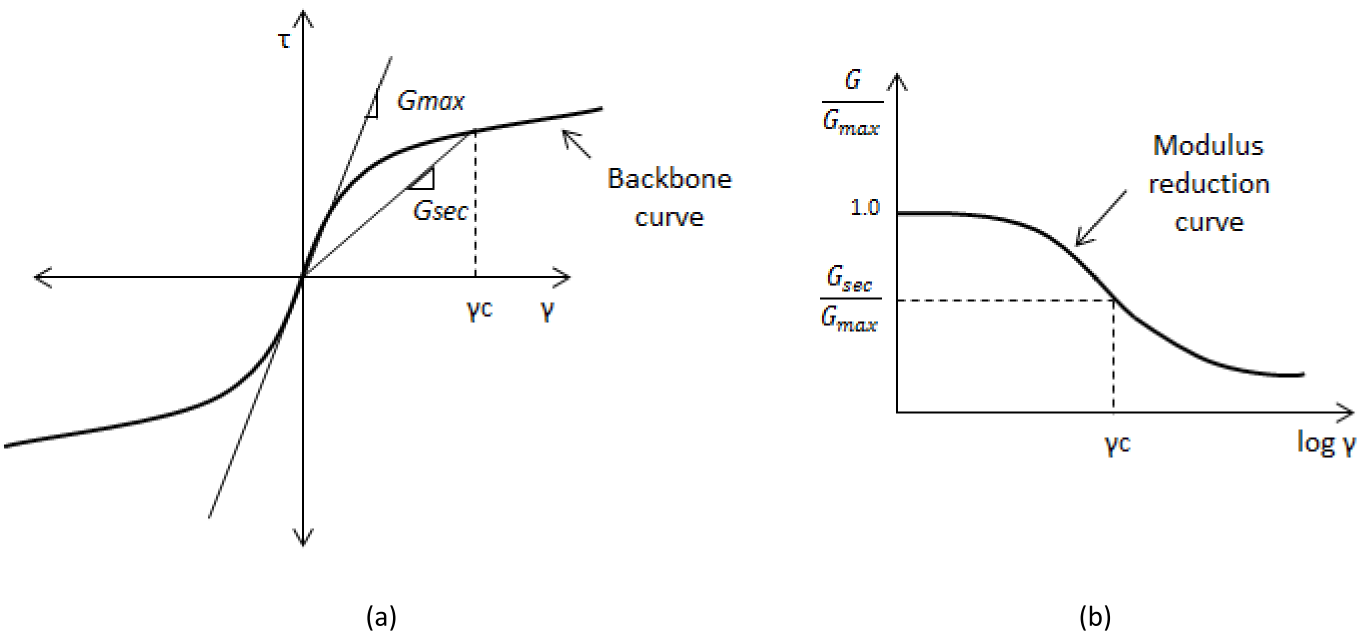

Figure 3.1: Backbone curve showing typical variation of Gsec with shear strain

Plasticity Index	k
0	0.00
20	0.18
40	0.30
60	0.41
80	0.48
≥100	0.50

Table 3.1: Over consolidation Ratio Exponent, k
Source :After Hardin and Drnevich (1972b)

e	$K_{2,max}$	Dr(%)	$K_{2,max}$
0.4	70	30	34
0.5	60	40	40
0.6	51	45	43
0.7	44	60	52
0.8	39	75	59
0.9	34	90	70

Table 3.2: Estimation of K2,max
Source: Adapted from Seed and Idriss (1970)

	Overconsolidation Ratio, OCR		
Plasticity Index	1	2	5
15-20	1100	900	600
20-25	700	600	500
35-45	450	380	300

Table 3.3: Values of Gmax/Su
Source: After Weiler (1988)

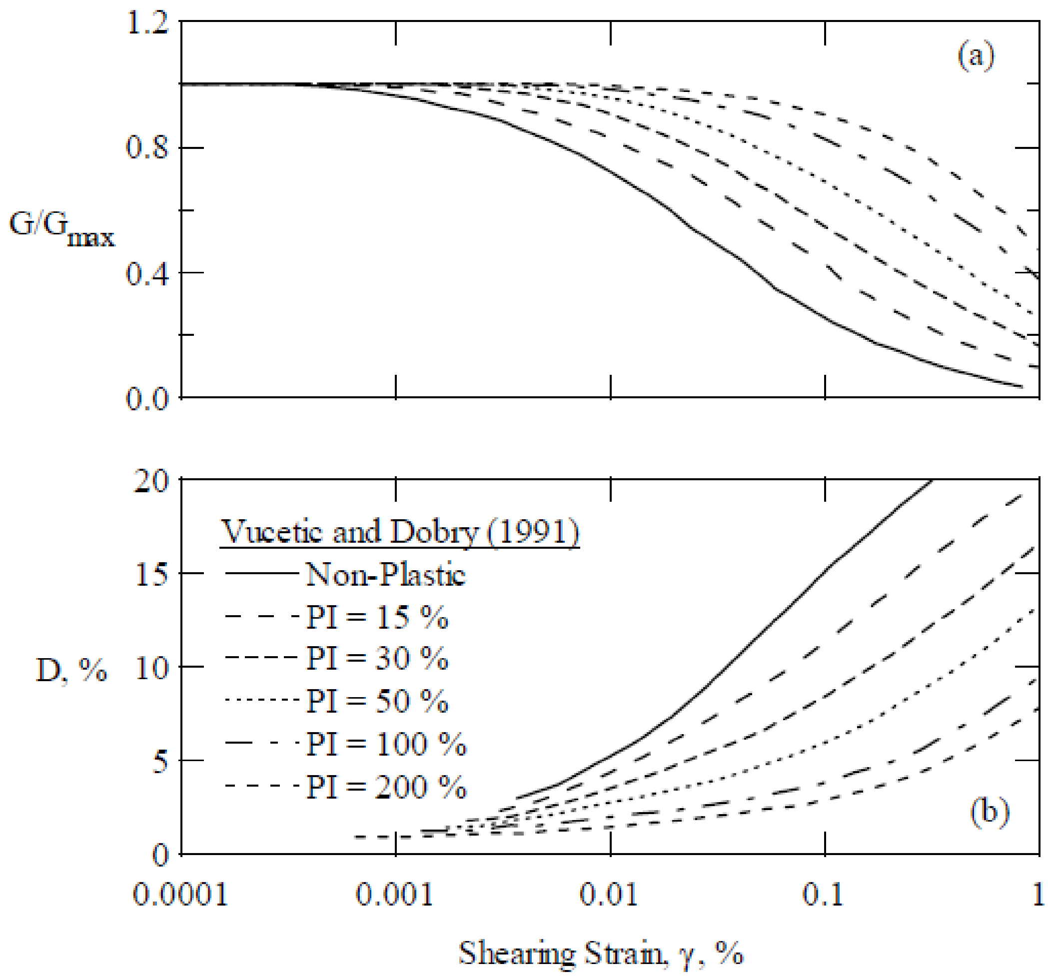

Figure 3.2: (a) Modulus reduction curves and (b) variation of damping ratio for fine- grained soils of different plasticity. with cyclic shear strain amplitude (After Vucetic and Dobry (1991). Effect of soil plasticity on cyclic resdponse. Journal of Geotechnical engineering, Vol. 117, No. 1. Reprinted by permission of ASCE)

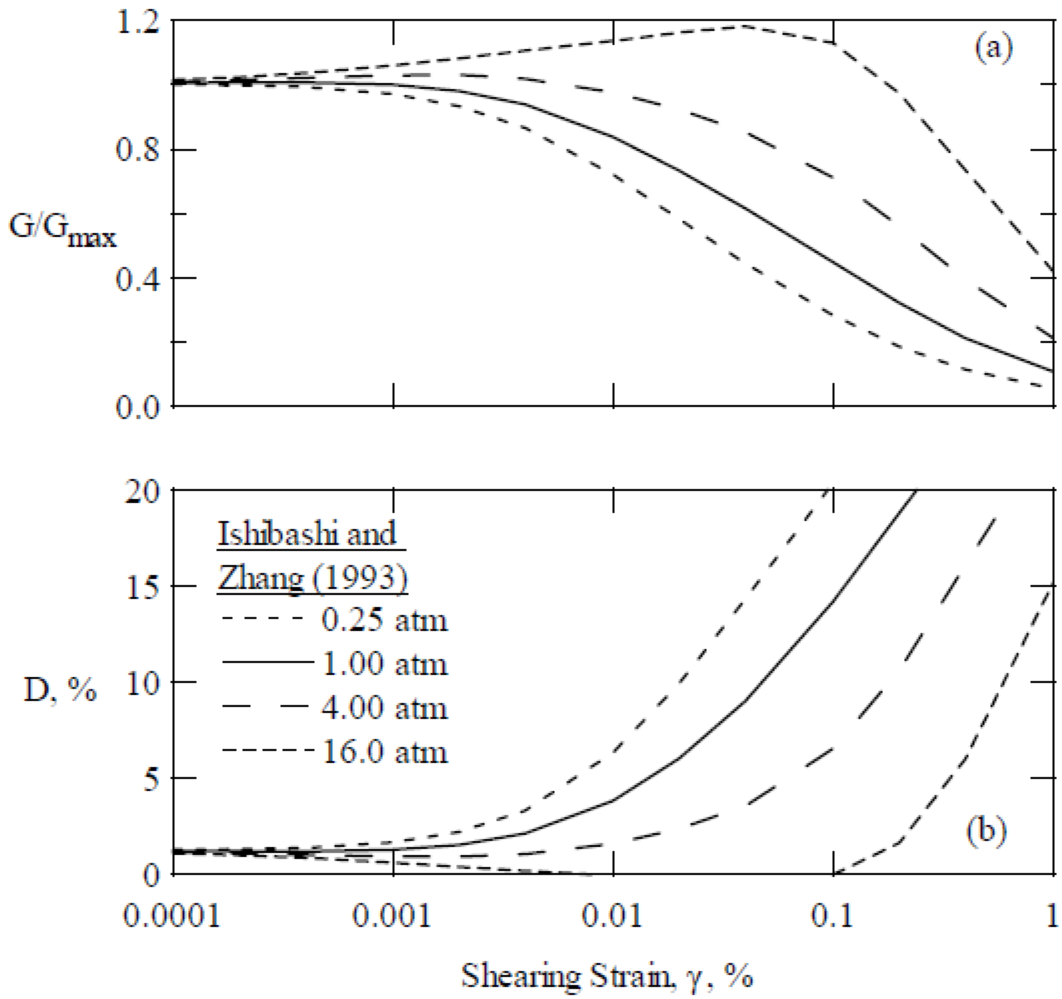

Figure 3.3: Influence of mean effective confining pressure on (a) modulus reduction curves and (b) variation of damping ratio for nonplastic (PI=0) soil with cyclic shear strain amplitude (After Ishibashi and Zhang (1993)).

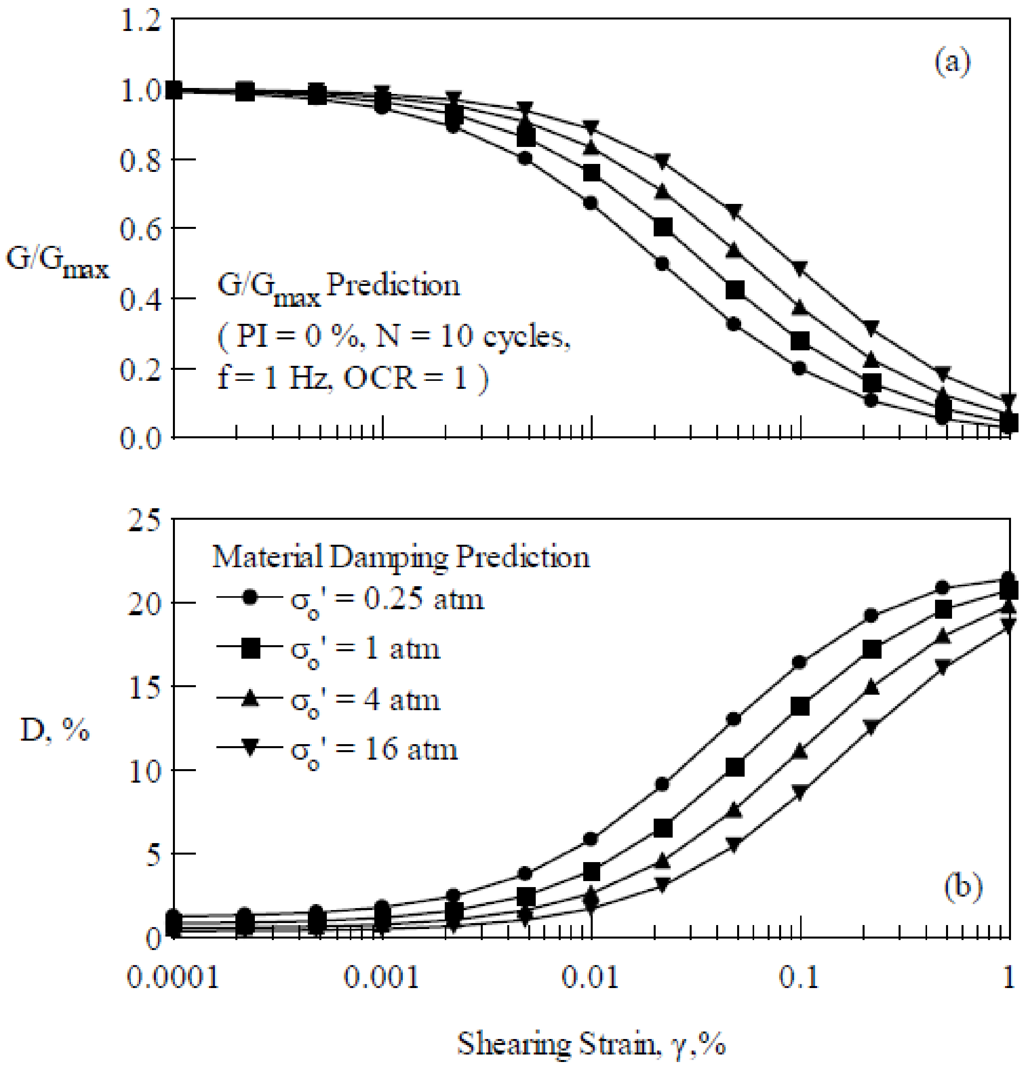

Figure 3.4: Effect of mean effective stress on (a) normalized modulus reduction and (b) material damping curves of a nonplastic soil
After: Mehmat Baris Darendeli, Doctor Of Philosophy, The University of Texas at Austin, August, 2001

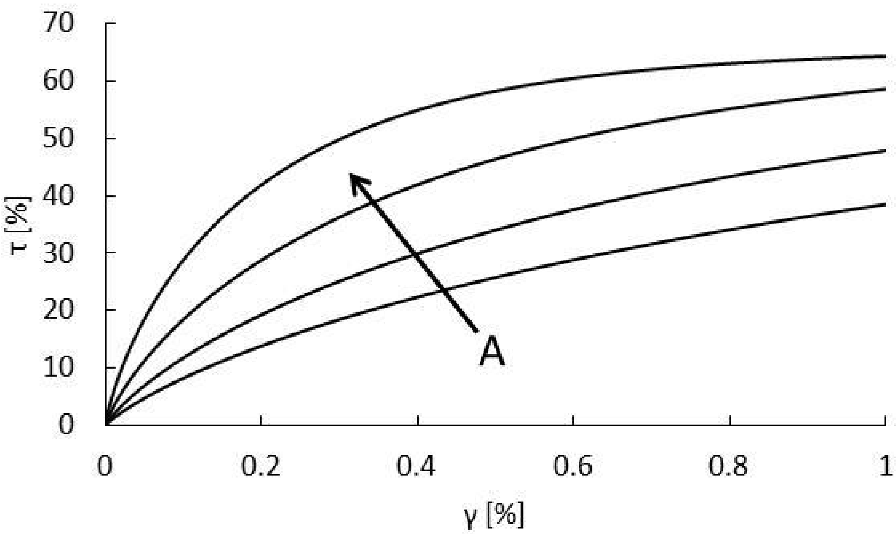

Figure 3.5: Influence of the parameter A in the monotonic stress - strain curve.

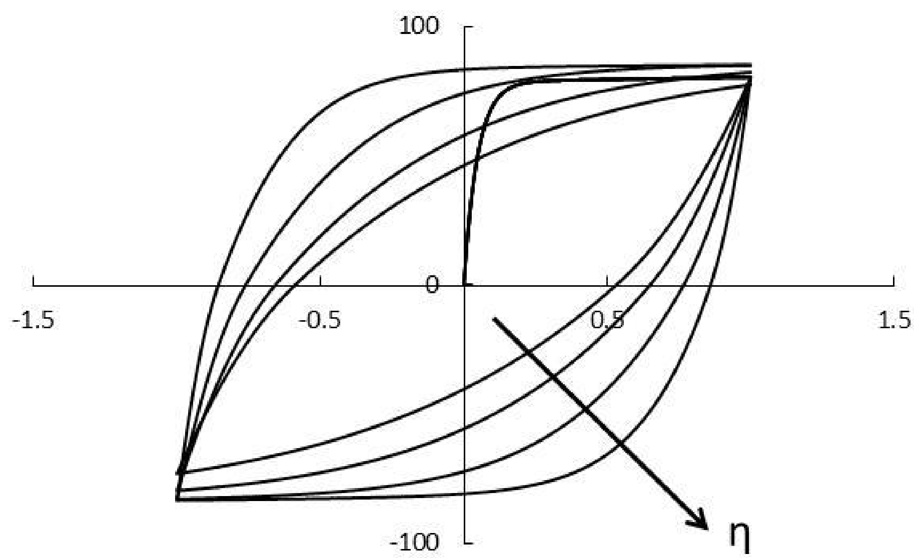

Figure 3.6: Influence of the parameter η in the expansion of the hysteretic shear stress – strain loop.

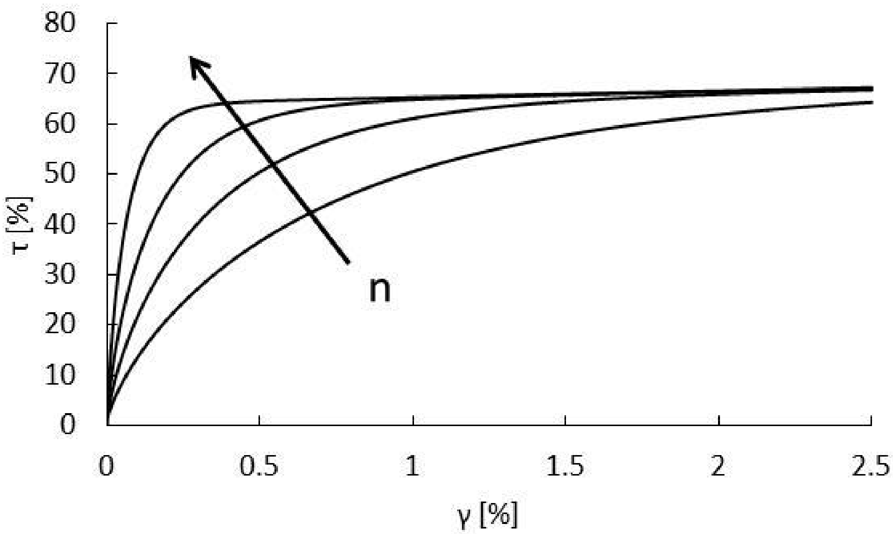

Figure 3.7: Influence of the exponent n in the monotonic stress - strain curve.

	A	S1	S2	n
Vucetic et al.	5700	3.5	0.9	0.75
Darendeli et al.	5000	3.4	0.955	0.8

Table 3.4: Values of calibrated model parameters A, s_1, s_2 and n according to Vucetic and Dobry (1991) curves and according to Darendeli et al. (2001) curves

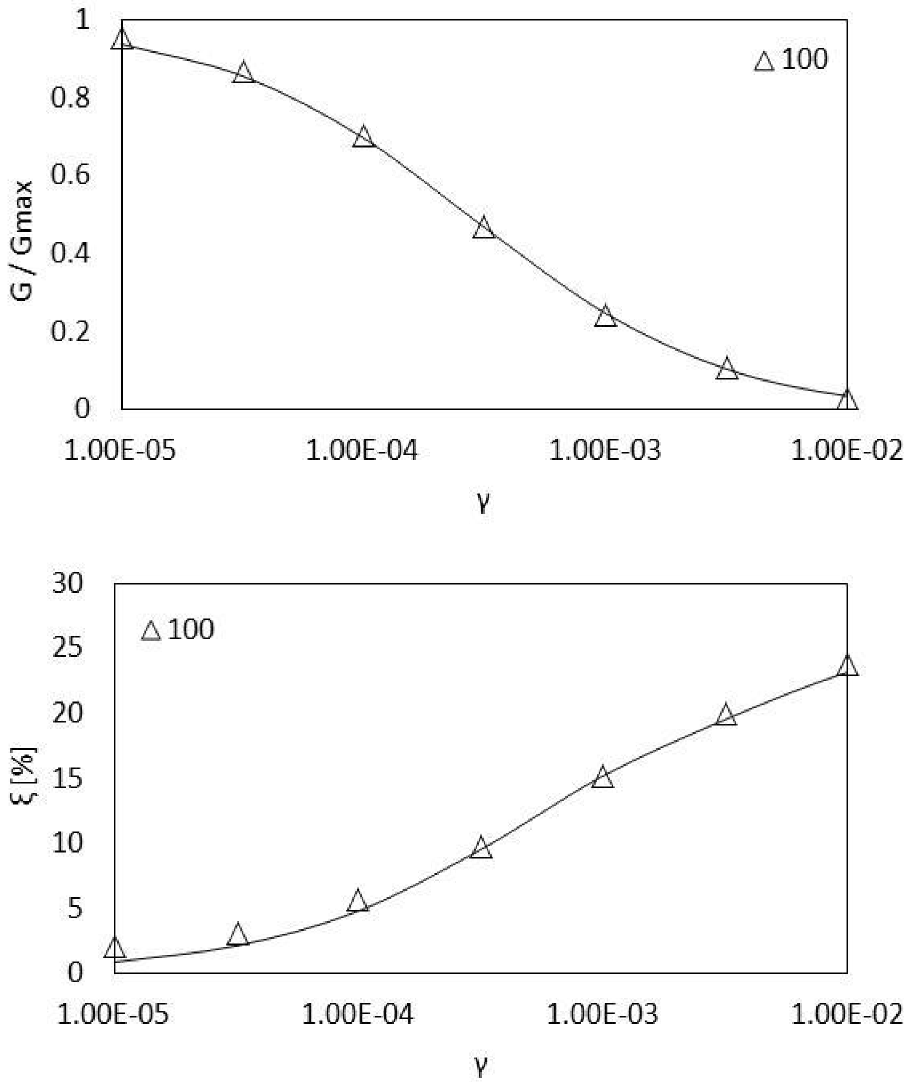

Figure 3.8: Approximation of the Vucetic and Dobry (1991) shear modulus and damping curves for sands (PI=0) of 100KPa confinement pressure. Published data is depicted with markers; Model results with continuous lines.

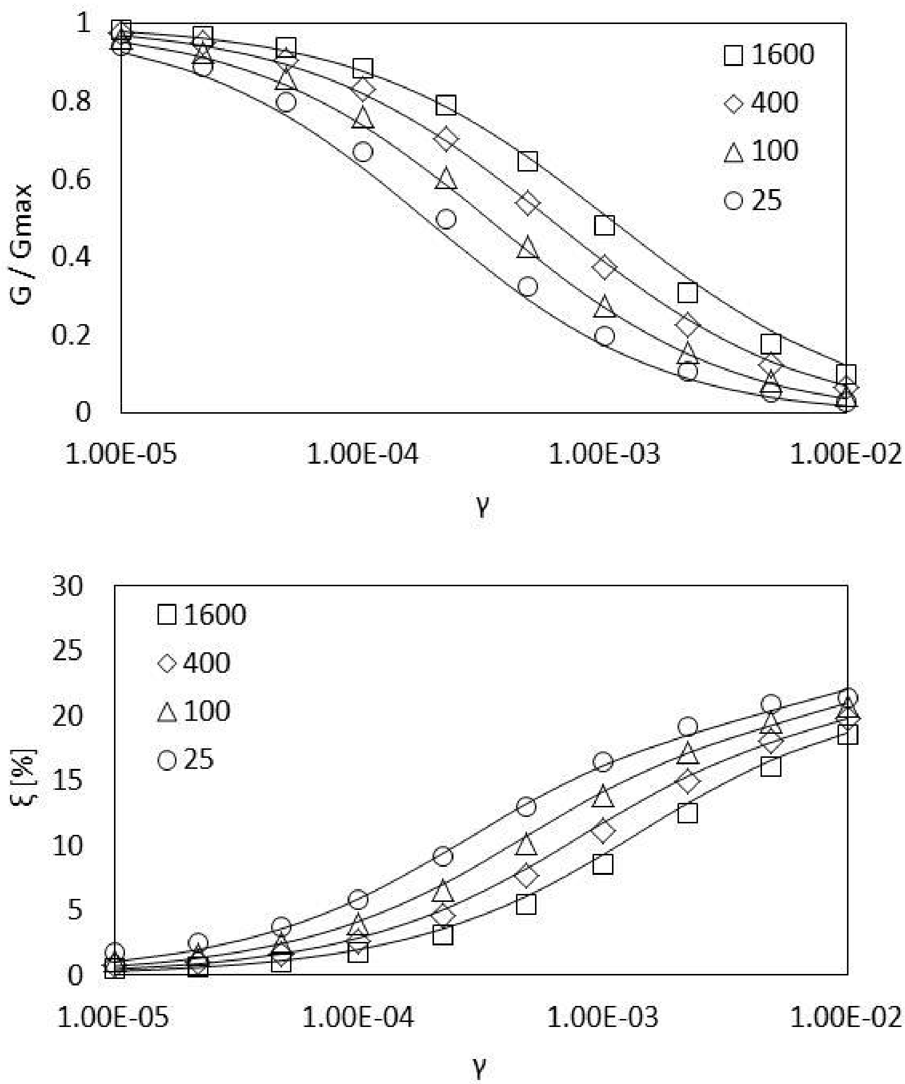

Figure 3.9: Approximation of the Darendeli et al. (2001) shear modulus and damping curves for sands (PI=0) of various confinement pressure levels. Published data is depicted with markers; Model results with continuous lines.

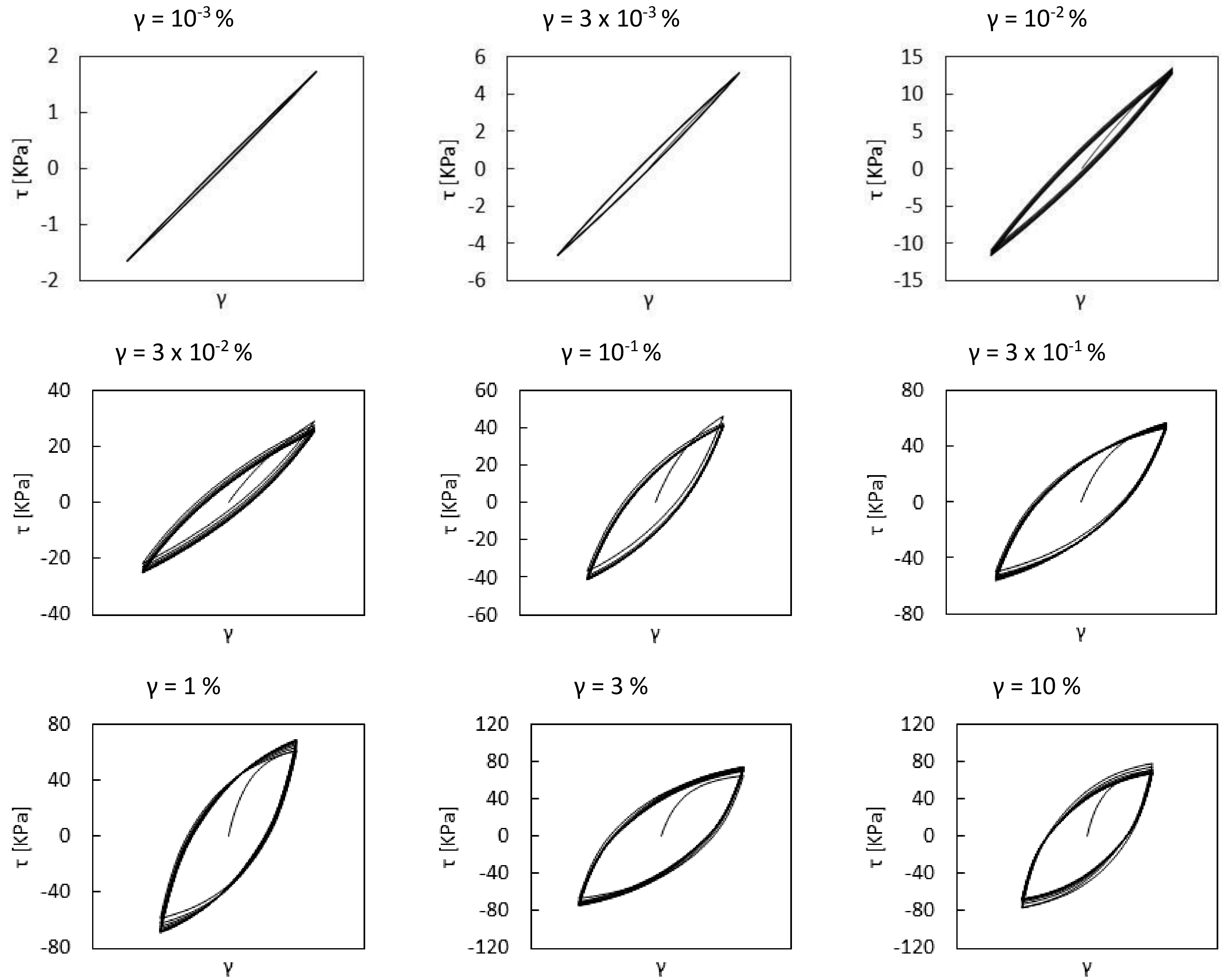

Figure 3.10: Hysteretic shear – stress strain loops corresponding to the calibrated model against Vucetic and Dobry (1991) shear modulus reduction and damping curves for the strain amplitudes depicted with markers in Fig 3.8.

Chapter 4
Numerical modelling of 1-Dimensional wave propagation

4.1 Ground response analysis

One of the most important and most commonly encountered problems in geotechnical earthquake engineering is the evaluation of ground response under earthquake loading. Ground response analyses are used to predict ground surface motions for development of design response spectra, to evaluate dynamic stresses and strain for evaluation of liquefaction hazard and to determine the earthquake – induced forces that can lead to instability of earth structures.

Despite the fact that seismic waves may travel through tens of kilometers of rock and often less than 100 m of soil, the soil plays a very important role in determining the characteristics of the ground surface motion. The influence of local soil conditions on the nature of earthquake damage has been recognized for many years. Seismologists and geotechnical earthquake engineers have worked toward the development of quantitative methods for predicting the influence of local soil conditions on strong ground motion. Over the years, a number of techniques have been developed for ground response analysis.
One of the most commonly used methods is a linear approach according to which transfer functions can be used to compute the response of single-degree-of-freedom systems. For the ground response problem, transfer functions can be used to express various response parameters, such as displacement, velocity, acceleration, shear stress and shear strain to an input motion parameter such as bedrock acceleration. Because it relies on the principle of superposition, this approach is limited to the analysis of linear systems. Since the nonlinearity of soil behavior is well known, the linear approach must be modified to provide reasonable estimates of ground response for practical problems of interest. Non-linear behavior can be approximated using an iterative procedure with equivalent linear soil properties. The equivalent linear shear modules G, is generally taken as a secant shear modulus and the equivalent linear damping ratio ξ, as the damping ratio that produces the same energy loss in a

single cycle as the actual hysteresis loop. A known time history of bedrock (input) motion is represented as a Fourier series, usually using the FFT. Each term in the Fourier series of the input motion is then multiplied by the transfer function to produce the Fourier series of the of the ground surface (output) motion. The ground surface (output) motion can then be expressed in the time domain using the inverse FFT. Thus, the transfer function determines how each frequency in the bedrock (input) motion is amplified, or deamplified, by the soil deposit.

Even though the process of iteration toward strain compatible soil properties allows non-linear soil behavior to be approximated, it is important to remember that the response method is still a linear method of analysis. The strain compatible soil properties are constant throughout the duration of the earthquake, regardless of whether at a particular time are small or large. The method is incapable of representing the changes in soil stiffness that actually occur during the earthquake.

The equivalent linear analysis is generally more flexible than many non-linear analysis methods and ground response is adequately approached (for a certain shear strain amplitude) with the calibration of only two parameters. However, it appears considerable disadvantages:

- It is incapable of describing basic cyclic soil behavior properties (e.g. shear modules degradation, development-reallocation-reduction of the pore water pressure, residual strains etc).
- Using a reduced effective shear strain for the shear modules reduction and the damping ratio increment, may lead to under-prediction of the stiffness and overestimation of the hysteretic damping when the inflicted shear strains time history is close to a harmonic one.
- Since soil properties are constant throughout each analysis step, the input ground motion may be over-amplified due to a fictitious soil resonance of one or more components of the input accelerogram. However, this is not happening in reality since soil properties are constantly changing over time.
- The variation of the dynamic soil parameters on each analysis step is common for every frequency component, regardless the corresponding strain amplitude. This results in high frequencies “depression”, which are usually characterized by small amplitude, since soil damping is overestimated for these components. This fictitious “depression” of the high frequency components leads to considerable deviations on predicting seismic response of deep soil deposits.

An alternative approach is to analyze the actual non-linear response of a soil deposit using direct numerical integration in the time domain. By integrating the equation of motion in small time steps, any linear or non-linear stress-strain model or advanced constitutive model can be used. At the beginning of each time step, the stress-strain relationship is referred to obtain the appropriate soil properties to be used in that time step. By this method a non-linear inelastic stress-strain relationship can be followed in a set of small incrementally linear steps. The available non –linear analysis methods outclass the equivalent linear methods concerning the cyclic soil response, however they suffer serious disadvantages:

- They over-predict hysteretic soil damping in great shear strains. The maximum hysteretic damping ratio appears to be two times greater that the experimentally measured one.
- They are not versatile in readjusting the hysteretic stress-strain loop shape, depending on variation of the dynamic soil parameters.
- Their capability to approach the experimental data of cyclic soil test is limited.

At present, a great number of computer programs has been developed for non-linear one-dimensional Seed (1978 ground response analysis such as DESPA-2 by Lee and Finn (1978), MASH by Martin and), DYNA 1D by Prevost (1989), NONLI3 by Joyner (1977), TESS1 by Pyke (1985), CHARSOIL by Streeter et al. (1973), CYCLIC 1D by Elgamal and DEEPSOIL by Hashash.

4.2 Mathematical framework

A number of techniques can be used to integrate the equations of motion. Of these, the explicit finite difference technique is the most easily explained.

Consider the soil deposit of infinite lateral extent shown in Figure 4.1. If the soil layer is subjected to horizontal motion at the bedrock level, the response will be governed by the differential equation of the one –dimensional vertical shear wave propagation through a continuum:

$$\rho \frac{\partial^2 u}{\partial t^2} = \frac{\partial \tau}{\partial z} + c\,\frac{\partial^3 u}{\partial z^2 \partial t}$$

where u is soil displacement, τ is shear stress and c is the viscoelastic constant, ρ is soil density, z is depth from surface and t is time.

Finite difference method aims to approximate the values of the continuous function $f\ (t,N)$ on a set of discrete points in (t,N) plane. We divide the N-axis into equally spaced nodes at distance ΔN apart, and, the t-axis into equally spaced nodes a distance Δt apart. Then (t,N)

plane becomes a mesh with mesh points on ($i\Delta t$, $j\Delta N$). We are interested in the values of $f\ (t,N)$ at mesh points ($i\Delta t$, $j\Delta N$), denoted as $f_{\ i,j}$ = f ($i\Delta t$, $j\Delta N$).

The basic idea of FDM is to replace the partial derivatives by approximations obtained by Taylor expansions near the point of interests. For example

$$\frac{\partial f\ (t,N)}{\partial t} = \lim_{\Delta t \to 0} \frac{f(t+\Delta t, N) - f\ (t,N)}{\Delta t} \approx \frac{f(t+\Delta t, N) - f\ (t,N)}{\Delta t}$$

for small Δt using Taylor expansion at point (t,N)

$$f(t+\Delta t, N) = f(t,N) + \frac{\partial f(t,N)}{\partial t}\Delta t + O((\Delta t)^2)$$

Then, the following three approximations to 1st order derivatives are formed (Fig. 4.2):

forward: $$\frac{\partial f\ (t,N)}{\partial t} \approx \frac{f(t+\Delta t,N) - f(t,N)}{\Delta t} + O(\Delta \mathrm{t})$$

backward: $$\frac{\partial f\ (t,N)}{\partial t} \approx \frac{f(t,N) - f(t-\Delta t,N)}{\Delta t} + O(\Delta \mathrm{t})$$

central: $$\frac{\partial f\ (t,N)}{\partial t} \approx \frac{f(t+\Delta t,N) - f(t-\Delta t,N)}{2\Delta t} + O((\Delta t)^2)$$

and for the 2nd order derivatives a symmetric central-difference approximation is formed:

$$\frac{\partial^2 f(t,N)}{\partial N^2} \approx \frac{-2f(t,N) + f(t, N-\Delta N)}{(\Delta N)^2} + O((\Delta N)^2)$$

Using Taylor's expansions for $f(t, N + \Delta N)$ and $f(t, N - \Delta N)$ around point (t, N) we derive the finite difference approximations:

forward difference: $\frac{\partial f}{\partial t} \approx \frac{f_{i+1,j} - f_{i,j}}{\Delta t}$ $\frac{\partial f}{\partial N} \approx \frac{f_{i,j+1} - f_{i,j}}{\Delta N}$

backward difference: $\frac{\partial f}{\partial t} \approx \frac{f_{i,j} - f_{i-1,j}}{\Delta t}$ $\frac{\partial f}{\partial N} \approx \frac{f_{i,j} - f_{i,j-1}}{\Delta N}$

central difference: $\frac{\partial f}{\partial t} \approx \frac{f_{i+1,j} - f_{i-1,j}}{2\Delta t}$ $\frac{\partial f}{\partial N} \approx \frac{f_{i,j+1} - f_{i,j-1}}{2\Delta N}$

As to the second derivative, we have:

$$\frac{\partial^2 f}{\partial t^2} \approx \frac{f_{i+1,j} - 2f_{i,j} + f_{i-1,j}}{\Delta t^2} \quad \text{and} \quad \frac{\partial^2 f}{\partial N^2} \approx \frac{f_{i,j+1} - 2f_{i,j} + f_{i,j-1}}{\Delta N^2}$$

As with any integration problem the boundary conditions must be satisfied. Since the ground surface is a free surface, τ_1=0, so

$$\frac{du(1,t)}{dz} = 0$$

The boundary condition at the bottom of the soil deposit depends on the nature of the underlying bedrock. If the bedrock is rigid, its particle velocity $\dot{u}_b(t) = \dot{u}_{N+1,t}$, can be specified directly as the input motion. If the bedrock is elastic, continuity of stresses requires that the shear at the bottom of the soil layer $\tau_{N+1,t}$, be equal to the shear stress at the top of the rock layer. Thus:

$$\tau_{N+1,t} + c\,\frac{\partial^2 u}{\partial z \partial t} = C\left[\frac{du(N+1,t)}{dt} - \frac{du_g(t)}{dt}\right]$$

Once the boundary conditions have been established, the integration calculations proceed from the bottom to the top of the soil deposit in each time step, and step by step in time.

If the soil deposit is initially at rest, then $\dot{u}_{i,t=0} = 0$ and $\tau_{i,t=0} = 0$ for all i. We also need to discretize the boundary and initial conditions accordingly.

Depending on which combination of schemes we use in discretizing the equations, we will have explicit, implicit, or Crank-Nicolson methods.

According to the explicit method, the variables at the time $i + 1$ are exclusively expressed using the same variables at the time i. Thus, it outclasses numerous numerical methods for solving differential equations systems, such as the implicit method, since the differencial equations solution is being approached without the solution of an algebraic equations system in every time step. However, despite being computationally simple, it appears a defect. Integration time step $\Delta t = k$, must be multiple smaller than the respective space step $\Delta z = h$, for the algorithm to converge. Space step h, should be very small as well, for the accuracy to be satisfactory. Nevertheless, present-day computational progress renders explicit method one of the most powerful tools for non-linear dynamic systems.

The integration progress can be summarized as follows:

1. At the beginning of each time step, the particle velocity $\dot{u_{i,t}}$,and total displacement $u_{i,t}$,are known at each layer boundary.
2. The particle displacement profile is used to determine the shear strain $\gamma_{i,t}$, within each layer.
3. The stress-strain relationship (as it is presented in ch. 2) is used to determine the shear stress, $\tau_{i,t}$, in each layer.
4. The input motion is used to determine the motion of the base of the soil layer at time $t + \Delta t$.
5. The motion of each layer boundary at time $t + \Delta t$ is calculated, working from bottom to top. The progress is then repeated from step 1 to compute the response in the next time step.

Although equivalent linear and non- linear methods are both used to solve one- dimensional ground response analysis problems, their formulations and underlying assumptions are quite different. Consequently, it is reasonable to expect to find some differences in their results. Comparing the results of equivalent linear and non- linear ground response analysis the following general conclusions can be extracted:

1. The inherent linearity of equivalent linear analyses can lead to *spurious resonances* (i.e., high levels of amplification that result from coincidence of a strong component of the input motion with one of the natural frequencies of the equivalent linear soil deposit). Since the stiffness of an actual noni- linear soil changes over the duration of a large earthquake, such high amplification levels will not develop in the field.

2. The use of an effective shear strain in an equivalent linear analysis can lead to an over-softened and over- damped system when the peak shear strain is much larger than the remainder of the shear strains, or to an under- softened, underdamped system when the shear strain amplitude is nearly uniform.
3. Equivalent linear analyses can be much more efficient than non- linear analyses, particularly when the input motion can be characterized with acceptable accuracy by a small number of terms in a Fourier series. For example, most earthquakes contain relatively little elastic wave energy at frequencies above 15 to 20 Hz. Consequently, the response can usually be computed with reasonable accuracy by considering only the frequencies below 15 to 20 Hz (or lower, in some cases0. As the power, speed and accessibility of computers have increased in recent years, the practical significance of differences in the efficiency of one- dimensional ground response analyses has decreased substantially.
4. Non- linear methods can be formulated in terms of effective stresses to allow modeling of the generation, redistribution and eventual dissipation of excess pore pressure during and after earthquake shaking. Equivalent linear methods do not have this capability.
5. Non- linear methods require a reliable stress- strain or constitutive model. The parameters that describe such models are not as well established as those of the equivalent linear model.
6. Differences between the results of equivalent linear and non- linear analyses depend on the degree of nonlinearity in the actual soil response. For problems where strain levels remain low (stiff soil profiles and/or relatively weak motions), both analyses can produce reasonable estimates of ground response. For problems involving high strain levels, particularly problems in which the induced shear stresses approach the available shear strength of the soil, nonlinear analyses are likely to provide reasonable results.

In summary, both equivalent linear and non-linear techniques can and have been used successfully for one-dimensional ground response analysis. The use and interpretation of each requires knowledge of their underlying assumptions, understanding of their operation, and recognition of their limitations. Neither can be considered mathematically rigorous or precise, yet the accuracy is not inconsistent with the variability in soil conditions, uncertainty in soil properties, and scatter in the experimental data upon which many of their input parameters are based.

4.3 Comparison with other methods

The downgrated in p-q space version of the three dimensional constitutive sand model TA-GER [9], [10], as it was described in chapter 2 is implemented into an inhouse computer code which uses the explicit finite-difference technique to integrate the equations of motion for the nonlinear one-dimensional ground response analysis of layered sites.The procedure is being followed as it was described in the previous paragraph. In order to obtain the maximum accuracy, integration time step $\Delta t = k$, must be multiple smaller than the respective space step $\Delta z = h$ for the algorithm to converge, thus *k*= 10^{-4} s and *h*=0.5m.

Using the finite difference approximation we derive the following expressions for the soil velocity and acceleration respectively:

$$v_{i,j} = \frac{u_{i,j} - u_{i-1,j}}{k}$$

$$a_{i,j} = \frac{u_{i-1,j} - 2u_{i,j} + u_{i+1,j}}{k^2}$$

Soil response in each space node j and each time step i is expressed using the variables at the previous time step., as follows:

$$u_{i+1,j} = \frac{k^2}{2rh}\left(\tau_{i,j+1,} - \tau_{i,j-1}\right) +$$

$$\frac{ck}{h^2 r}\left(u_{i,j+1} - 2u_{i,j} + u_{i,j-1} - u_{i-1,j-1} + 2u_{i-1,j} - u_{i-1,j+1}\right) + 2u_{i,j} - u_{i-1,j}$$

where:

u is the soil displacement

τ is the shear stress

k is the integration time step

h is the integration space step

r is the soil density =2 Mg/m^3

c is the viscocity coefficient =50 KN*sec/ m^3

The boundary conditions impose that the shear stress at the top of the bedrock and therefore the shear strain at the same position be equal to zero. The above constraint is expressed through the equation:

$$u_{i,2} = u_{i,1}$$

The boundary condition at the bottom of the soil deposit requires that the shear stress at the top of the underlying bedrock be equal to the shear stress at the bottom of the soil and thus:

$$u_{i+1,N+1} = \frac{k}{C_{rock}} \tau_{i,N+1} + \frac{c}{C_{rock} * h} \left(u_{i,N} - u_{i,N+1} - u_{i-1,N} + u_{i-1,N+1} \right) + ug_i - ug_{i-1}$$

where:

C_{rock} is the dashpot coefficient of the bedrock accounting for radiation damping and is taken equal to 5000 KN*sec/ m^3

ug is the displacement imposed by the excitation

The initial conditions, e.g. zero initial displacement and zero initial velocity at the whole soil column, should also be accounted and they are expressed in the well known finite difference form as follows:

$$u_{1,j} = 0$$
$$\frac{u_{0,j} - u_{1,j}}{k} = 0$$

The effectiveness of the proposed model is checked against the hysteretic model by Gerolymos and Gazetas [4] implemented in the finite difference code NL-DYAS ([4], [5]). To serve as a yardstick, an equivalent linear soil response analysis was also carried out with the use of code STRATA [2] — one of the current state-of-practice soil amplification codes. The goal is twofold: the validation between three different models, that represent three different schools and the estimation of the range of applicability of each one of the tree methods, a plasticity based model which is governed by an physical law for connecting the volumetric strain with the shear strain, a phenomenological model, which lucks a plastic flow rule and the equivalent linear method.

To compare the aforementioned methods a 30-m deep dense sand profile with density ρ = 2.1 Mg/m^3, constant with depth, and shear wave velocity distribution illustrated in Fig 4.3, is excited at its base and its response is calculated.

In order to reveal the drawbacks of every method, two analyses with different excitations will be carried out. A strong motion, the JMA 090 record from the Kobe (1995) earthquake and a moderate one from Kalamata 1986 earthquake are used as excitations at the base of the soil column. We consider the sand to behave according to the Derendeli curves.

The results of the three analyses (TA–GER, NL-DYAS, STRATA) are portrayed in terms of : (a) the distributions with depth of the peak values of acceleration, displacement, shear strain, and shear stress (Figs 4.4 and 4.5), (b) the acceleration time histories at the ground surface (Figs 4.6 and 4.8), (c) the stress–strain hysteresis loops of the two nonlinear models at the depth of 5m and 15m (Figs 4.10 and 4.11), and (d) the corresponding acceleration response spectra (Figs 4.12 and 4.13). The following remarks can be made:

- Results corresponding to Kalamata 1986 medium intensity excitation are very similar for all the three methods in terms of distributions with depth and quite similar acceleration time histories, with STRATA exhibiting slightly higher amplitudes. The predicted accelerations at the surface are:

  - Tager: 0.51g and -0.48g maximum and minimum acceleration the surface
  - NL – Dyas: 0.50g and -0.48g maximum and minimum acceleration the surface
  - Strata: 0.57g and -0.50 g maximum and minimum acceleration the surface

  for 0.23g and 0.24g excitation accelerations respectively.

  Accelerations spectra at the surface are also in well agreement denoting that the equivalent linear method is sufficiently adequate and provides reliable results for excitations in this level of intensity. The consistency of predictions indicates also that the plasticity based method Tager is correctly validated.

  The similarity between the shear stress – strain diagrams of TA-GER and NL-DYAS analyses is evident for this motion. Slight differences are within expectations.

- Regarding the strong seismic excitation, a fairly similar response is predicted by the two non-linear models, considerably deviating from strata predictions. In terms of distributions with depth the equivalent linear method under – predicts the maximum displacement. Differences exist also between the two non – linear methods, especially in terms of maximum strain with depth but are less intense and are completely eliminated in terms of acceleration time histories at the surface:

- Tager :0.85g and -0.72g maximum and minimum acceleration at the surface
- NL – Dyas: 0.86g and -0.73g maximum and minimum acceleration at the surface
- Strata: 1.39g and -0.97g maximum and minimum acceleration at the surface

for 0.60g -0.45g excitation accelerations respectively.

In terms of acceleration spectra at the surface STRATA significantly exaggerates the long-period pulses, while it depresses the high-frequency components — a performance within expectations, as such "depression" of high frequencies has been already noted in the literature (e.g. [13], [14], [15], [16]). The response acceleration spectra from the three codes reinforce this conclusion: whereas the two inelastic soil models produce almost identical spectra, the equivalent-linear analysis, having filtered-out the short-period components, underpredicts the spectral values for periods less than 0.45 sec. It is worth mentioning that an improved equivalent-linear method that avoids the overdamping of high frequencies has been developed by Assimaki and Kausel [14]. Such overdamping stems from the facts that damping is a function of strain amplitude and that high frequencies are usually associated with small amplitudes of motion; thus, these components experience substantially less damping than the dominant frequencies and are artificially suppressed when hysteretic damping is taken as constant. The overestimation of the long period spectral accelerations by the equivalent linear method is due to resonance phenomena that take place in a linear analysis. Such phenomena phenomena cannot be developed when nonlinearity is accounted for, as the shear modulus, therefore the natural periods of soil, are not fixed but change over time.

There are sharp differences between the hysteretic shear stress – stain loops, for the two non - linear models for z=5m and z=15m, with Tager predicting higher values of shear strain, but this deviation is expected, considering that the models exhibit differences and loops are very sensitive. However, the TA-GER model predicts broader hysteresis loops that are more regular in shape.

Figures

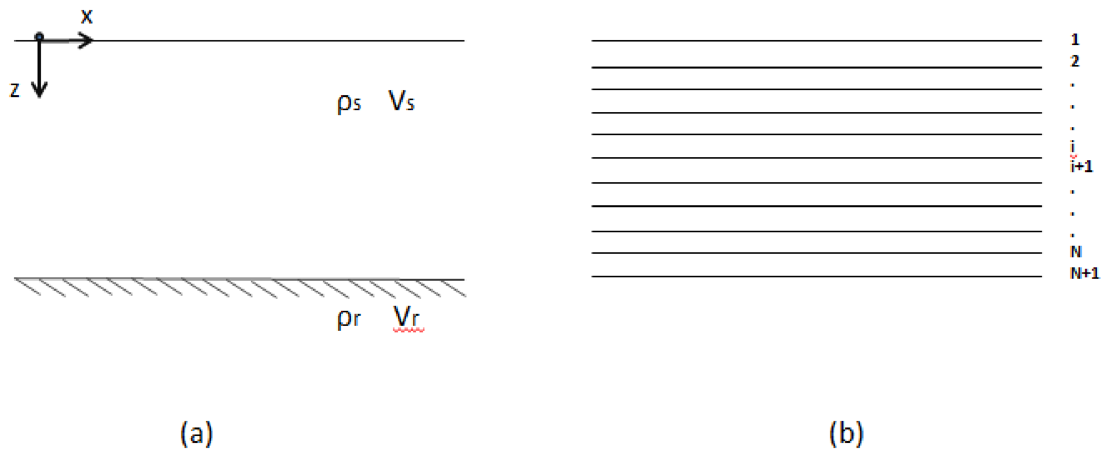

Figure 4.1: (a) Uniform soil deposit of infinite lateral extent overlying bedrock (b) discretization of soil deposit into N sub-layers

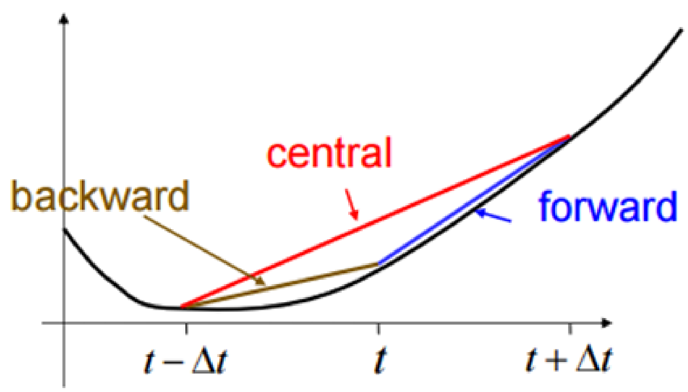

Figure 4.2: Forward, central and backward derivatives approximation

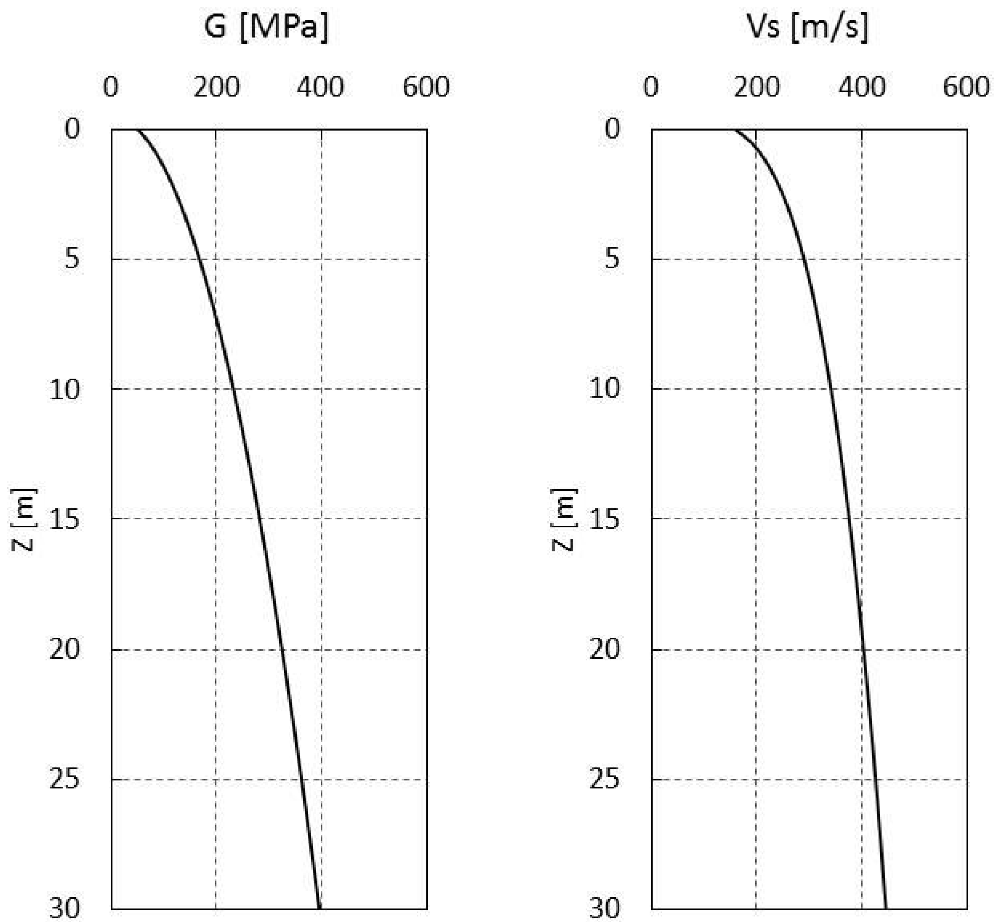

Figure 4.3: Shear modulus and shear wave velocity distribution with depth for the 30m deep soil profile

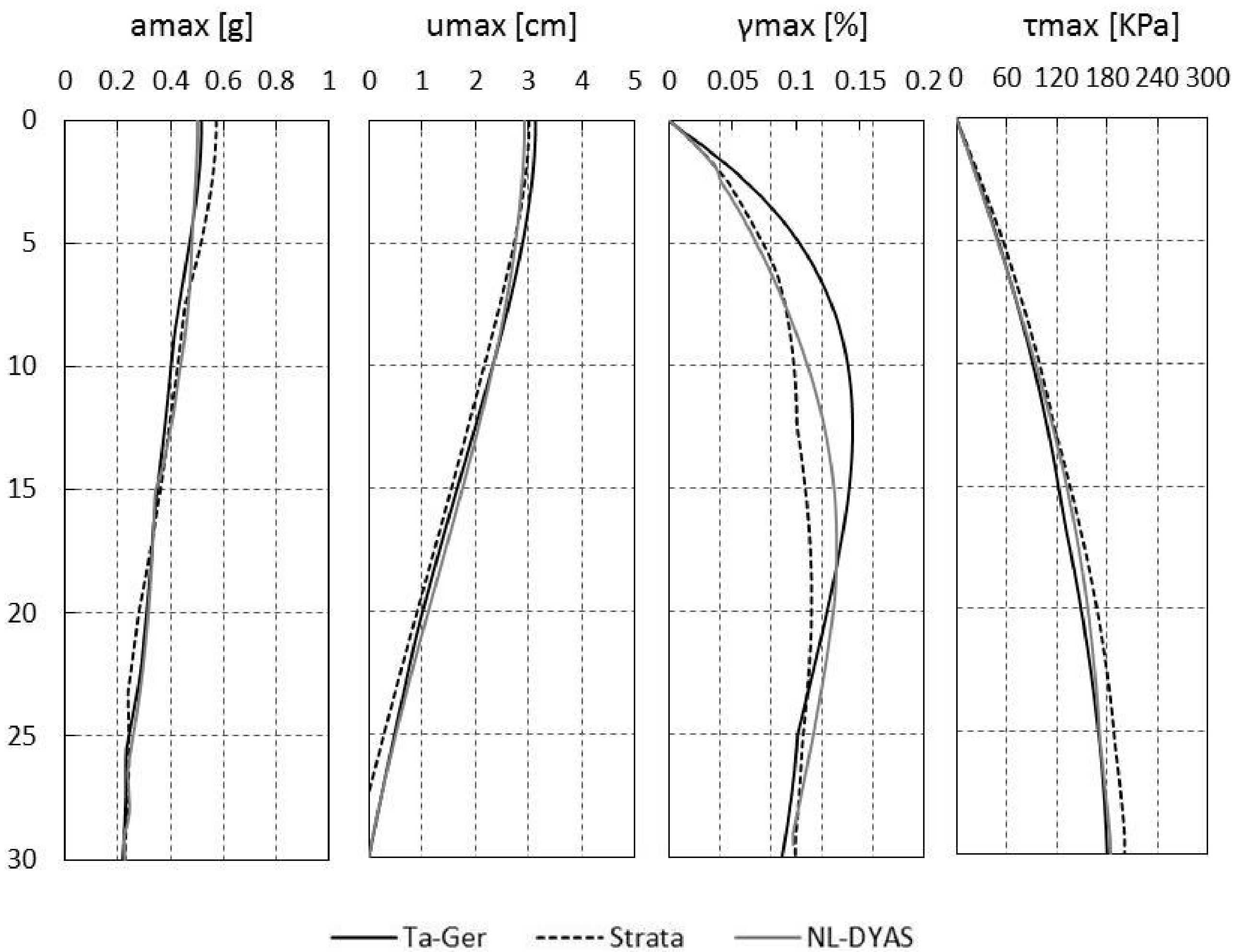

Figure 4.4: *Distributions with depth of the peak values of acceleration, displacement, shear strain, and shear stress. Shaking with Kalamata 1986 record*

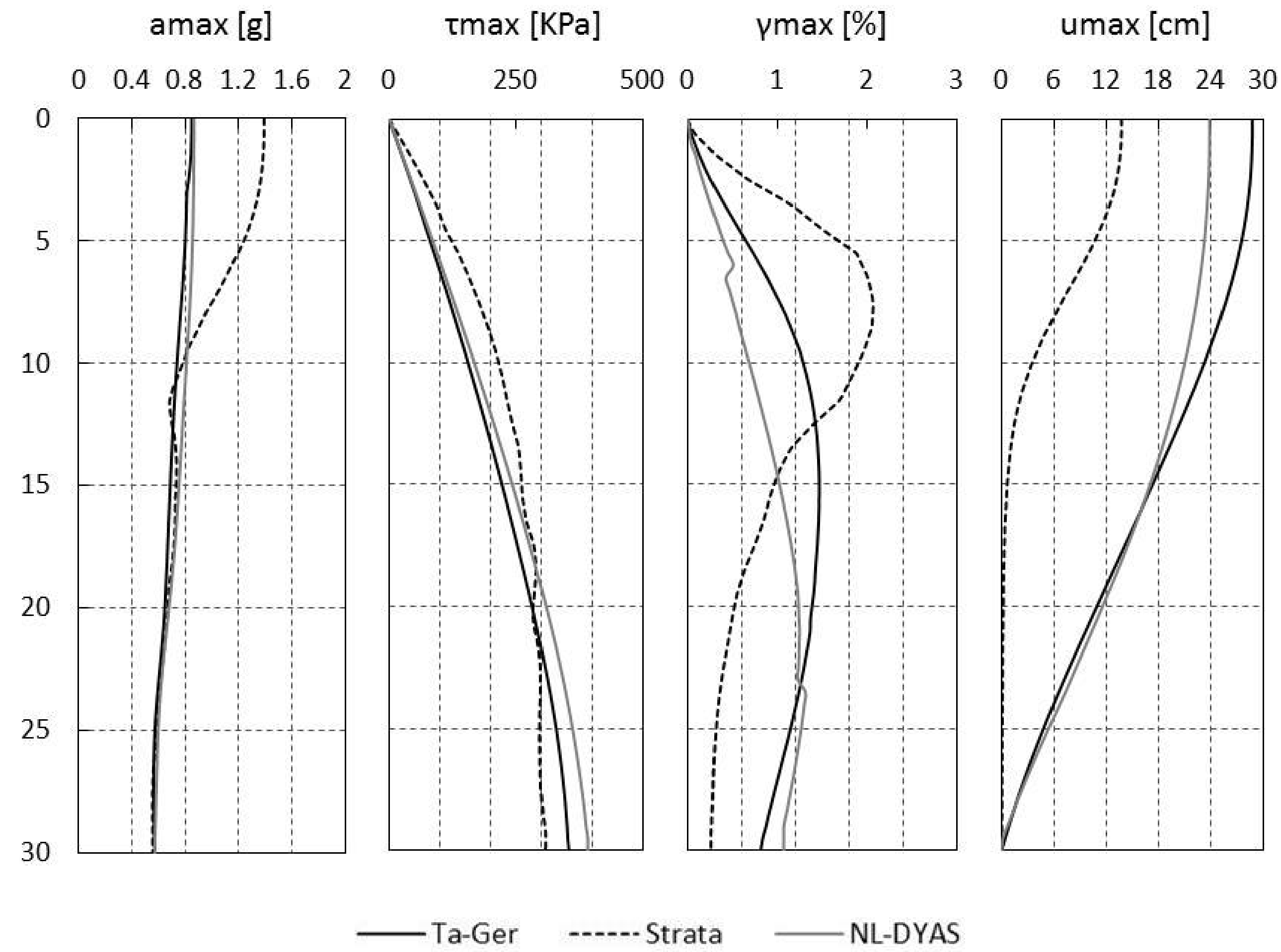

Figure 4.5: *Distributions with depth of the peak values of acceleration, shear stress, shear strain and displacement. Shaking with Kobe JMA 090 1995 record*

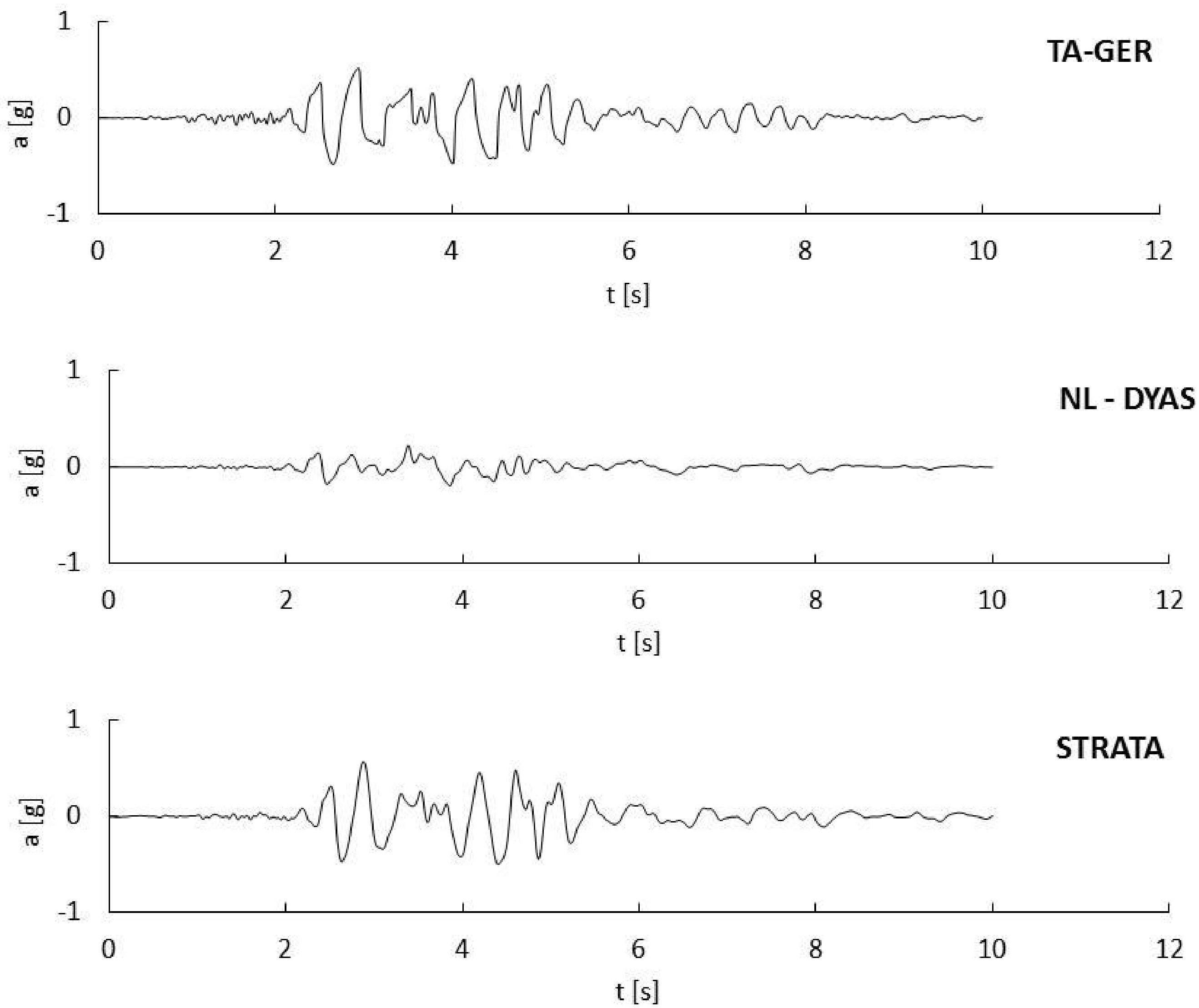

Figure 4.6: *Comparison of acceleration time histories at the surface computed with the three models. Shaking with Kalamata 1986 record*

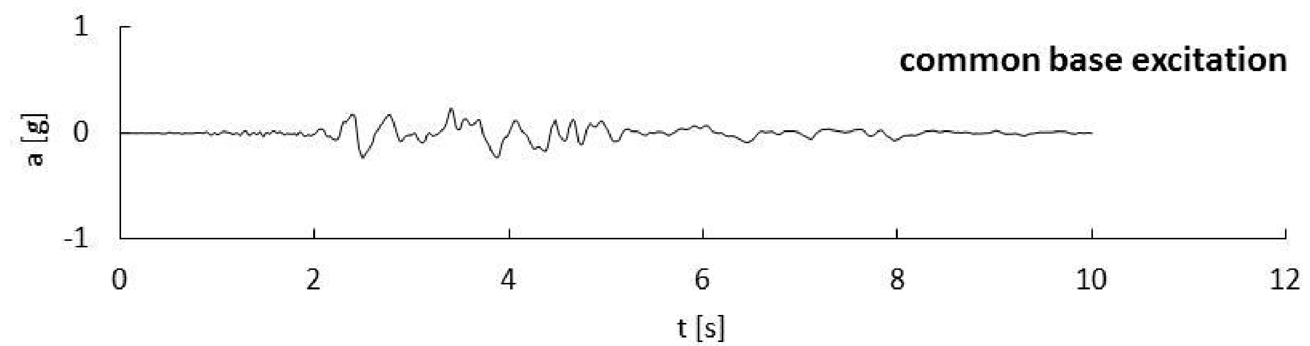

Figure 4.7: Acceleration time history for the common base excitation of with Kalamata 1986 record

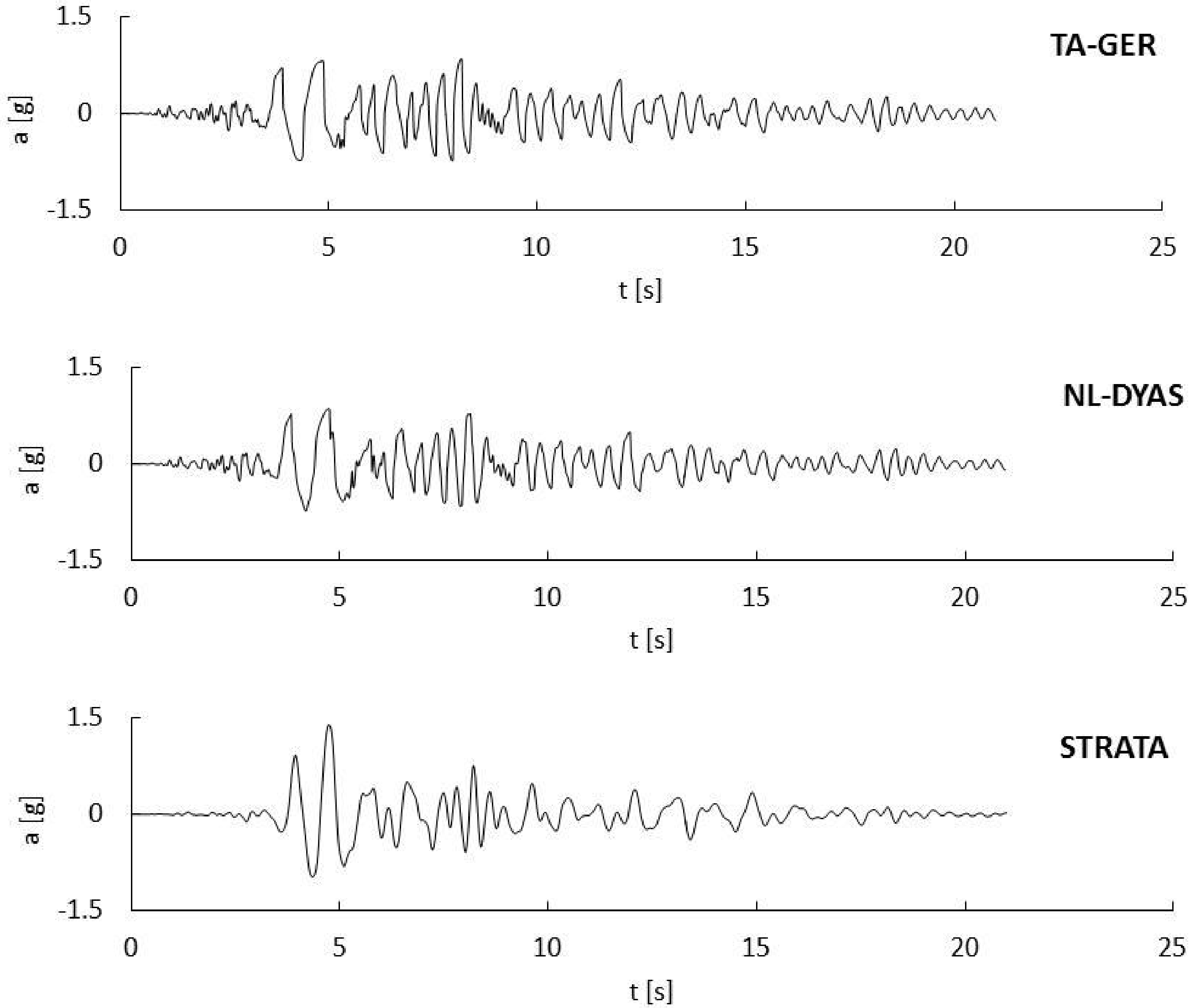

Figure 4.8: *Comparison of acceleration time histories at the surface computed with the three models. Shaking with Kobe JMA 090 1995 record*

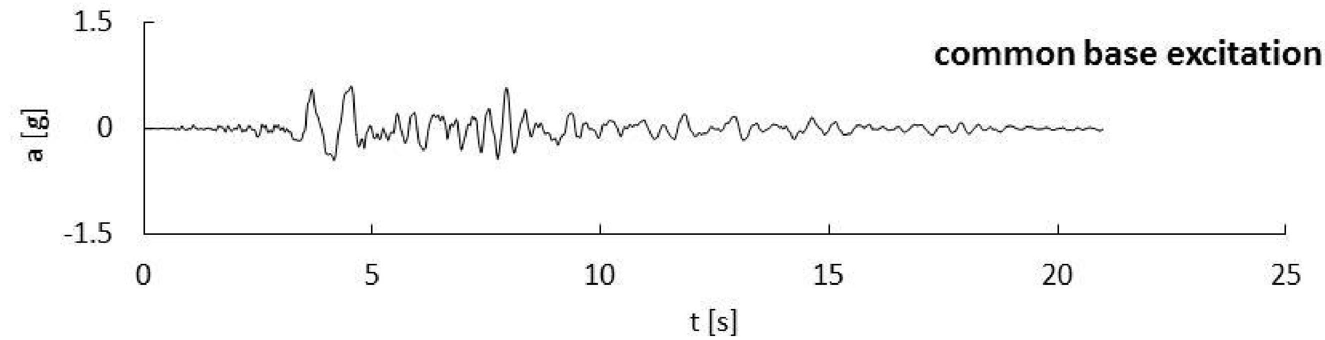

Figure 4.9: Acceleration time history for the common base excitation of with Kobe JMA 090 1995 record

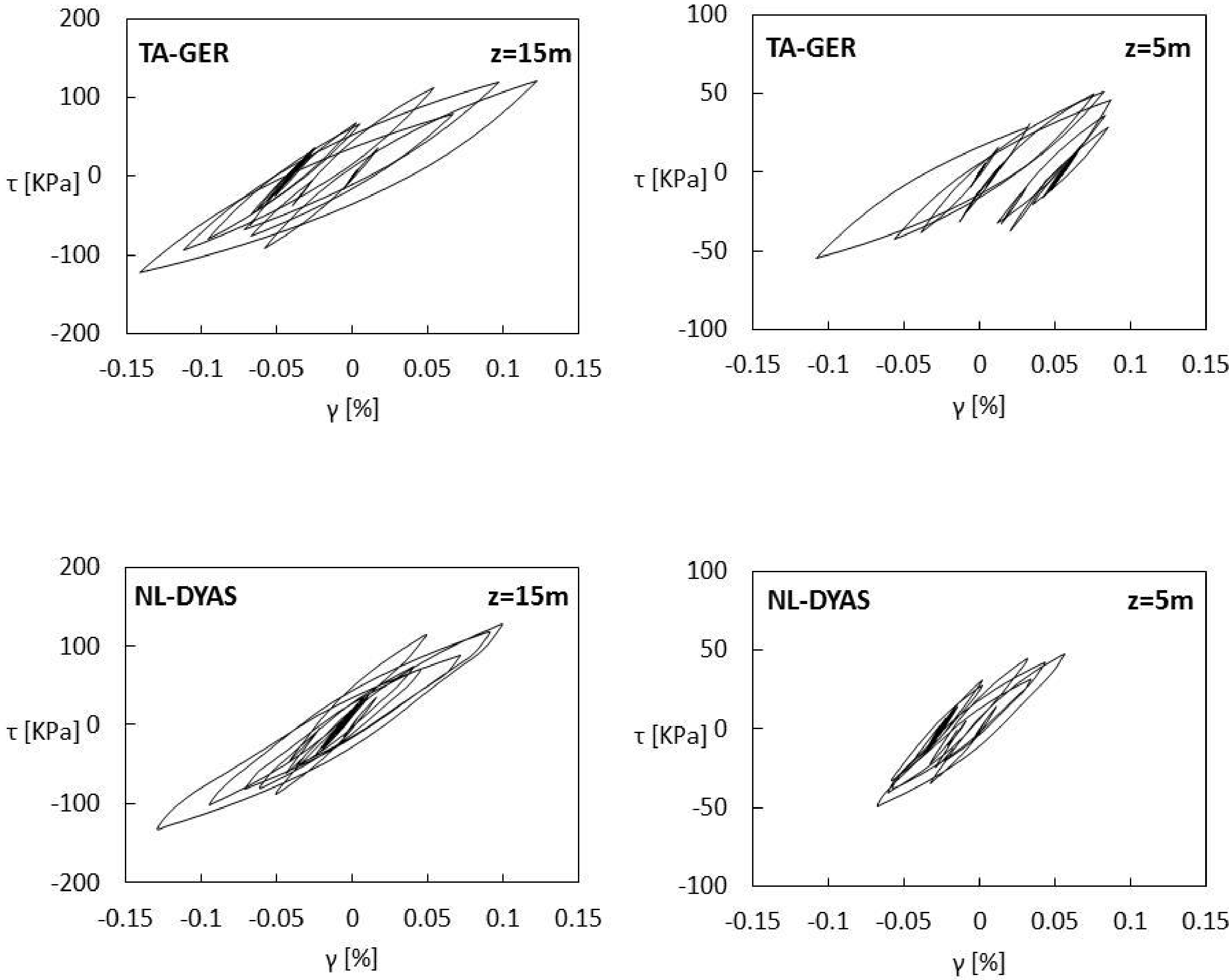

Figure 4.10: *Comparison of stress – strain loops computed with Ta- Ger and NL – DYAS at z=15m and z=5m. Shaking with Kalamata 1986 record*

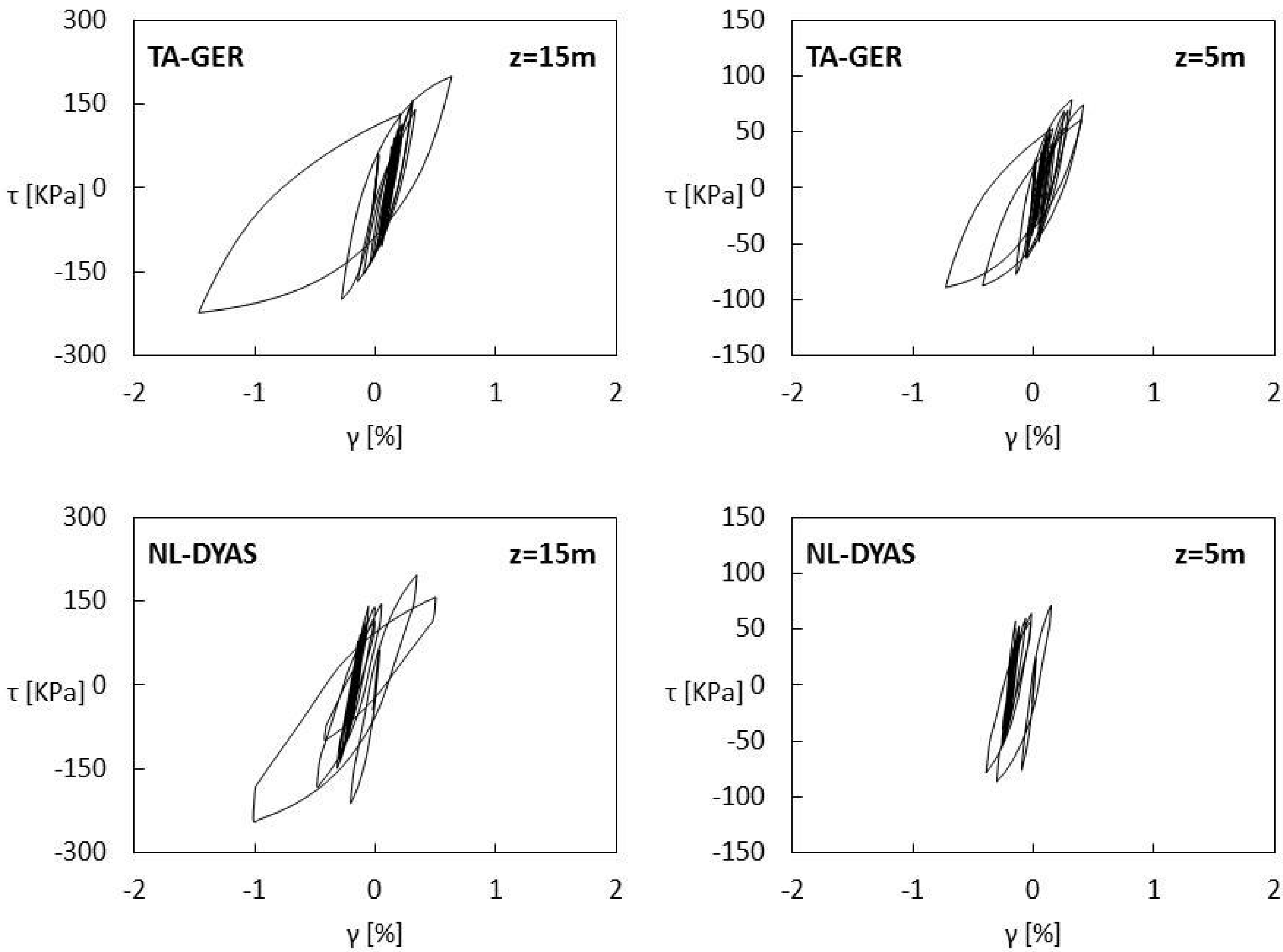

Figure 4.11: *Comparison of stress – strain loops computed with Ta- Ger and NL – DYAS at z=15m and z=5m. Shaking with Kobe JMA 090 1995 record*

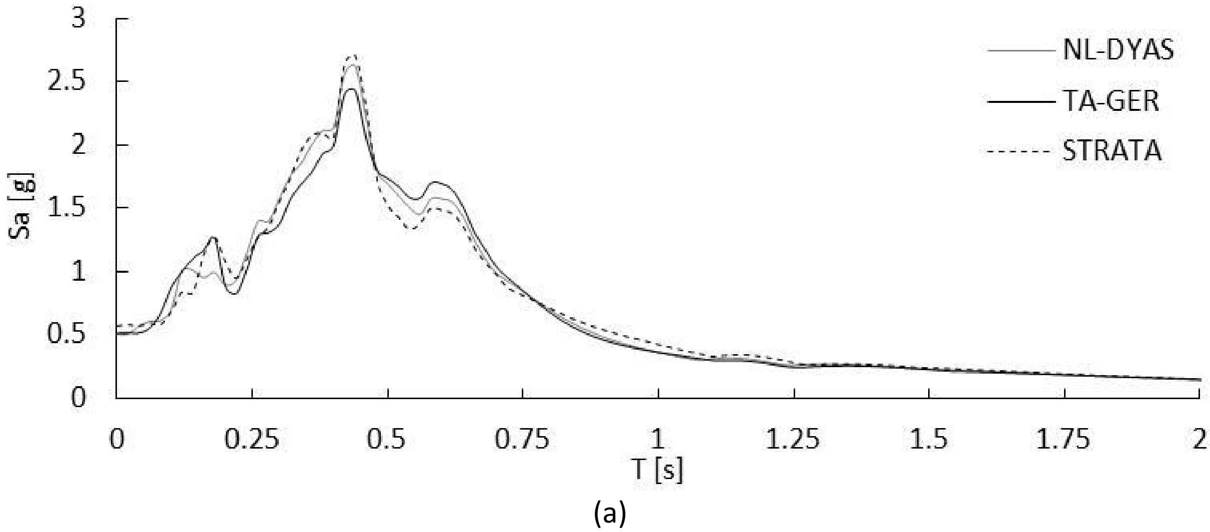

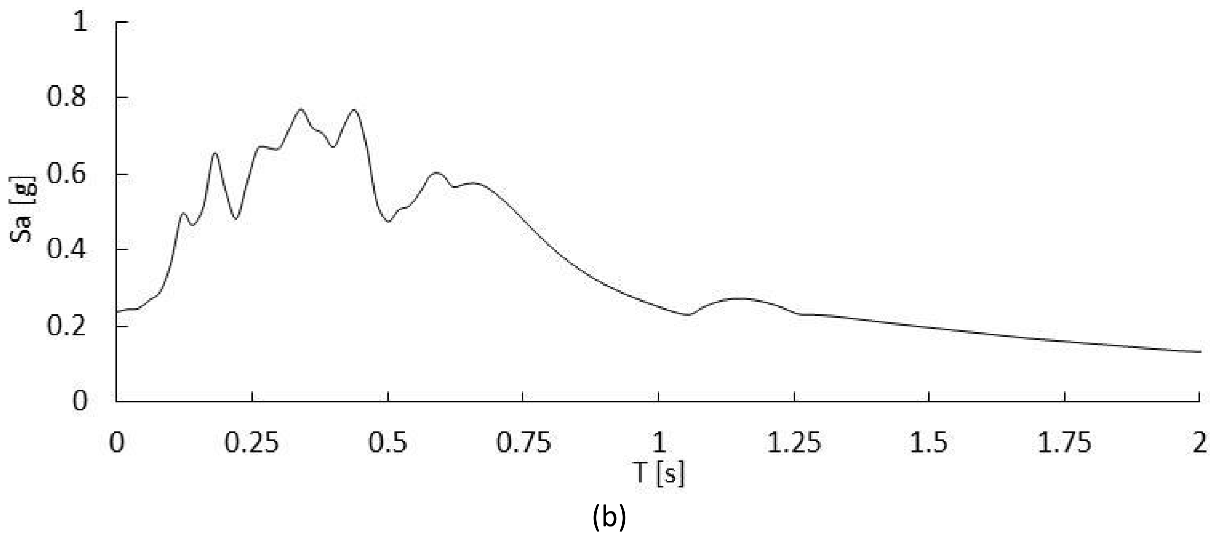

Figure 4.12: (a) Acceleration response spectra at the surface calculated with the three models and (b) common base acceleration spectra. Shaking with Kalamata 1986 record

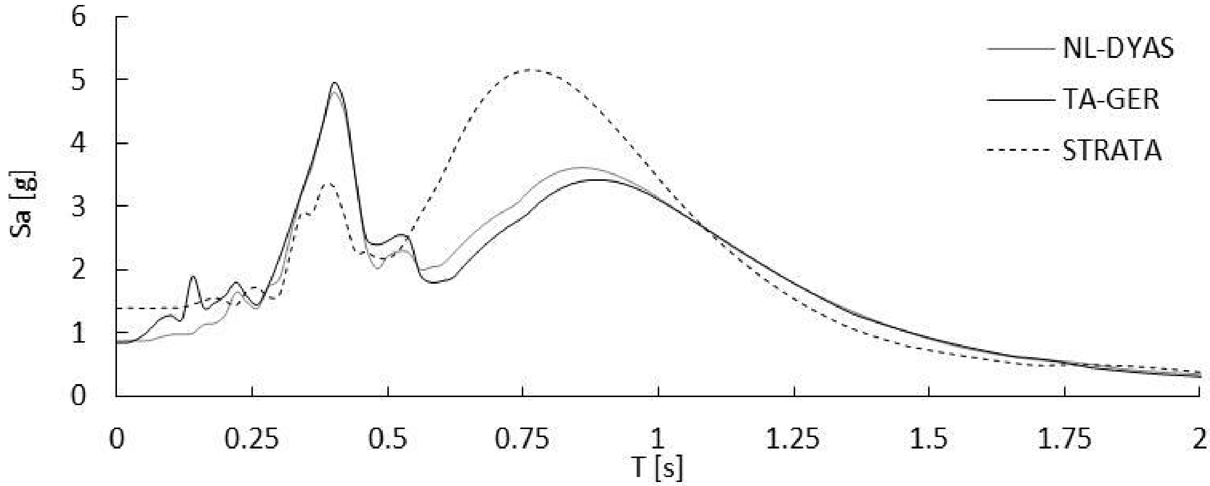

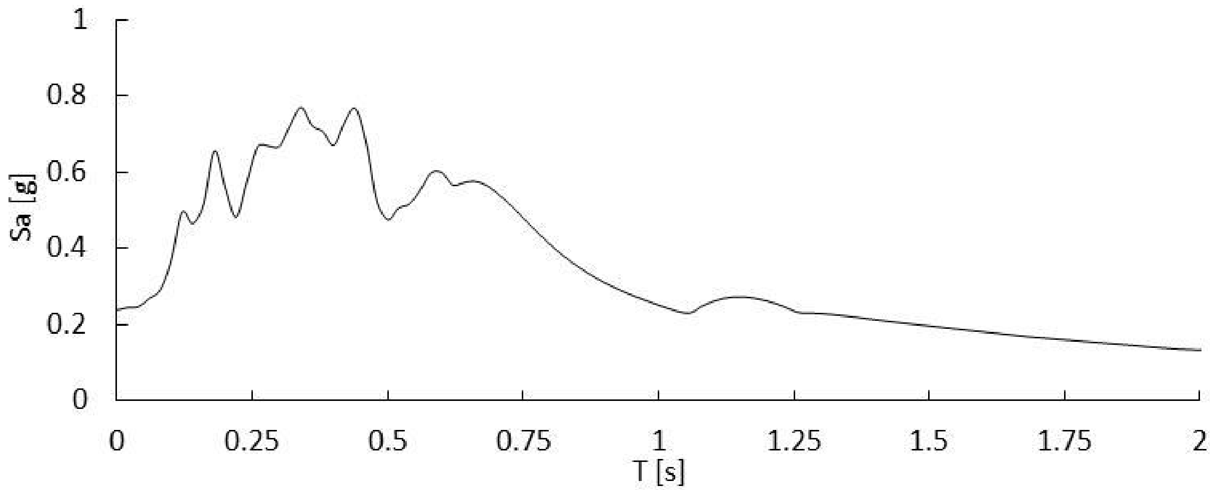

Figure 4.13: (a) *Acceleration response spectra at the surface calculated with the three models and (b) common base acceleration spectra. Shaking with Kobe JMA 090 1995 record*

Chapter 5
Conclusions

5.1 Conclusions

A recently proposed by Tasiopoulou and Gerolymos constitutive model for sand, was downscaled from the three dimensional space (6 stresses and 6 strains) to the two dimensional space (2 stresses and 2 strains). The model is based on a modified elastoplasticity scheme and founded on the effective stress and critical state concepts. The constitutive formulation combines features of classical elastoplasticity with a hardening law and an unloading-reloading rule of the Bouc-Wen type. The model performance was demonstrated through a series of simulations on drained condition with monotonic and cyclic loading. It was shown that the model is capable of reproducing the basic aspects of sand behavior, such as, hysteretic loops, progressing stiffening, densification, etc.

Afterwards, the capability of the model on fitting the experimental shear modulus reduction and damping curves was tested. Two families of published experimental data were utilized, those proposed by Vucetic and Dobry (1991) and those proposed by Darendeli et al. (2001). Only four model parameters were selected for calibration. Curve fitting revealed that values of the parameters selected for calibration are unique for every mean effective stress level, for each one of the family curves, i.e. there is no need to recalibrate the model parameters to account for different values of p.

The model is finally implemented into a finite differences in - house computer code. The equations of motion, the boundary conditions and the initial conditions were approached using the explicit finite difference method technique. The model was validated against two different methods established in literature, a non – linear method that utilizes a hysteretic (phenomenological) model and the well - known equivalent linear method. Validation proved the model capable of predicting efficiently the 1D nonlinear site response. The capability of the model in simulating the nonlinear response of horizontally layered deposits was checked testing a 30 m deep dense sand profile to two different levels of seismic excitation on its base, a moderate and a strong one. While the three codes exhibited similar results for the moderate seismic excitation case, validating the proposed plasticity-based model, the equivalent linear method fails to yield satisfactory results for the strong motion case, significantly underestimating the high-frequency components of the ground response and overestimating the low-frequency ones. Thus, it is evident that equivalent linear method is incapable of predicting accurate results when soil non linearity is dominant and should be used carefully when simulating strong seismic excitations. On the contrary, the phenomenological hysteretic non – linear method is in well agreement with the plasticity based non – linear method for both the excitations. However, the lack of a physically motivated plastic flow rule for the connection of the plastic volumetric strain with the plastic shear strain, that the phenomenological model suffers from, leads to difficulties in extending the model to account for undrained conditions, while plasticity based models are perfectly able to account for drained and undrained conditions as well. Furthermore, phenomenological models can not be extended to three dimensional space to predict system failure but are limited to soil element response and are also incapable of simulating two face analyses. Thus, it is a worthly procedure to calibrate and validate a plasticity based model even in the two – dimensional space since it is the first step for more complex and sophisticated analyses that only this type of constitutive models can provide.

5.2 Future work

The calibration of the model according to the published shear modulus reduction and damping curves and its validation in predicting the one dimensional soil response was carried out only for drained conditions in the present work. The next step, would be the implementation of the same procedure to account for undrained conditions. The constitutive model should be reformed and it’s ability to accurately predict pore pressure generation should be tested against the experimental data for the cyclic liquefaction resistant ratio curves. Model is potentially capable for simulating partially drained conditions as well.

References

[1] Schnabel PB, Lysmer J and Seed HB. "SHAKE: A computer program for earthquake response analysis of horizontally layered sites," Rep. EERC 72-12, Univ. of California, Berkeley, 1972.

[2] Rathje, E.M., Ozbey, M.C., and Kottke, A. 2006. "Site Amplification Predictions using Random Vibration Theory," Proceedings, First European Conference on Earthquake Engineering and Seismology, Paper No. 337, Geneva, Switzerland, September (CD-ROM).

[3] Lee MKW and Finn WDL. "DESRA-2, Dynamic effective stress response analysis of soil deposits with energy transmitting boundary including assessment of liquefaction potential," Soil Mechanics Series No. 38, University of British Columbia, 1978.

[4] Gerolymos N, Gazetas G. Constitutive model for 1-D cyclic soil behavior applied to seismic analysis of layered deposits. Soils Found 2005; 45(3):147–59.

[5] Drosos V, Gerolymos N, Gazetas G. Constitutive model for soil amplification of ground shaking: Parameter calibration, comparisons, validation. Soil Dyn Earthq Eng 2012; 42:255–74

[6] Hashash, Y.M.A. and Park D. (2001). "Non-linear one-dimensional wave propagation in the Mississippi Embayment". Engineering Geology, v. 62 (1-3), 185-206.

[7] Yang, Z., Lu, J., and Elgamal, A. (2004). "A Web-Based Platform for Computer Simulation of Seismic Ground Response." Advances in Engineering Software, 35(5), 249-259.

[8] Ching JY and Glaser SD. "1D time-domain solution for seismic ground motion prediction," *Journal of Geotechnical and Geoenvironmental Engineering*, ASCE, 36-47, 2001.

[9] Tasiopoulou P, Gerolymos N. (2016), "Constitutive modeling of sand: Formulation of a new plasticity approach", Soil Dynamics and Earthquake Engineering 82, pp. 205-221.

[10] Tasiopoulou P., Gerolymos N. (2016), "Constitutive Modelling of Sand: A Progressive Calibration Procedure accounting for Intrinsic and Stress-Induced Anisotropy", Geotechnique 66(9), 1-17.

[11] Vucetic, M. and Dobry, R. (1991) "Effect of soil plasticity on cyclic response." *Journal of Geotechnical Engineering,* 117(1), 89–107.

[12] Darendeli, M.B., Stokoe, K.H., II, Rathje, E.M. and Roblee, C.J. (2001) "Importance of Confining Pressure on Nonlinear Soil Behavior and Its Impact on Earthquake Response Predictions of Deep Sites." *Proc., 15th International Conference on Soil Mechanics and Geotechnical Engineering*, August 27-31, Istanbul, Turkey

[13] Constantopoulos, I.V., Roesset J.M., and Christian, J.T. (1973) "A comparison of linear and exact nonlinear analysis of soil amplification," *Proc., 5th World Conference on Earthquake Engineering*, vol. 2, 1806–1815.

[14] Assimaki, D. and Kausel, E. (2002) "An equivalent linear algorithm with frequency- and pressure-dependent moduli and damping for the seismic analysis of deep sites." Soil Dynamics and Earthquake Engineering, 22, 959–965.

[15] Rathje, E.M., and Kottke, A.R. (2011) "Relative differences between equivalent linear and nonlinear site response methods." *Proc., 5th International Conference on Earthquake Geotechnical Engineering*, January 10 – 13, Santiago, Chile.

[16] Travasarou, T. and Gazetas, G. (2004) "On the linear seismic response of soils with modulus varuing as a power of depth – the Maliakos marine clay." *Soils and Foundations*,44(5), 85–93.

[17] Kyriazis Pitilakis, Geotechnical Earthquake Engineering, published by ZHTH, Thessaloniki

[18] Steven L. Kramer, University of Washington, Geotechnical Earthquake Engineering, published by Prentice – Hall Inc., Simon & Schuster / A Viacom Company, Upper saddle River, NJ 07458, 1996

[19] Mehmet Baris Darendeli, B.S., M.S., Doctoral Dissertation, Development of a new family of normalized modulus reduction and material damping curves, The university of Texas at Austin, August 2001

[20] Panagiota Tasiopoulou, Doctoral Dissertation, Development and Calibration of Constitutive Model for Sand, National technical University of Athens, October 2015

[21] Nikos Gerolymos, Doctoral Dissertation, Constitutive model for the static and dynamic soil, soil – pile and soil – caisson response, National technical University of Athens, February 2002